EXTENDED ABSTRACTS

THE 1990 U.S. WORKSHOP on the PHYSICS and CHEMISTRY of MERCURY CADMIUM TELLURIDE and NOVEL IR DETECTOR MATERIALS

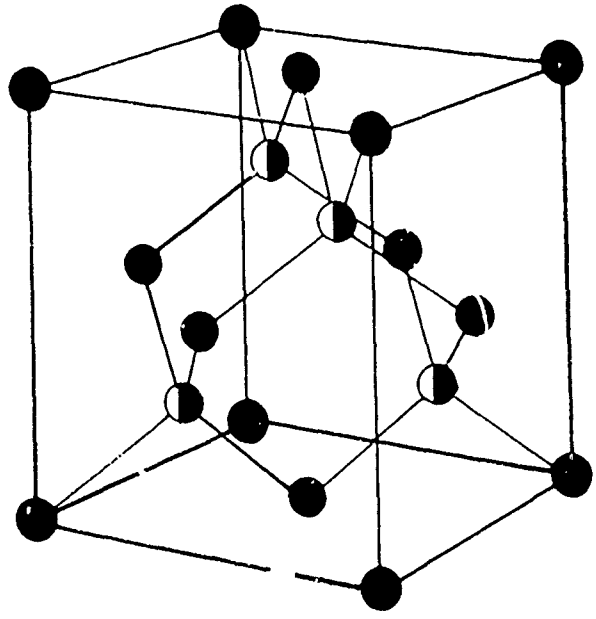

Sponsored by

CECOM Center for Night Vision and Electro-Optics
Office of Naval Technology
Air Force Office of Scientific Research
Electronic Materials & Processing Division —American Vacuum Society

October 2, 3, 4, 1990
San Francisco, California

"The views, opinions, and/or findings contained in this report are those of the author(s) and should not be construed as an official Department of the Army position, policy, or decision, unless so designated by other documentation."

MASTER COPY KEEP THIS COPY FOR REPRODUCTION PURPOSES

REPORT DOCUMENTATION PAGE

Form Approved
OMB No. 0704-0188

1. AGENCY USE ONLY (Leave blank)	2. REPORT DATE	3. REPORT TYPE AND DATES COVERED
	Oct 1990	Final 24 Sep 90 - 23 Sep 91

4. TITLE AND SUBTITLE
Extended Abstracts on U.S. Workshop on the Physics and Chemistry of Mercury Cadmium Telluride and Novel IR Detector Materials

5. FUNDING NUMBERS
DAAL03-90-G-0202

6. AUTHOR(S)
Mark Goldfarb - principal investigator

7. PERFORMING ORGANIZATION NAME(S) AND ADDRESS(ES)
Palisades Institute for Research Services, Inc.
201 Varick Street
New York, NY 10014

8. PERFORMING ORGANIZATION REPORT NUMBER

9. SPONSORING/MONITORING AGENCY NAME(S) AND ADDRESS(ES)
U. S. Army Research Office
P. O. Box 12211
Research Triangle Park, NC 27709-2211

10. SPONSORING/MONITORING AGENCY REPORT NUMBER
ARO 27876.1-EL-CF

11. SUPPLEMENTARY NOTES
The view, opinions and/or findings contained in this report are those of the author(s) and should not be construed as an official Department of the Army position, policy, or decision, unless so designated by other documentation.

12a. DISTRIBUTION/AVAILABILITY STATEMENT
Approved for public release; distribution unlimited.

12b. DISTRIBUTION CODE

13. ABSTRACT *(Maximum 200 words)*
The workshop was held as scheduled. Extended abstracts of the presentations have been distributed.

14. SUBJECT TERMS
Mercury Cadmium Telluride, IR Detectory Materials, Workshop, Novel Devices

15. NUMBER OF PAGES
177

16. PRICE CODE

17. SECURITY CLASSIFICATION OF REPORT	18. SECURITY CLASSIFICATION OF THIS PAGE	19. SECURITY CLASSIFICATION OF ABSTRACT	20. LIMITATION OF ABSTRACT
UNCLASSIFIED	UNCLASSIFIED	UNCLASSIFIED	UL

ACKNOWLEDGEMENTS

The Workshop would like to acknowledge the special contributions, pertinent to the success of the Workshop, which were made by the following institutions:

MASSACHUSETTS INSTITUTE OF TECHNOLOGY

ROCKWELL INTERNATIONAL SCIENCE CENTER

LORAL IR AND IMAGING SYSTEMS

SANTA BARBARA RESEARCH CENTER

CO-CHAIRMEN

R.L. Aggarwal
Massachusetts Institute of Technology
E.R. Gertner
Rockwell International

PROGRAM COMMITTEE

J.P. Faurie
University of Illinois
J.K. Furdyna
Notre Dame University
S.K. Ghandhi
Rensselaer Polytechnic Institute
C.R. Helms
Stanford University
P.R. Norton
Santa Barbara Research Center
P.W. Norton
Loral IR and Imaging Systems
H.F. Schaake
Texas Instruments
J.F. Schetzina
North Carolina State University
A. Sher
SRI International
C.J. Summers
Georgia Institute of Technology

GOVERNMENT ADVISORS

P.M. Amirtharaj
CECOM Center for NV&EO
R.L. Denison
WRDC
D.G. Seiler (Proceedings Editor)
NIST
J.R. Waterman
NRL
H. Wittmann
AFOSR

WORKSHOP COORDINATOR

J. Morreale
Palisades Institute for Research
Services, Inc.

WORKSHOP SPONSORS

CECOM Center for NV&EO
Office of Naval Technology
Air Force Office of Scientific Research
American Vacuum Society

PROGRAM

MONDAY, OCTOBER 1, 1990

7:00–10:00 pm Pre-Workshop Check-In

TUESDAY, OCTOBER 2, 1990

7:00– 8:00 am Workshop Check-In
8:00– 8:30 am Keynote Address
8:30–10:20 am Growth I
10:20–10:40 am BREAK
10:40–12:40 pm Growth II
12:40– 2:00 pm LUNCH
2:00– 3:50 pm Doping I
3:50– 4:10 pm BREAK
4:10– 5:30 pm Doping II
5:30– 7:00 pm Wine and Cheese

WEDNESDAY, OCTOBER 3, 1990

7:00– 8:00 am Workshop Check-In
8:00– 9:30 am Devices I
9:30–10:00 am BREAK
10:00–12:35 pm Devices II
12:35– 2:00 pm LUNCH
2:00– 3:20 pm Devices III
3:20– 3:40 pm BREAK
3:40– 5:20 pm Superlattices
5:20– 7:30 pm Wine and Cheese
6:00– 7:30 pm Panel Discussion

THURSDAY, OCTOBER 4, 1990

7:30– 8:30 am Workshop Check-In
8:30–10:10 am Defects I
10:10–10:30 am BREAK
10:30–11:30 am Defects II
11:30– 1:00 pm LUNCH
1:00– 3:40 pm Surfaces and Miscellaneous

TABLE OF CONTENTS

DIFFUSION MECHANISMS IN MCT

D. A. Stevenson and M F. S. Tang

Department of Materials Science and Engineering
Stanford University, Stanford, CA 94305

For elemental semiconductors, the control of the position and concentration of dopant atoms is a major concern in device fabrication. In the mercury cadmium telluride (MCT) system there are additional concerns: the mercury to cadmium ratio controls the bandgap to the desired value; native defects introduced by mercury annealing (interstitials and vacancies of the component atoms) influence the electrical properties (1); and the quality of superlattices and heterojunctions depends on the sharpness of composition profiles. The practical interest for diffusion in MCT has therefore focussed on component diffusion, specifically: interdiffusion of the components; and intrinsic diffusion of mercury. The three relevant diffusion quantities for component diffusion are: interdiffusion (D); intrinsic diffusion D_i ; and tracer self-diffusion (D_i^*), where the subscript i refers to one of the components (Hg, Cd, Te). These three diffusion quantities are interrelated for the MCT system by theory based on the thermodynamics of diffusion (2). An important limiting form of the resulting theory applies to the MCT system; when the common non-metal species (Te) diffuses more slowly than the two metal species, then D and D_i^* are related with a Nernst-Planck type of equation and the interdiffusion process is controlled by the more slowly diffusing species (2). The interdiffusion is consequently slower than would be predicted from relevant diffusion theory for binary systems.

There are several interdiffusion studies in the MCT System and there is generally good agreement for studies performed above 400°C (3-10). There is an exponential dependence of the interdiffusion coefficient on x (the CdTe mole fraction in MCT), with substantially higher D values at low x values. This dependence has been related to the dependence of the vacancy and interstitial concentrations and formation energies on the x

value, as determined by experiment or calculated from theory (9-16). These interdiffusion values provide a good basis for predicting interdiffusion above 400°C. The prediction of the stability of heterojunctions and superlattices, however, concerns interdiffusion values at lower temperatures where epitaxy is performed, namely, 180 - 250°C. Interdiffusion studies have been performed below 400°C by conventional methods (9,10), by x-ray studies of satellite peaks (17) and by chemical lattice imaging (18). These results indicate that the high temperature behavior can not be extrapolated to lower temperatures and that the diffusion mechanism changes at lower temperatures. At the lower temperatures, there is a lower activation energy, a decreased dependence on x, and an increased dependence on the Hg overpressure (9,10). Furthermore, the use of high spacial resolution methods at low temperatures indicates that D depends on the distance of the diffusion interface from the sample surface (18).

Tracer self-diffusion measurements for all three components in MCT are reported by several investigators for a wide range of samples and experimental conditions (19-23). All these studies show complex tracer profiles that are fit with a superposition of more than one analytical diffusion profile and are represented with D values for slower and faster diffusion processes (D_s and D_f). Complex diffusion profiles and fast diffusion processes are observed when diffusion short circuits are present, such as grain boundaries and sub-grain boundaries, however, the complex profiles in MCT are observed for a wide variety of samples having different grain structure. It is also possible that a faster diffusion process could be chemical diffusion arising from incomplete preannealing, however, the observed diffusion behavior is independent of the preannealing conditions. It is proposed that D_f represents true self-diffusion and D_s represents intrinsic diffusion for Hg and Cd components (22). The basis for this premise is the good fit to the interdiffusion coefficients given by theory if one makes these assignments. Diffusion isotherms for D_{Hg}^* (D_{Hg}^* versus Hg overpressure) show evidence for a vacancy and an intersititial mobile Hg species respectively at low and high Hg overpressure, a species independent of

stoichiometry for Cd, and a Te interstitial for Te (22). The relative D_i^* values for the three components shows the following relation: $D_{Hg}^* > D_{Cd}^* >> D_{Te}^*$. Since the Te sublattice is essentially immobile, in contrast to the metal sublattice, the Nernst-Planck limiting form of the general diffusion equation is appropriate to relate D to D_i^* (22), and the interdiffusion is limited by the more slowly moving cation, namely, Cd.

Annealing kinetics in mercury ambients is related to the intrinsic diffusion coefficient. The mercury intrinsic diffusion coefficient has been assigned to the slower of the mercury tracer diffusion coefficients (22) and can be calculated from D_{Hg}^* and the thermodynamic factor calculated from data in the literature (24).

References

1. C. L. Jones, M. J. T. Quench, P. Cooper and J.J. Gosney, J. Appl. Phys. **53** 9080 (1982).
2. M-F. S. Tang and D. A. Stevenson, J. Phys. Chem. Solids **51**, 563 (1990).
3. V. I. Ivanov-Omskii, K. E. Mironov, and V. K. Ogorodnikov, Phys. Status Solidi A **58**, 543 (1980).
4. V. Leute, H. M. Schmidtke, W. Stratmann, and W. Wink'ng, Phys. Status Solidi A **67**, 183 (1981).
5. K. Zanio and T. Massopust, J. Electron Mater. **15**, 103 (1986).
6. F. Bailly, C. R. Acad. Sci. **262**, 635 (1966).
7. L. Svob, Y. Marfaing, R. Triboulet, F. Bailly, and G. Cohen-Solal, J. Appl. Phys. **46**, 4251 (1975).
8. J. G. Fleming and D. A. Stevenson, Phys. Stat. Sol. (a) **105**, 77 (1987)
9. M-F. S. Tang and D. A. Stevenson, Appl. Phys. Lett. **50**, 1272(1987)
10. M-F. S. Tang and D. A. Stevenson, J. Vac. Sci. Technol. **A (515)**, 3124 10.
11. J. Strauss and R. F. Brebrick, J. Phys Chem. Solids **31**, 2283 (1970)
12. C. G. Morgan Pond and R. Raghavan, Phys. Rev. **B31**, 6616 (1985)
13. H. R. Vydyanath, J. Electrochem. Soc. 128, 260 (1981)
14. H. R. Vydyanath, J. C. Donovan, and D. A. Nelson, J. Electrochem. Soc. **128**, 2685 (1981)
15. J. Nishizawa and K. Suto, J. Phys. Chem. Solids **37**, 33 (1976)
16. H. F. Schaake, J. Electron. Mater. **14**, 513 (1985)
17. D. K. Arch, J. L. Staudenmann, and J. P. Faurie, Appl. Phys. Lett. **48**, 1588 (1986)
18. Y. Kim, A. Ourmazd, and R. D. Feldman, J. Vac. Sci. Technol. **A 8**, 1117 (1990)
19. F. A. Zaitov, A. V. Gorshkov, and G. M. Shalyapina, Sov Phys Solid State **21** (1), 112 (1979)
20. J. S. Chen, Ph. D. Thesis, University of Southern California, 1985
21. M. Brown and A. F. Willoughby, J. Cryst. Growth **59**, 27 (1982)
22. M-F. S. Tang and D. A. Stevenson, J. Vac. Sci. Technol. A 7, 544 (1989)
23. N. Archer and H. Palfrey, presented at the Electronic Materials Conference, Santa Barbara, CA, June 27-29, 1990
24. T. Tung, L. Golonka, and R. F. Brebrick, J. Electrochem. Soc. **128**, 451 (1981)

SELECTIVE ANNEALING FOR PLANAR PROCESSING OF HgCdTe DEVICES†

K.K. Parat, H. Ehsani, I.B.Bhat and S.K. Ghandhi

Rensselaer Polytechnic Institute
Troy, New York 12180

$Hg_{1-x}Cd_xTe$ layers grown by OMVPE are typically p-type due to Group II vacancies, and can be converted to n-type by subjecting them to a low temperature annealing under Hg overpressure. We have investigated the effect of a CdTe cap on the annealing behavior of these layers. It is found that the diffusion rate of Hg through CdTe is significantly lower than through $Hg_{1-x}Cd_xTe$ at 220°C, so that the CdTe cap can be used as a diffusion barrier for Hg. By opening windows in the CdTe cap, the underlying $Hg_{1-x}Cd_xTe$ can be selectively annealed, thus making it possible to form n-type regions selectively in a p-type layer. This technique of selective annealing was used for forming planar p-n junction photodiodes and n-channel enhancement mode MISFETs.

Undoped $Hg_{1-x}Cd_xTe$ layers were grown at 370°C by a process described earlier [1]. After the growth of a 10 μm thick $Hg_{1-x}Cd_xTe$ layer, an undoped CdTe cap of 0.8 μm thickness was grown in the same reactor run. The as grown laye , were p-type with typical carrier concentrations in the mid $10^{16}/cm^3$ range. Figure 1 shows the temperature dependence of the Hall coefficient of two layers which were annealed at 220°C under Hg overpressure. Here sample A was annealed with the CdTe cap intact, and the sample B was annealed after removing the CdTe cap. The alloy composition of the layers were 0.23, and the thickness of the $Hg_{1-x}Cd_xTe$ layer was 11.0 μm. Here, the capped sample remains p-type whereas the uncapped sample is converted to n-type after annealing. At 77K, the measured hole concentration in the p-type layer was $4.9 \times 10^{16}/cm^3$, and the measured electron concentration in the n-type layer was $6.5 \times 10^{14}/cm^3$. It is seen from these results that, at 220°C, a CdTe cap is a good diffusion barrier for Hg, and thus can be used for selective annealing of $Hg_{1-x}Cd_xTe$.

P-N junction photodiodes were fabricated by opening an array of windows 600 μm in diameter and spaced 1000 μm apart, in the CdTe cap, and later annealing the layer

†This research was supported by the Defense Advanced Research Projects Agency (Contract No. N-00014-85-K-0151) and by a grant from the Raytheon Corp.

under Hg overpressure at 220°C for 24 hours in a sealed quartz ampoule. The p-n junctions thus formed are of a cylindrical nature, with a junction area equal to πdt, where d is the diameter of the window, and t is the $Hg_{1-x}Cd_xTe$ layer thickness. For these devices, the CdTe cap acts as a diffusion barrier for Hg during annealing, and also serves the purpose of the junction passivant.

Figure 2 shows the dark I-V characteristic of such a diode at 77K. Here the thickness of the $Hg_{1-x}Cd_xTe$ layer was 10.4 μm, and the alloy composition was 0.32. The junction area was 2 $\times 10^{-4}$ cm^2. The forward cut-in of the diode is about 0.2 volts, and the reverse breakdown voltage is about 9 volts. The R_oA product of the diode is 8.8 $\times 10^7$ ohm-cm^2, which is comparable to the best values reported for $Hg_{1-x}Cd_xTe$ p-n junction diodes with this alloy composition [2].

Figure 3 shows the spectral response of this photodiode measured at 77K. The response is almost flat in the wavelength range of 2.5 μm to 4.0 μm, denoting low recombination velocities at the front and back $CdTe/Hg_{1-x}Cd_xTe$ interface. The response falls to about 50% of the peak value at a wavelength of 4.5 μm, which is the expected cut off for a $Hg_{1-x}Cd_xTe$ photodiode of $x = 0.32$.

Figure 4 shows the source drain I-V characteristic of a MISFET fabricated on $Hg_{1-x}Cd_xTe$ of $x = 0.30$. The threshold voltage of this device is about 1.2 volts. The surface mobility of the electrons estimated from the triode region of the I-V characteristic is about 6700 cm^2/Vsec, which is the typical value for this composition [3].

In summary, selective annealings were achieved in $Hg_{1-x}Cd_xTe$ using a CdTe cap as the barrier for Hg diffusion. This allows planar processing for the fabrication of p-n junctions. P-N junction photodiodes and n-channel MISFETs were formed using this process.

References

1. S.K.Ghandhi, I.B. Bhat and H. Fardi, Appl. Phys. Lett., 52, 392 (1988).
2. A. Rogalski, Infrared Phys., 28, 139 (1988).
3. G.M. Williams and E.R. Gertner, Electr. Lett., 16, 839 (1980).

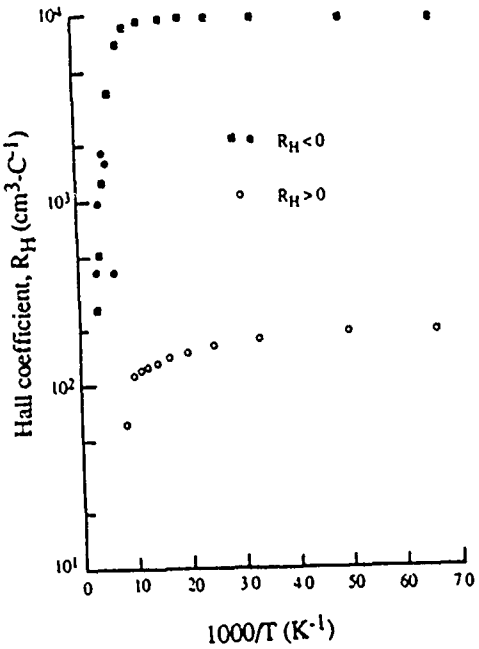

Fig. 1. R_H vs. 1000/T for two annealed samples. Sample A (● o): capped layer. Sample B (■): uncapped layer.

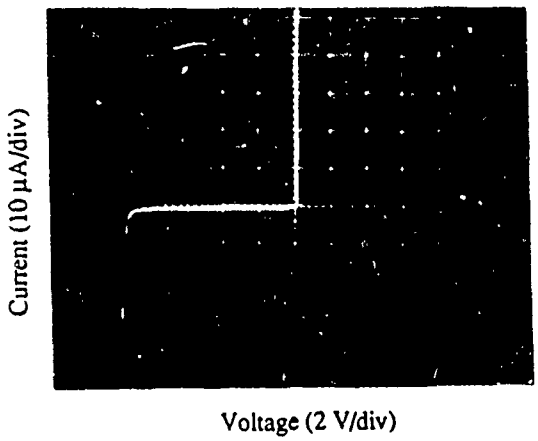

Fig. 2. Dark I-V characteristic of a $Hg_{.68}Cd_{.32}Te$ p-n junction diode at 77K.

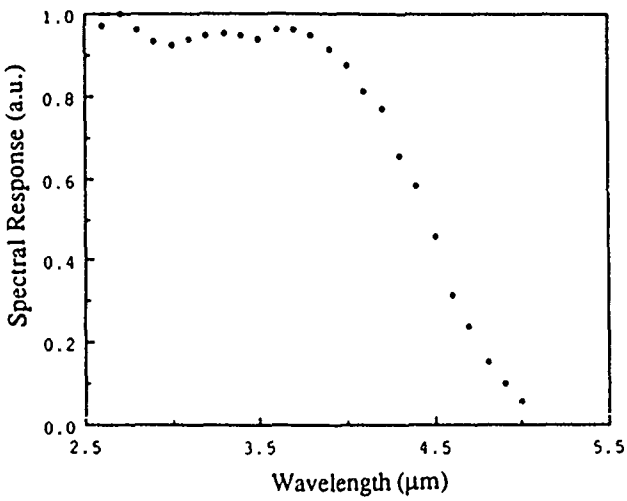

Fig. 3. Spectral respose of the $Hg_{.68}Cd_{.32}Te$ photodiode at 77K.

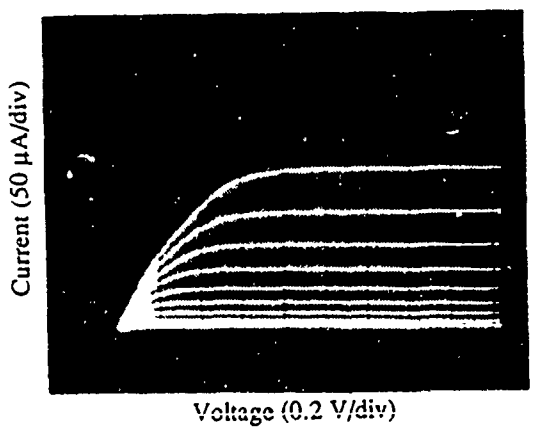

Fig. 4. I-V characteristic of n-channel $Hg_{0.7}Cd_{0.3}Te$ MISFET. Gate voltage: 1.2, 1.4,...3.2 volts.

The MOCVD Growth of HgCdTe on GaAs at 300°C Using Diisopropyltelluride

R. Korenstein, B. MacLeod and P. Hallock

Raytheon Company, Research Division, Lexington, MA 02173

GaAs is currently being pursued as an alternative substrate for $Hg_{1-x}Cd_xTe$ (MCT) epitaxy due to its high crystalline perfection, low price, ruggedness and availability in large area. Typically, MCT is deposited by metalorganic chemical vapor deposition (MOCVD) on (100) oriented GaAs at temperatures in the range of 360-400°C. Doping of the MCT layer by either gallium or arsenic from the GaAs substrate has not been observed to any significant extent for the (100) orientation. For example, Taskar *et al.* report the growth of n-type material on (100)CdTe/GaAs with a carrier concentration of $3.5x10^{15}$ cm^{-3} at 77K.[1] However, we have reported significant gallium doping when MCT is grown in the (111)B orientation at a temperature of 360°C on GaAs substrates.[2] A corresponding carrier concentration in excess of $1x10^{17}$ cm^{-3} is observed for this n-type material. The difference in gallium incorporation as a function of crystallographic orientation can be explained in terms of the chemical reactivity of each surface.[2]

Growth of (111)B MCT is preferred due to the smoother surface morphology obtained in this orientation. In order to reduce gallium incorporation in (111)B MCT, we have reduced the growth temperature to 300°C. A lower growth temperature is expected to reduce the chemical reactions between the metalorganic compounds and the GaAs substrate believed to be responsible for gallium incorporation in MCT grown at higher temperatures.[2]

MCT was grown on both CdTe and GaAs substrates by MOCVD at 300°C using elemental mercury, dimethylcadmium and diisopropyltelluride (DIPTe) in an atmospheric pressure reactor. For GaAs substrates, a (111)B CdTe buffer layer was first grown by hot wall

epitaxy prior to MCT growth. A DIPTe partial pressure of 2.9×10^{-3} atm and a Hg partial pressure of 1.0×10^{-2} atm resulted in growth rates on the order of 1.5 μm/Hr. As expected for this orientation, the grown layers have very smooth surfaces free of the hillocks and microterraces typical of (100) MCT. The compositional uniformity (defined by the maximum variation divided by the mean) is typically between 2-4% over an area of 3 cm^2. From Hall effect measurements, MCT with x values between 0.21 to 0.23 is n-type after a 220°C anneal under a Hg ambient with carrier concentrations between $6\text{-}10 \times 10^{14}$ cm^{-3} and mobilities in excess of 7×10^4 cm^2/Vs at 77K. The n-type doping has been reduced by approximately two orders of magnitude in (111)B MCT as a result of decreasing the growth temperature from 360°C to 300°C. To the best of our knowledge these are the lowest doped MCT layers grown on GaAs by the MOCVD process.

References

1. N.R. Taskar, I.B. Bhat, K.K. Parat, D. Terry, H. Ehsani, and S.K. Ghandi, J. Vac. Sci. Technol. A7, 281 (1989).

2. R. Korenstein, P. Hallock, B. MacLeod, W. Hoke, and S. Oguz, J. Vac. Sci. Technol. A8, 1039 (1990).

THE EFFECT OF GROWTH ORIENTATION ON THE MORPHOLOGY, COMPOSITION, TWIN FORMATION AND GROWTH RATE OF MCT LAYERS GROWN BY MOVPE

G. Cinader, A. Raizman and A. Sher
Solid State Physics Department, Soreq Nuclear Research Center,
Yavne 70600, Israel

The purpose of this investigation was to find the growth conditions for smooth and twin-free HgCdTe (MCT) layers, using the IMP method[1]. A study of the growth mechanism of CdTe and HgTe layers was carried out. The HgTe layers exhibit very smooth morphology and their growth rates were found to be nearly directional independent, except for (111)A and vicinal directions. The grown reaction was concluded to be an homogenious one, and the growth rate was found to be proportional to the tellurium precursor (DIPTe) partial presure. On the other hand, under our growth conditions, the growth rate of CdTe was found to depend strongly on the crystallographic growth direction. The relative growth rates R of CdTe were found to be as following:
R(223)B > R(255)B > R(112)B > R(111)B > R(012)B > R(001)B >> R(111)A, R(112)A. Here the growth mechanism was concluded to be heterogenious and surface kinetically limited. At 350°C and P(DIPTe) ≈ P(DMCd) the rate limiting reactant is DMCd. The pyrolysis of the tellurium precursor seems to be catalyzed by cadmium on the growth surface[2]. It was noticed that the growth mechanism of CdTe is similar to that of GaAs, under proper conditions[3].

We have found that crystallographic directions which exhibit higher growth rate result in MCT layers of better morphology. Directions having nearly maximum growth rates (with respect to other directions) yield layers of featureless morphology.

A model was proposed explaining the formation of morphological features such as hillocks. This model explains the faceted structure of the hillocks, their compositional inhomogeneity[4], and possible formation of lamella twins inside some of them. The model assumes that thermal etch pits are formed around crystallographic defects at the substrate surface during the pregrowth process, or in the

layer-substrate interface region, during the early stage of the layer growth. The pyramidal hillocks originate from the faster growth rate of CdTe on the pits facets[5], which are usually in a prefered direction, such as (111)B. Hence the local increase of the layer thickness at the hillocks site is associated with an appropriate increase in the cadmium concentration of the MCT alloy. Realizing the role of sublimation in revealing thermal pits a proper atmosphere was held during the substrate heating stage, prior to growth, yielding a reduction of the hillocks density, in (001) layers. Growth of CdTe on a (100) GaAs substrate, under mass transport limited conditions, has resulted in a morghology with no hillocks at all.

X-ray double crystal diffractometry have been used to assess the presence of twin defects in layers grown in different crystallographic directions. Our measurements indicate that the twin population is strongly reduced in layers that deviate a few degrees from the (111)B direction. Our findings can explain the different structure of the twins[6] that exists in MCT layers grown on CdTe (111)B and (111)A substrates. Practically, the preferred growth orientation for CdTe and MCT layers, free of hillocks and twins, should deviate fron the (111) direction and be of the highest CdTe growth rate.

Further evaluation of the growth quality on the new directions was carried out by measuring the electrical properties of several MCT layers grown on (112)B CdTe substrates. All the as grown layers were found to be low n-type, with $n \approx 10^{15}/cm^3$ and $\mu=(1\text{-}2)10^5$ $cm^2/V\cdot S$ at 77°K, and show normal field and temperature dependence. These results differ from previously reported results and theoretical calculations[7] that have predicted p-type conductivity with $p \approx 6x10^{16}/cm^3$. The role of the expected lower mereury condensation coeficient[8] for the (112)B direction, with respect to the standart (100) surface, is not yet clear.

Reference list

1. S.C.J. Irvine, J. Tunnicliffe and J.B. Mullin, Materials Letters 2 (1984), 305.
2. Ishwara B. Bhat, Nikhil R. Taskar and Sorab K. Ghandhi, J. Electrochem. Soc. (1987), 92.
3. Don W. Shaw, J. Crystal Growth 31 (1975), 130.
4. P. Capper, C.D. Maxey, P.A.C. Whiffin and B.C Easton, J. Crystal Growth 96 (1989), 519.
5. J.J. Dubowski, J.M. Wrobel, D.F. Mitchell and G.I. Spraulc, J. Crystal Growth 94 (1989), 41.
6. M. Oron, A. Raizman, Hadas Shtrikman and G. Cinader, Appl. Phys. Lett. 52 (1988), 1059.
7. J.B. Mullin, A. Royle, J. Giess, J.S. Gough and S.J.C. Irvine, J. Crys. Growth 77 (1986), 460.
8. S. Sivanathan, X. Chu and J.P. Faurie, J. Vac. Sci. Technol. B5 (1987), 694.

GROWTH AND CARRIER CONCENTRATION CONTROL OF $Hg_{1-X}Cd_XTe$ HETEROSTRUCTURE USING ISOVPE AND VPE TECHNIQUES

S. B. Lee, D. Kim and D. A. Stevenson
Department of Materials Science and Engineering, Stanford University
Stanford, CA 94305

Heterostructures are proposed as a way of overcoming some of the problems inherent in single layer narrow bandgap $Hg_{1-X}Cd_XTe$ devices.[1] Advantages of heterostructure $Hg_{1-X}Cd_XTe$ (wide bandgap material on the surface of a narrow bandgap material) include: the improvement in MIS (metal-insulator-semiconductor) performance by increasing well capacity and reducing dark current; and the integration of associated signal processing circuitry on-chip in the wide bandgap region of $Hg_{1-X}Cd_XTe$. We describe a study employing isothermal vapor phase epitaxy (ISOVPE) and vapor phase epitaxy (VPE) for growth of wider bandgap $Hg_{1-X}Cd_XTe$ on narrow bandgap $Hg_{1-X}Cd_XTe$, along with the electrical and compositional control and characterization of the layers.

The ISOVPE conversion technique (2) and a two stage conversion technique (illustrated in Fig. 1) are used to fabricate the $Hg_{1-X}Cd_XTe$ heterostructures on the solid state recrystallized (SSR) narrow bandgap $Hg_{1-X}Cd_XTe$ (X=0.2). Roughly 1 to 2 μm of wide bandgap $Hg_{1-X}Cd_XTe$ is appropriate to increase the well capacity of the MIS structure by improving the breakdown electric field.[1] Precise control of composition is not necessary for this purpose and graded junction profiles are acceptable. The ISOVPE conversion technique is used for this purpose and the typical converted profile is shown as figure 2. For on-chip fabrication of signal processing circuitry, thicker layers (>10 μm) are required and there is no preference about the junction shape as long as the compositional profile at the surface region is flat. A two stage conversion is used mainly for this purpose; in its first stage, CdTe is grown on top of narrow bandgap $Hg_{1-X}Cd_XTe$ (X=0.2) and in the second stage, the desired composition ($0.3<X<0.7$) of $Hg_{1-X}Cd_XTe$ is grown on a CdTe layer using the ISOVPE technique. The first stage of the conversion is conducted using a

conventional evaporation chamber with the CdTe source at 625°C and the $Hg_{1-X}Cd_XTe$ substrate at 200°C.

Both conversion methods produce p-type heterostructures, which are converted into n-type by annealing in a mercury ambient. Carrier concentrations of $5X10^{14}/cm^3$ to $1X10^{15}/cm^3$ and mobilities of 70,000 to 80,000cm^2/V-s are measured reproducibly. Two zone mercury annealing (the Hg reservoir at a lower temperature than the annealed sample) is effective to lower the carrier concentration to the $5X10^{14}/cm^3$. Two zone mercury annealing is also effective to lower carrier concentration of ISOVPE-grown narrow bandgap $Hg_{1-X}Cd_XTe$.

The chemical composition and the concentration profiles are evaluated using electron probe microanalysis (EPM). The surface morphology of converted $Hg_{1-X}Cd_XTe$ is evaluated using optical microscopy and a scanning electron microscopy (SEM). The surface morphology is strongly dependent on the orientation of the SSR $Hg_{1-X}Cd_XTe$ and the surface usually requires polishing. Etchpit density of the heterostructures is comparable to the conventional ISOVPE-grown single layers ($5X10^4/cm^2$ to $5X10^5/cm^2$) after polishing. The Laue method and Read camera are used for investigating crystal quality and crystal orientation. Electrical characterization of the as-grown and post-growth treated layers is performed by Hall measurements at 77K using the van der Pauw technique and differential etching.

The main achievements of the present work are: the growth of heterostructures with wider bandgap $Hg_{1-X}Cd_XTe$ at the surface region for better performance of MIS devices and on-chip signal processing, utilizing relatively easy and inexpensive methods like the ISOVPE and VPE techniques; and the development of a two zone mercury annealing method to control the carrier concentration.

REFERENCES

1. M. W. Goodwin, M. A. Kinch, and R. J. Koestner, J. Vac. Sci. Technol. A 8 (2), 1226-1232(1990)
2. S. B. Lee, L. K. Magel, M. F. S. Tang, D. A. Stevenson, J. H. Tregilgas, M. A. Goodwin, and R. L. Strong, J. Vac. Sci. Technol. A 8 (2), 1098-1102(1990)

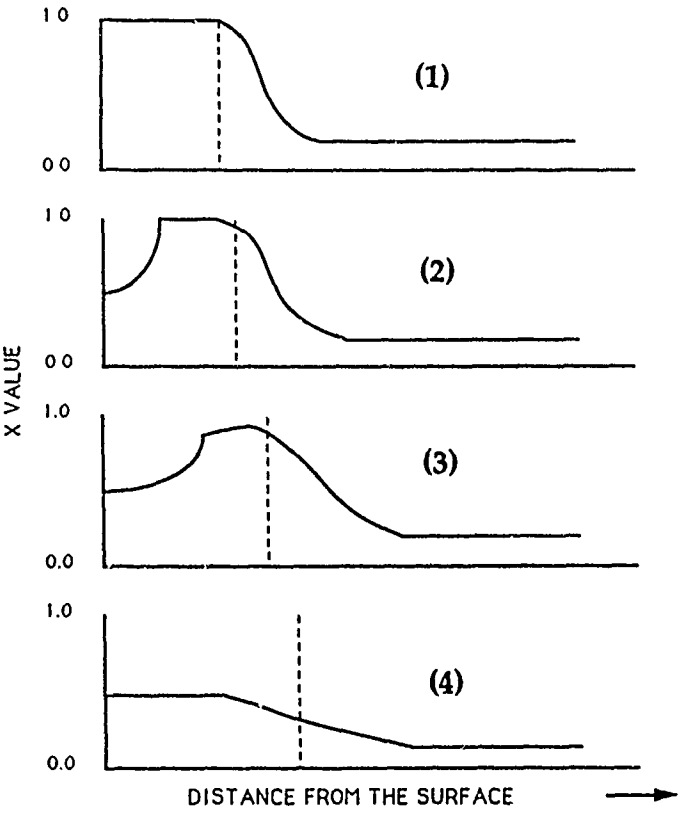

Figure 1. Mechanism of two stage growth, (1) CdTe is deposited on top of narrow bandgap (HgCd)Te, (2), (3) Wide bandgap (HgCd)Te is grown on CdTe interlayer by ISOVPE technique, (4) Further growth flattens the hump of the composition profile.

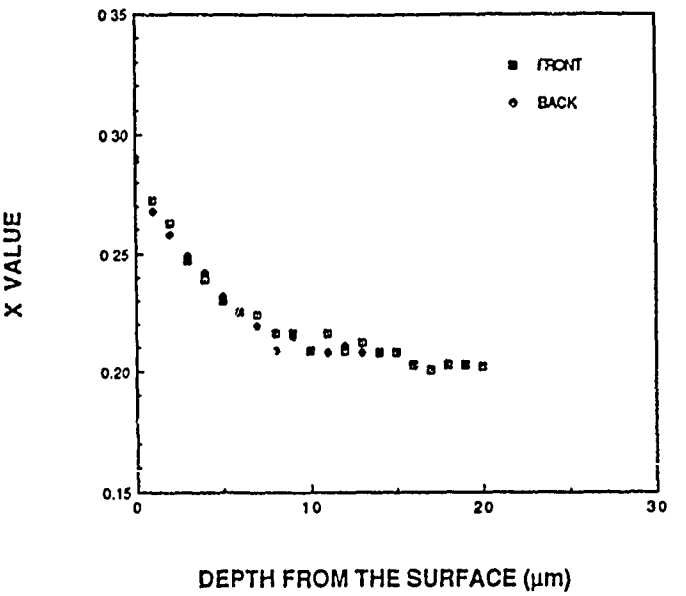

FIgure 2. Typical concentration profile of ISOVPE converted (HgCd)Te heterostructure. (X=0.2, 450°C, 24 hrs)

Low Dislocation Density HgCdTe Grown on GaAs and Si Substrates by MBE

J.M. Arias, S.H. Shin, M. Zandian, J.G. Pasko and R.E. DeWames
Rockwell International Science Center

The use of GaAs and Si substrates for HgCdTe epitaxial growth is highly desirable because of the possibility of manufacturing very large focal plane arrays (greater than 128x128) using the hybrid approach. These HgCdTe multilayer structures make it also conceivable to integrate signal processing and infrared (IR) detection in a monolithic structure.

One of the major problems in obtaining high quality HgCdTe films on GaAs is the high defect density generation due to the large lattice mismatch (14.5 %) between the CdTe buffer layer and the GaAs substrate. A threading dislocation density in the mid 10^6 cm^{-2} range occurs for MBE HgCdTe epilayers[1] grown on (211)B GaAs and (211)B GaAs/Si substrates. Dislocations affect LWIR HgCdTe dark currents for devices operating at low temperatures[1,2] ($\leq$77K) because they are thought to produce mid-gap states in the band gap, it is highly desirable to reduce the dislocation density.

We have developed a post-growth thermal annealing method to consistently reduce the threading dislocation density by an order of magnitude for large area HgCdTe epilayers grown on (211) GaAs and GaAs/Si substrates. Etch pit densities (EPD) as low as $2x10^5$ cm^{-2} have been obtained. This is a significant result since the EPD values of these highly mismatched systems are comparable to high quality (device quality) MBE HgCdTe epilayers grown on lattice-matched CdZnTe substrates[3].

In this paper, we present the methodology followed to achieve the reduction of the dislocation density, from fundamental nucleation and MBE growth (GaAs thermal cleaning, CdTe and HgCdTe growth temperature, Te-stabilized conditions, etc.) to the thermal annealing studies (annealing temperature, time, overpressure, etc.). Structural (x-ray, top and cross section EPD studies), as well as electrical (Hall and lifetime measurements) characterizations will be presented. We will also discuss the mechanisms for the annihilation of dislocations and the consequence of these results.

1. J.M. Arias, R.E. DeWames, S.H. Shin, J.G. Pasko, J.S. Chen, and E.R. Gertner, Appl. Phys. Lett. 54, 1025 (1989).
2. J.H. Tregilgas, T.L. Polgreen and M.C. Chen, J. Crystal Growth 86, 460 (1988).
3. J.M. Arias, S.H. Shin, J.G. Pasko, R.E. DeWames and E.R. Gertner, J. Appl. Phys.65, 1747 (1989).

Partially Suported by DARPA/CNVEO Contract NO. DAAL03-87-C-0014

MOLECULAR BEAM EPITAXY OF CdTe ON LARGE AREA Si(100)

R. Sporken, M.D. Lange, and J.P. Faurie

Microphysics Laboratory, Department of Physics

University of Illinois at Chicago, P.O. Box 4348, Chicago, IL 60680

Recently, there has been considerable interest for the use of silicon as a substrate for epitaxial growth of CdTe[1-3] and HgCdTe.[3] The goal is to develop a technique to produce large-area monolithic infrared (IR) focal plane arrays combining HgCdTe IR detectors with Si integrated circuits for signal processing. Moreover, Si has some other advantages over conventional substrates for II-VI semiconductors. So far, CdTe and CdZnTe single crystals are the most widely used substrates for the epitaxial growth of HgCdTe, but they are expensive and difficult to produce with a large area; they are also very fragile and difficult to process. Silicon substrates are available in large area and are inexpensive compared to CdTe or GaAs, and silicon is much stronger than CdTe or GaAs.

We have grown CdTe directly on 2-inch and 5-inch diameter Si(100) by molecular beam epitaxy (MBE) and characterized these layers by in-situ reflection high-energy electron diffraction (RHEED) and by double-crystal x-ray diffraction, scanning electron microscopy (SEM) and low-energy photoluminescence (PL). The films are up to 10μm thick and mirror-like over their whole surface. RHEED shows that smooth monocrystalline films are obtained with a $(2\sqrt{3} \times 2\sqrt{3})$ R30° reconstruction, which is typical for CdTe (111)B surfaces prepared by MBE. Two domains are observed in the CdTe layers corresponding to the $[\bar{2}11]$ CdTe axis parallel to either the [011] or the [011] Si axis. Single-domain films are grown on misoriented Si(100) substrates. SEM shows that these single-domain films are of better surface morphology than those grown on oriented Si(100).

The crystalline quality of the CdTe layers was checked by double-crystal x-ray diffraction. The best value of the full-width at half maximum (FWHM) of the CdTe (333) reflection is slightly below 500 arcsec for a layer grown on a 5-inch substrate, and the standard deviation is only 17 arcsec. The thickness of the CdTe layers on Si(100) was measured by IR transmission. Fig. 1 shows the thickness variation for a 6μm thick CdTe layer on Si(100) compared to the average thickness along a 5-inch diameter. The standard deviation is 2.3% whereas on 2-inch wafers, standard deviations below 0.4% were obtained. PL spectra measured at 12K confirm the improved quality of these layers compared to earlier results. The bound exciton peak at 1.593eV has a FWHM of 3 to 4.5 meV, whereas previously reported values[2-4] range from 5.6 to 12 meV at low temperature and 20 meV at 77K. These results demonstrate the possibility of producing CdTe layers with 5-inch diameter, which has never been possible before by any other technique. They also prove the success of MBE for the growth of semiconductors on large area substrates, with excellent structural and thickness uniformity.

References

1) Y. Lo, R.N. Bicknell, T.H. Meyers, J.F. Schetzina, and H.H. Saldmeier, J. Appl. Phys. 54, 4238 (1983)

2) R.L. Chou, M.S. Lin, and K.S. Chou, Appl. Phys. Lett. 48, 523 (1986)

3) R. Sporken, S. Sivananthan, K.K. Mahavadi, G. Monfroy, M. Boukerche and J.P. Faurie, Appl. Phys. Lett. 55, 1879 (1989)

4) H. Zogg and S. Blunier, Appl. Phys. Lett. 49, 1531 (1986)

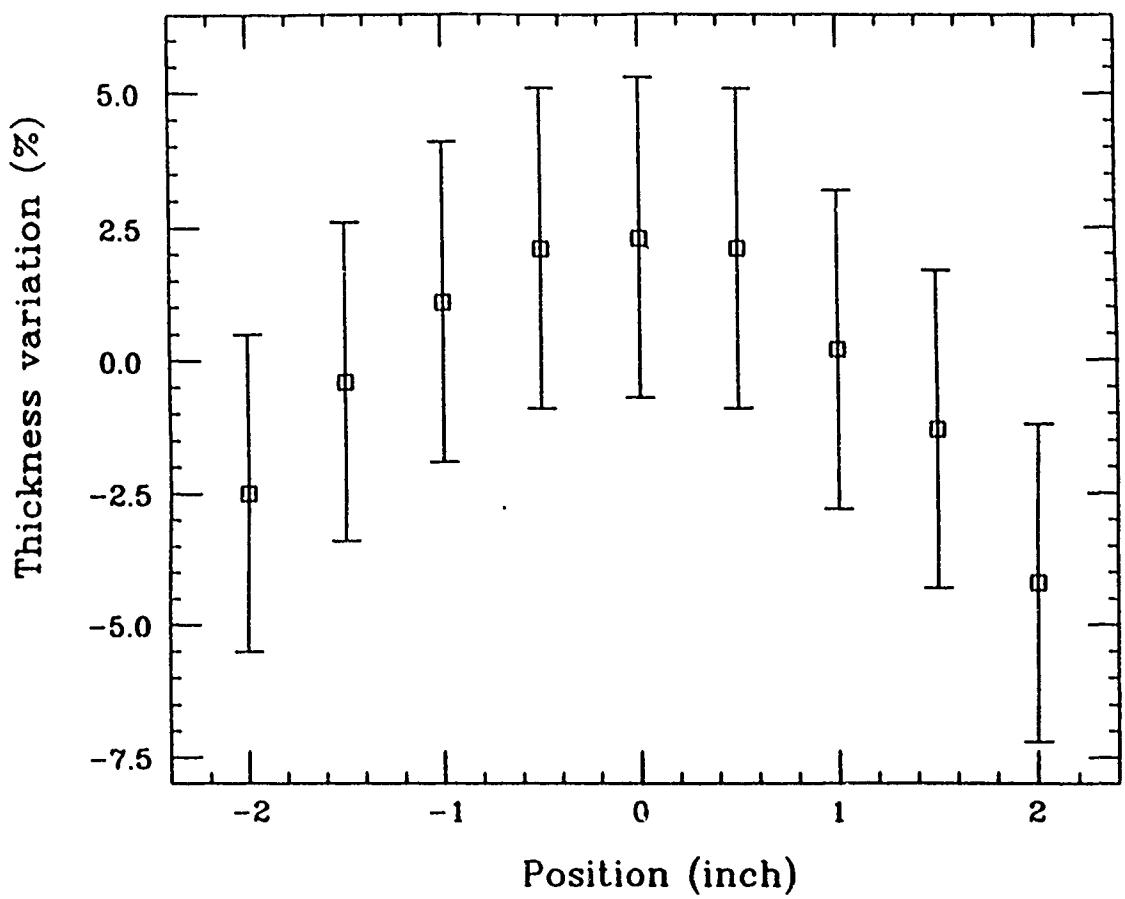

Fig. 1: Thickness variation of a CdTe layer grown by MBE on a 5-inch Si(100) wafer with rotation. The average layer thickness is 6µm.

RHEED STUDIES OF CdTe AND HgTe GROWN BY CBE

R. G. Benz II, B. K. Wagner, D. Rajavel and C. J. Summers
Physical Sciences Division
Georgia Tech Research Institute
Atlanta, Georgia 30332

Chemical beam epitaxy (CBE) is a newly-developed growth technique which uses organometallic vapors to deposit epitaxial materials. CBE offers improved flexibility and control over growth parameters compared to molecular beam epitaxy (MBE). Although CBE has demonstrated the ability to deposit certain high-quality III-V and II-VI materials, this technique has only recently been applied to the growth of CdTe and HgTe. However, no comparison has been made between the microscopic growth process occurring on the surface of CBE and MBE layers. Differences are expected due to the presence of organic radicals, partially-cracked organometallic molecules and Te-monomers in CBE. This work presents correlated studies of the growth rate and surface quality of CdTe and HgTe by CBE and MBE as determined by reflection high energy electron diffraction (RHEED) image analysis and intensity oscillations.

In particular, the RHEED intensity oscillations were studied for optimum conditions of the incident electron beam angle, azimuthal angle and diffracted beam to measure the growth rate and conditions of growth for CdTe and HgTe. These studies included variations in the DeCd to DipTe (cracked and uncracked) flux ratios, absolute flux intensities and the substrate temperature. Analysis of the surface nucleation condition was obtained from RHEED streak profile analysis to estimate the step density. Preliminary results indicate a linear increase in CdTe growth rate with cracked DipTe flow for a constant cracked DeCd flow. The growth rate saturated at a DipTe/DeCd ratio of ~ 1.3 at 250°C. For growth on a nominally singular surface, the growth rate then decreased at larger DipTe/DeCd ratios, while intensity oscillations disappeared on a vicinal surface. Thus, using RHEED intensity oscillations the Cd- and Te-rich growth conditions can be quantitatively determined and directly related to the atomic surface morphology as measured by the RHEED image. Results are compared between solid Cd(Hg) and Te sources, and uncracked DeCd and DipTe to estimate the effect of organometallic cracking on the growth surface. Additional results will be presented on vicinal surfaces to determine the surface diffusion length and on the phase behavior of the intensity oscillations to determine surfaces with minimum roughness for superlattice growth.

CHARACTERIZATION OF CdTe AND $Hg_{1-x}Cd_xTe$ GROWN BY CHEMICAL BEAM EPITAXY

B. K. Wagner, R. Rejavel, R. G. Benz II, C. J. Summers

Physical Sciences Division
Georgia Tech Research Institute
Atlanta, Georgia 30332

We report on the growth of $Hg_{1-x}Cd_xTe$ ($0<x<1$) by chemical beam epitaxy (CBE). The epitaxial layers were grown in a Varian GEN II MBE system modified to handle gas sources. These modifications include direct injection diethylcadmium (DeCd) and diisopropyltelluride (DipTe) flow controllers, separate group II and VI high temperature cracking injectors, gas dopant sources, and a turbomolecular pumping system.

Growth of HgCdTe was undertaken on (001) GaAs, CdTe, and ZnCdTe substrates at growth rates from 0.3 to 1.3 um/hr and substrate temperatures from 160 to 300°C. Growth was carried out using both conventional solid and gas sources. In each case the elemental Hg flux was supplied by a Hg-pressure controlled vapor source.

The precise control obtained with the Hg source and direct injection flow controllers allowed the effect of flux ratios on layer quality to be accurately controlled and investigated. The effect of the DipTe/DeCd flux ratio (0.8 to 2) on the photoluminescence (PL) spectra of (001) CdTe layers grown on CdTe substrates at 250°C is shown in figure 1. The layers exhibit strong band edge luminescence and for the best samples no defect band was observed at longer wavelengths. Carrier concentration and mobility measurements support the trend of crystal quality as indicated by the PL measurements. The PL data is currently being analyzed to identify the donor and acceptor species present in the material.

Further results of PL, infrared transmission, and electrical characterizations of CdTe and HgCdTe layers comparing solid and gas source growth as a function of substrate temperature will be reported along with preliminary arsine doping results.

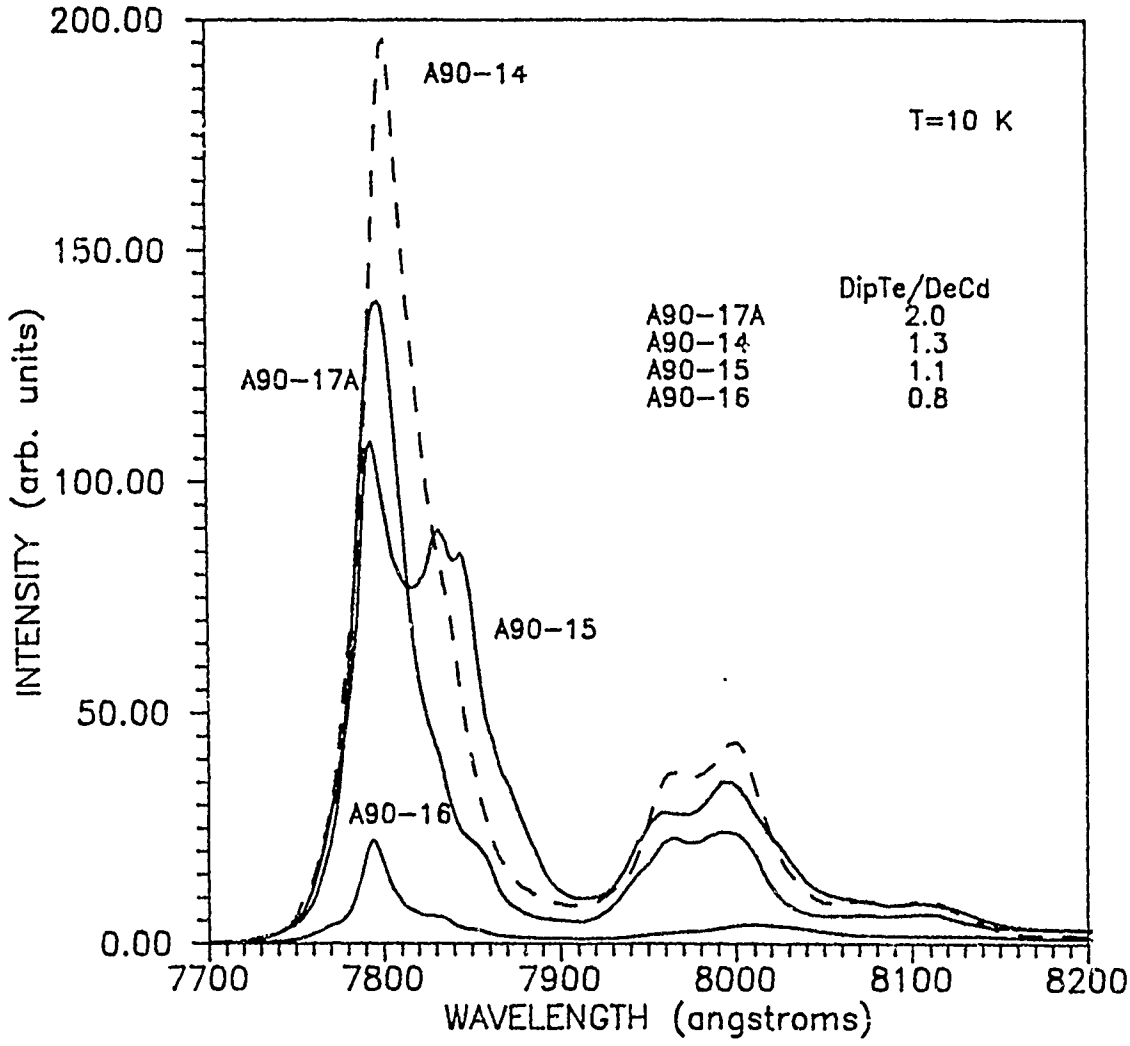

Figure 1. Photoluminescence spectra of (001) CdTe layers grown at 250°C by CBE.

NUMERICAL AND EXPERIMENTAL RESULTS ON THE GROWTH OF (Hg,Cd)Te BY LIQUID PHASE EPITAXY

Pok-Kai Liao, Luigi Colombo, J. H. Hurst, and D.W. Shaw
Texas Instruments Incorporated
Central Research Laboratories
Dallas, TX 75265

Growth of (Hg,Cd)Te by liquid phase epitaxy (LPE) using the dipping technique is numerically simulated by coupling mass transport and the equilibrium phase diagram information.[1] A one dimensional, two-layer model including the solutal boundary layer is assumed for the melt and it is assumed that local equilibrium is established at the melt-film interface. The models are then compared to experimental results. Fluid flow in the LPE melts was also simulated numerically using a commercially available code, FLUENT[2], in order to understand the effects of substrate rotation and natural convection on the melt behavior during film growth.

Figure 1 shows the film composition as a function of thickness for two growth techniques, programmed cooling and isothermal growth, from a two-phase solution of (Hg,Cd)Te solid and Hg-Cd-Te liquid. The simulation indicates that films grown under programmed cooling, curves 1, 2 & 3, have higher compositional gradients than those grown under isothermal grown conditions, curves a, b & c. This is in very good agreement with experimental results where compositional gradients, dx/dz, of about $0.7\text{-}2\times10^{-4}$ /μm are observed for films grown under cooling rates of 0.017°C/min, and gradients less than 5×10^{-5} /μm for isothermal growth. Figure 2 shows the composition across a (Hg,Cd)Te film grown under isothermal conditions as determined from IR transmission curves as a function of film thickness. The gradient is about 5×10^{-5}/μm in the upper 60% of the film.

One of the advantages of liquid phase epitaxy using the dipping technique is that the substrate can be rotated in order to minimize compositional non-uniformities and achieve boundary layer control. Figure 3 shows the growth rate as a function of substrate rotation. As the substrate rotation is increased, the growth rate increases approximately as predicted by the boundary layer expression given by Burton et al..[3] These results are in qualitative agreement with the numerical calculations when the solutal boundary is varied. In addition at higher rotation rates the surface morphology is greatly improved as a result of the lower

in comparison to films grown at the same growth rates without high rotation. Figure 3 also shows that at low rotation rates the growth rate does not follow the square root dependence of the rotation rate. This observation can be qualitatively explained by invoking fluid flow. Figure 4 shows the stream lines within the Te-rich liquid used to grow the films. A detailed analysis of the fluid flow indicates that at low rotation rates, 0 to 20 rpm, thermal convection dominates. This is usually unsteady and asymmetric , thus giving rise to compositional inhomogeneities and films with inclusions. For rotation rates higher than 30 rpm, steady symmetric forced convection is observed. This is in agreement with experimental results in that specular films can be achieved under these growth conditions for the chosen geometries.

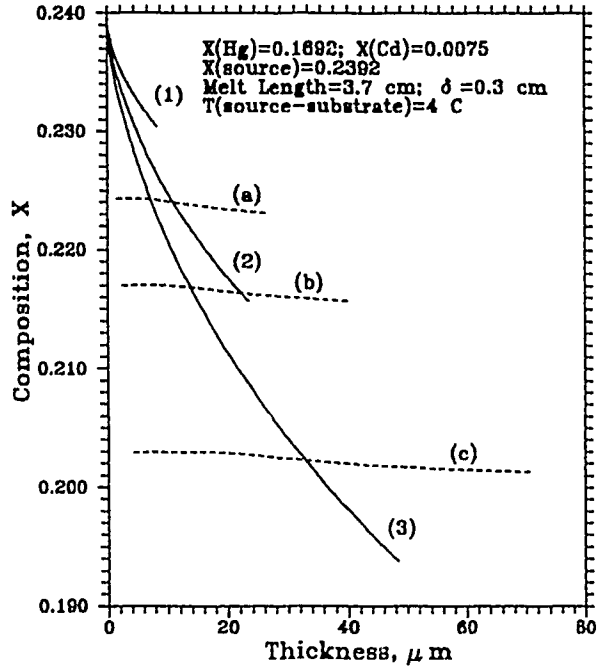

Figure1. Calculated composition as a function of film thickness for two growth techniques A) programmed cooling curves 1) 0.017, 2) 0.05°C/min and 3) 0.1°C/min and B) isothermal growth with the following undercoolings a) 4°C, b) 6°C and c) 10°C.

[1] D.W. Shaw, J. Crystal Growth 62, 247(1983).

[2] FLUENT, creare.x Incorporated, Etna Rd., P.O. Box 71, Hanover, NH 03755.

[3] J.A. Burton, R.C. Prim, W.P. Slichter, J. Chem. Phys. 21, 1987(1953).

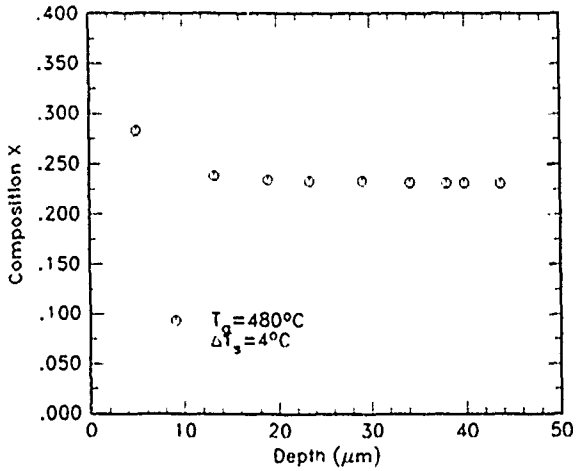

Figure 2. Composition of a (Hg,Cd)Te film grown by isothermal LPE.

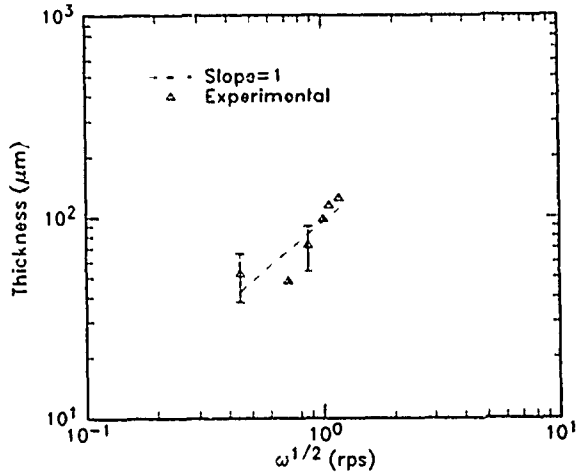

Figure 3. (Hg,Cd)Te film thickness versus subtrate rotation rate.

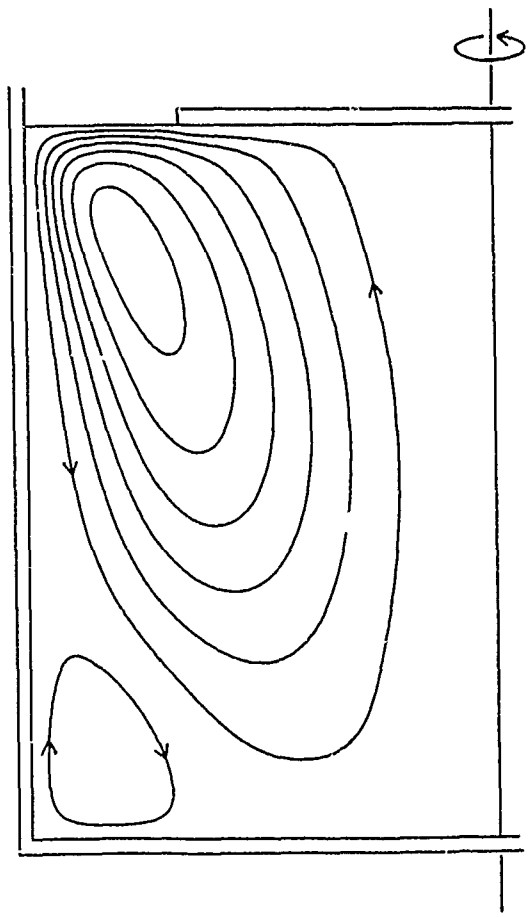

Figure 4. Contours of stream functions in an LPE melt with a radius of 27mm and a depth of 40mm, with a circular substrate of radius 18mm rotating at 20rpm. The small convection cell at the lower left corner is caused by thermal convection.

LOW TEMPERATURE GROWTH OF MWIR LPE HgCdTe ON SAPPHIRE

E.R. Blazejewski, S. Johnston, J.S. Chen, J. Bajaj, G. Williams,
and L. Bubulac

Rockwell Science Center
Thousand Oaks CA 91360

Consistently low dislocation density MWIR (x = .31) LPE HgCdTe epitaxial layers with excellent morphology were grown on CdTe/sapphire substrates (PACE-1) using a new low temperature Te melt process. Epitaxial layers of HgCdTe were grown at 420° C from a Te melt using the horizontal tipping technique. 2" Sapphire substrates with thin MOCVD grown (111) CdTe buffer layers were utilized.

Surface etch pit densities (EPD) between 5×10^5 cm^{-2} and 9×10^5 cm^{-2} were revealed using a previously reported chemical etch[1] on a 20 layer sample set. Cross sectional EPD profiles reveal a more rapid decrease of defects from the CdTe buffer layer interface for the 420° C PACE-1 material as compared to conventionally grown 500° C material. Figure 1 shows an SEM cross sectional photomicrograph of EPD distributions for the two growth temperatures. The high temperature layer shows dislocations distributed throughout the crystal while the low temperature layer shows a significantly reduced count beyond the interface.

Compositional depth profiles of both the same 500° C and the 420° C grown epilayers were obtained using EDAX as shown in Fig. 2. The high temperature grown layer exhibits compositional grading as indicated by the more rounded Hg and Cd curves around 4 μm. The low temperature grown layer exhibits a sharper transition from the CdTe buffer layer to the HgCdTe layer. The reduced compositional grading observed in the 420° C layer is consistent with a reduction of matrix interdiffusion associated with a reduction in temperature.

Comparison indicates the data is in qualitative agreement with that of Yoshikawa.[2] The reduction in growth temperature results in less interdiffusion of HgCdTe at the buffer layer interface. Less compositional interdiffusion requires that the lattice mismatch that occurs must be accommodated over a shorter distance. This accommodation results in increased misfit dislocations which are confined near the interface. Reduced EPD count is observed away from that interface.

The most significant result of this work is that the lattice mismatch system, $Hg_{.69}Cd_{.31}Te$/CdTe/sapphire (PACE-1), can be grown under conditions which produce high quality material with characteristics (x-ray rocking curves, Hall data and EPD) that mimic those obtained using the more lattice matched HgCdTe/CdTe system.

REFERENCES

1. J.C. Chen, United States Patent No. 4897152.

2. M. Yoshikawa, K. Maruyama, T. Saito, T. Maekawa, and H. Takigawa, J. Vac. Sci. Tech. A. Vol. 5, No. 5, Sept/Oct (1987).

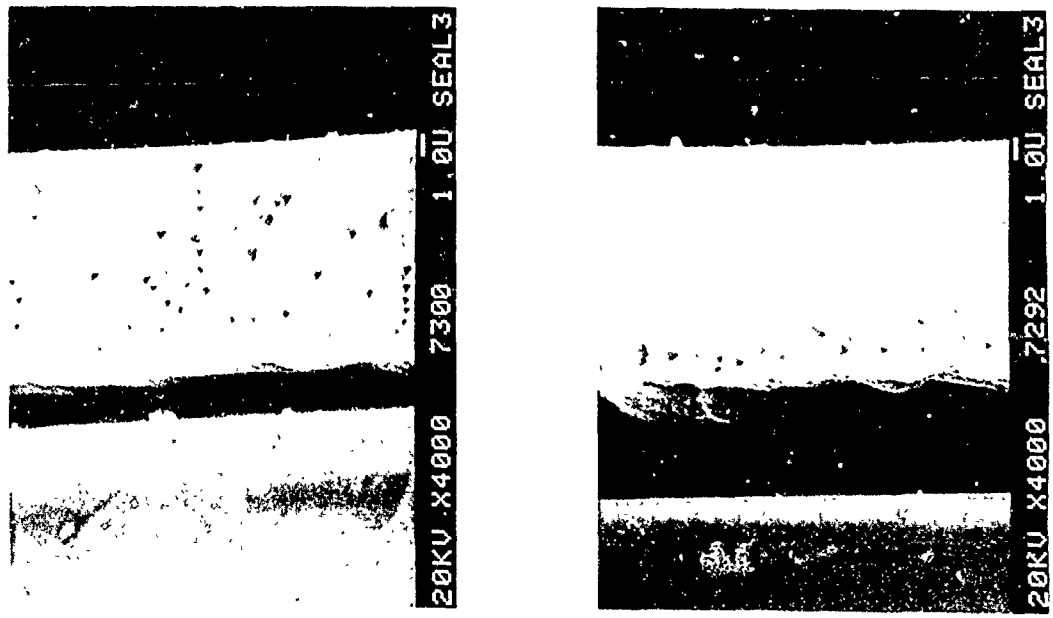

• 500°C LPE GROWTH

• 420°C LPE GROWTH

Fig. 1 SEM micrographs of the cross sections of 500° C and 420° C MWIR PACE-1 layers after exposure to a dislocation etch.

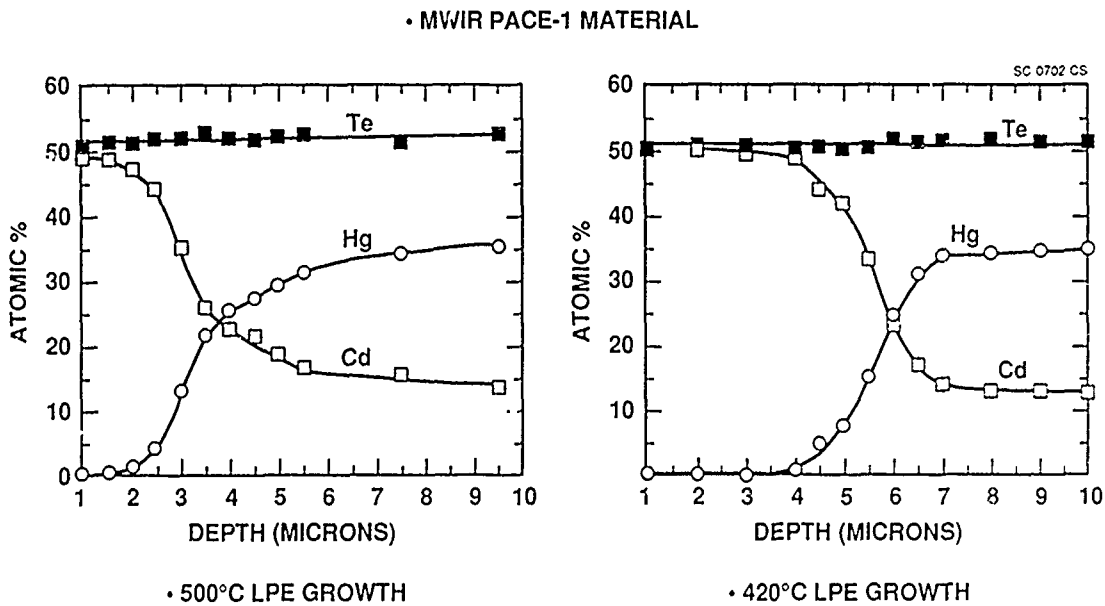

Fig. 2 EDAX compositional profile of MWIR PACE-1 HgCdTe material grown from Te-rich solutions at 500° C and 420° C temperatures.

A REVIEW OF IMPURITY BEHAVIOUR IN BULK AND EPITAXIAL MCT

P.Capper

Philips Components Ltd., Southampton, Hants, U.K.

Extrinsic doping using slow-diffusing elements will become increasingly important in future infra-red device structures based on MCT. This paper reviews the modes of incorporation and activition of dopants in the most widely used bulk and epitaxial growth techniquess. Stoichiometry at the growth temperature is shown to be the critical factor affecting dopant activity. A number of factors, including stoichiometry, can affect the as-grown electrical properties of MCT and the importance of determining the type of conduction in the as-grcwn state, if successful extrinsic doping is to be accomplished, will be stressed.

The minimum requirement to confirm successful doping is established as a correlation between electrical data, on an annealed sample, and chemical data from a well-calibrated analysis technique. Figure 1 gives an example for an x = 0.2, Arsenic-doped layer grown by metal-organic vapour phase epitaxy (MOVPE). At low levels of intentional doping, the absence of any other potentially active dopant impurities at significant levels needs to be established. Most elements are electrically active in accordance with their relative position in the Periodic Table. This is particularly true of material grown under metal-saturated conditions (e.g. Bridgman and Hg-rich liquid phase epitaxy (LPE)). In Te-rich LPE and MOVPE material, acceptor and donor activity, from Groups I and III respectively, is largely unchanged but Group V acceptor

elements require a high temperature 'activation' anneal to adjust site occupancy. Even this type of anneal does not produce acceptor activation in molecular beam epitaxy (MBE) layers; the Group V elements occupy metal sites as donors, and resort has been made to the faster diffusing Group I elements. Changing conditions from Te-rich to metal-rich in MOVPE growth gives acceptor activity using Group V elements with no need for 'activation' anneals which opens up the potential for the growth of controlled doped heterostructures (see figure 2).

In addition to the electrical activity of dopants this review will highlight the importance of other aspects of dopant behaviour. Knowledge of dopant segregation in growth from liquids is also important in achieving controlled doping. Acceptor ionization energies can be used to differentiate doped from undoped material but not, as yet, between dopants. There is some evidence that acceptor doping can improve lifetimes in Hg-rich LPE material (see figure 3), but this is not universally observed in other types of material, e.g. Bridgman and MBE. Data on annealed undoped Te-rich LPE (shown in figure 3) demonstrates that high lifetimes can also be obtained purely by defect control.

References

1. P.Capper, C.D.Maxey, P.A.C.Whiffin and B.C.Easton, J.Crystal Growth, 97, 833 (1989).
2. C.D.Maxey, P.Capper, P.A.C.Whiffin, B.C.Easton, I.Gale, J.B.Clegg, A.Harker and C.L.Jones, J.Crystal Growth, 101, 300 (1990).
3. D.E.Lacklison and P.Capper,Semicond.Sci&Technol.2,33(1987).
4. T.Tung, M.H.Kalisher, A.P.Stevens and P.E.Herning, Mat.Res.Soc.Symp.Proc. 90, 321 (1987).
5. J.S.Chen, J.Bajaj, W.E.Tennant, D.S.Lo, M.Brown and G.Bostrup, Mat.Res.Soc.Symp. 90, 287 (1987).
6. C.L.Jones, C.K.Ard, A.McAllister and S.Barton (Unpublished)

(This work was supported by MOD, Procurement Executive and

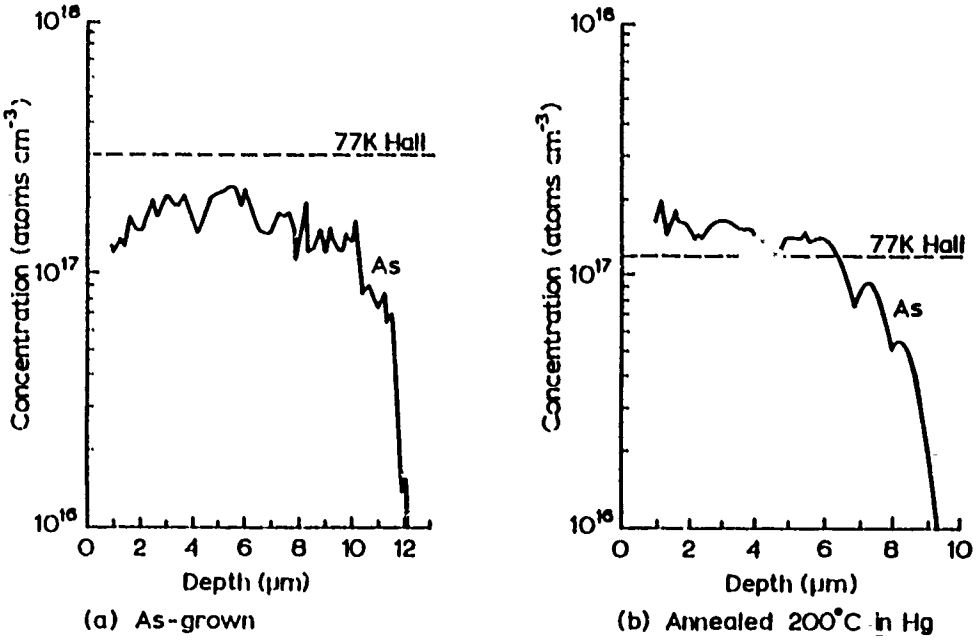

Figure 1) Secondary Ion Mass Spectrometry (SIMS) profiles and carrier concentrations a) before and b) after Hg annealing in an x = 0.2 As-doped MOVPE layer (from ref.1).

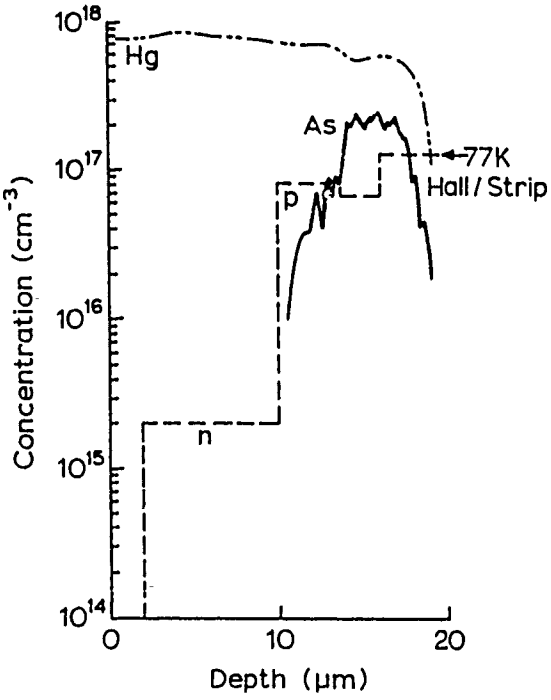

Figure 2) SIMS and Hall/strip profiles of a doped/undoped MOVPE heterostructure, after annealing (from ref.2).

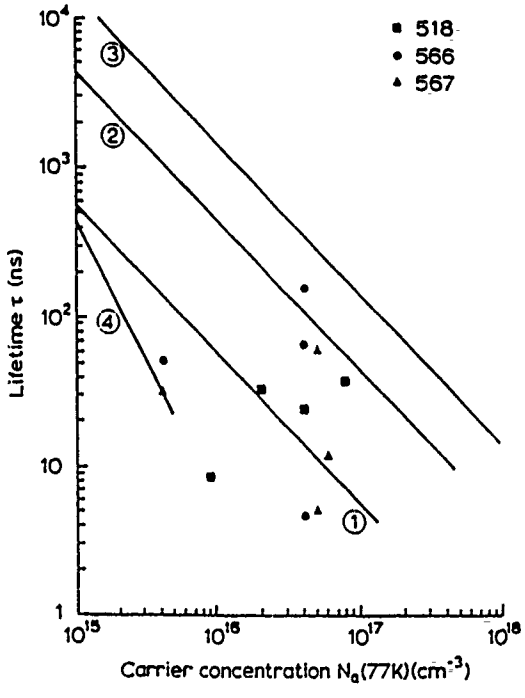

Figure 3) Minority carrier lifetime versus acceptor concentration (N_a) for 1 - bulk samples (from ref.3), 2 & 3 - x = 0.2 & 0.3 As-doped Hg-rich LPE (from ref.4) and 4 - undoped Te-rich LPE (from ref.5). Data points for three undoped Te-rich LPE samples after various post-growth anneal treatments (from ref.6).

IMPURITIES AND MOCVD GROWTH OF MCT*

B C Easton, C D Maxey, P A C Whiffin, J A Roberts, I G Gale and F Grainger

Philips Research Laboratories, Redhill, Surrey RH1 5HA, UK

P Capper

Philips Infra-red Defence Components Ltd, Southampton, Hants S09 7BH, UK

We report the correlation of chemical analysis results with the electrical activity and doping behaviour of impurities in epitaxial MCT, prepared by the Interdiffused Multilayer Process[1] (IMP) using a reactor system described in detail elsewhere[2]. Layers (x=0.21-0.23) were deposited on CdTe substrates (2-4°off (100)) at 410°C, using dimethyl tellurium and dimethyl cadmium. The advantages of the analytical techniques employed are discussed together with analyses of the residual impurities present in the layers.

Previously [3,4,5] we studied arsenic as an acceptor impurity. This work has now been extended to indium and iodine, as possible donor impurities. Unlike As, where the dopant was incorporated in the CdTe, it has been found that [In] is higher in the HgTe. After annealing in mercury vapour at 200°C, Hall measurements confirm donor behaviour of In in MCT both at low and at high concentrations, albeit at reduced activity in the latter case. Fig.1 shows the SIMS depth profile through an unintentionally doped layer, grown to investigate reactor system 'memory' effects from previous experiments. The In profile is consistent with a progressive 'clean-up' occurring during layer growth and reveals evidence of significant In diffusion into the substrate.

Because of the memory effect and the high diffusion rate of indium, iodine has been investigated as an alternative donor impurity. 6vpma of iodine in the reactant gas gave a concentration of $6x10^{15}cm^{-3}$ atoms in the layer. After a mercury anneal the layer was

* This research was supported by the Procurement Executive Ministry of Defence.

n-type with $N_{D-A}=4.6x10^{15}cm^{-3}$ and a mobility of 88,000 $cm^2v^{-1}s^{-1}$. As-grown layers are normally p-type from our growth system, as-grown iodine doped layers have shown both n-type and mixed conduction properties.

Laser scan mass spectrometry (LSMS)[7] has been developed in our laboratory, it is particularly suited to the survey analysis of impurities in MCT layers. Table 1 is an analysis of a layer deposited on CdTe. Aspects to note are the changes in impurity concentrations which occur in passing through the layer and interface region to the CdTe substrate. This sample, after annealing in mercury, was n-type at 77K with a mobility of $1.1x10^5$ $cm^2v^{-1}s^{-1}$ and a free carrier concentration of $4.8x10^{14}cm^{-3}$. Carbon and oxygen are the dominant impurities in the bulk of the layer, however their effect on electrical properties appears not to be significant, no particular impurity can be assigned as the major contributor to the donor background. Aluminium is probably rendered inactive by the presence of oxygen. There is evidence of high impurity levels in the interface region for some elements and the substrate region is seen to have impurities at levels below the detection limits in most cases.

Sodium is a common impurity and a potential acceptor in MCT layers, it is however highly mobile. Figs. 2 and 3 show SIMS sodium profiles for an as-grown layer and after an isothermal anneal treatment in mercury vapour at 200°C. After annealing the level of Na in the bulk of the layer is significantly reduced by out-diffusion.

References

(1) J B Mullin, S J C Irvine and J Tunnicliffe J. J. Cryst. Growth 68, 214, (1988).
(2) P A C Whiffin, B C Easton, P Capper and C D Maxey C.D. J. Crystal Growth 79, 935, (1986).
3) P Capper, P A C Whiffin, B C Easton, C D Maxey and I Kenworthy. Mat. Lett. 6, 356, (1988).
(4) C D Maxey, P Capper, P A C Whiffin, B C Easton, I Gale I. and J B Clegg. Mat. Lett. 8, 385, (1989).
(5) C D Maxey, P Capper, P A C Whiffin, B C Easton, I Gale and J B Clegg, A Harker and Growth 101, 300, (1990).
(6) F Grainger and J A Roberts. Semicond. Sci. Technol. 3, 802, (1988).

TABLE 1

SIMS ANALYSIS OF UNDOPED MCT LAYER

($x10^{15}$ atoms cm^{-3})

ELEMENT	SURFACE	BULK	INTERFACE	SUBSTRATE
C	3000	3000	3000	60
O	3000	30	600	0.6
F	9	0.9	1.5	<0.2
Na	9	0.9	1.5	6*
Al	6	3	0.6	0.3
Si	60	<0.9	1.5	<1.5
P	0.9	<0.2	0.3	<0.2
S	150	0.6	15	0.6
Cl	90	0.3	30	<0.3
K	6	0.9	0.6	6*
As	0.3	<0.2	0.6*	<0.2
Se	60	60	<0.3	<0.6
Br	15	<0.3	<0.3	<0.6

* Denotes heterogeneous distribution.

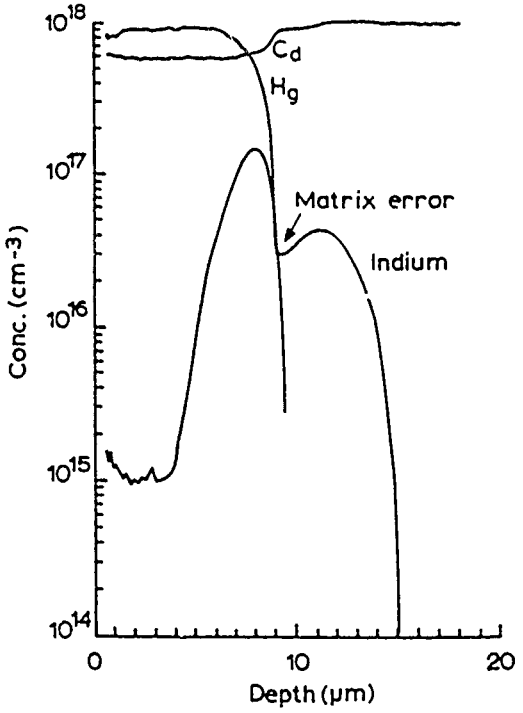

Figure 1. SIMS depth profile for In showing system memory effect and diffusion into the CdTe substrate.

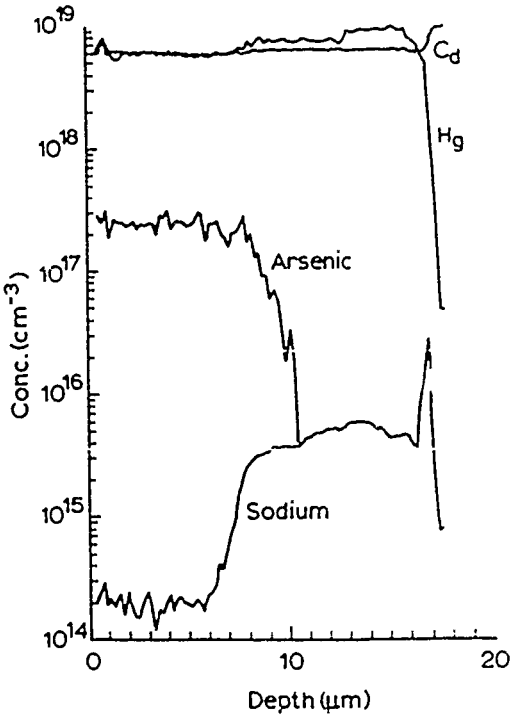

Figure 2. SIMS depth profile for Na through an "as-grown" MCT layer.

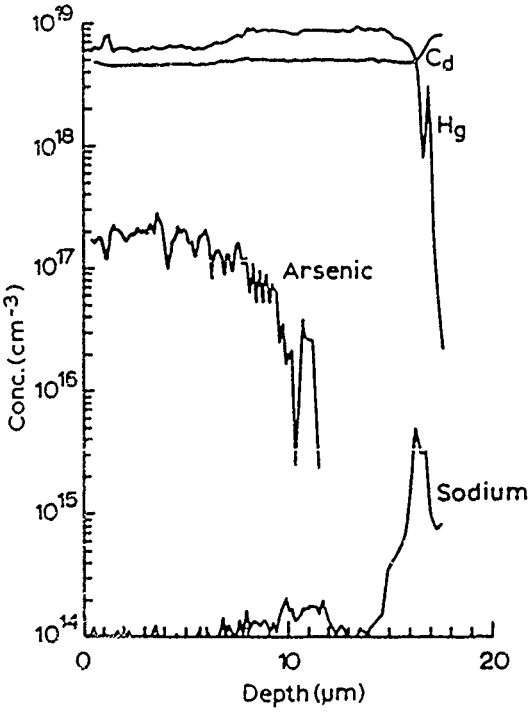

Figure 3 Profile for layer in fig.2 after an anneal in Hg vapour at 200°C to remove metal vacancies

EXTRINSIC DOPING IN MOCVD HgCdTe FOR GROWN JUNCTIONS

J.S. Chen, L.O. Bubulac, D.S. Lo, and R. Zucca
Rockwell International Science Center
Thousand Oaks, CA 91360

Reported here are the results of extrinsic doping in MOCVD HgCdTe which is part of the effort to develop high performance LWIR HgCdTe heterojunctions on GaAs substrates. GaAs orientation used is (100) 10° toward [110]. The HgCdTe epitaxial layers were grown by an interdiffused multilayer process (IMP)(1) at temperatures between 360 to 400 °C.

Ethyl-dimethyl indium (EDMIn) is the dopant for n-type extrinsic doping in MOCVD LWIR HgCdTe. We have developed procedures that allow control of indium levels from the mid 10^{14} to low 10^{18} cm^{-3} levels. Figure 1 shows the linear relationship between the indium level as determined by SIMS and the 77K n-type carrier concentration measured by Hall effect after low temperature anneals to remove Hg vacancies. Variable temperature and magnetic field Hall effect also show classical behavior. Minority carrier lifetime measurements as a function of temperature from 300K to 12.5K indicate Auger processes as the dominant recombination mechanism.(2) For a LWIR layer, x =0.23, with n-type carrier concentration of $2.7x10^{15}cm^{-3}$ and mobility of 92015 $cm^2/Vsec$, we measured a lifetime of 350 nsec at 77K.

Considerable progress in reproducible p-type doping during MOCVD HgCdTe will be reported. The alkyl source, di-ethyl arsine (DEAs), was successfully used to achieve extrinsically doped p-type MWIR and LWIR HgCdTe layers at 300 °C and 380 °C growth temperatures. Table 1 lists the pertinent layer and electrical properties including the As levels determined by SIMS. Initial measurements indicate longer lifetimes for As doped HgCdTe compared with Hg vacancy doped layers. A 800 nsec lifetime was measured for a layer with x = 0.28 and a hole concentration of $4x10^{15}$ cm^{-3} and mobility of 320 $cm^2/Vsec$. As diffusion profiles determined by SIMS are sharp for both 300 and 380 °C growths, making the realization of a grown HgCdTe heterojunction a distinct possibility in the near future.

REFERENCE:

1. J. Tunnicliffe, S.J.C. Irvine, O.D. Dosser, and J.B. Mullin
J. Crystal Growth, 68(1984), p245.

2. R. Zucca, D.D. Edwall, and J.S. Chen, to be published.

Work funded by SDIO/TNS, sponsored by AFSTC/SWS, managed by WRDC/MLPO, contract No. F33615-89-C-5557, Robert Hickmott, Technical Monitor.

Figure 1

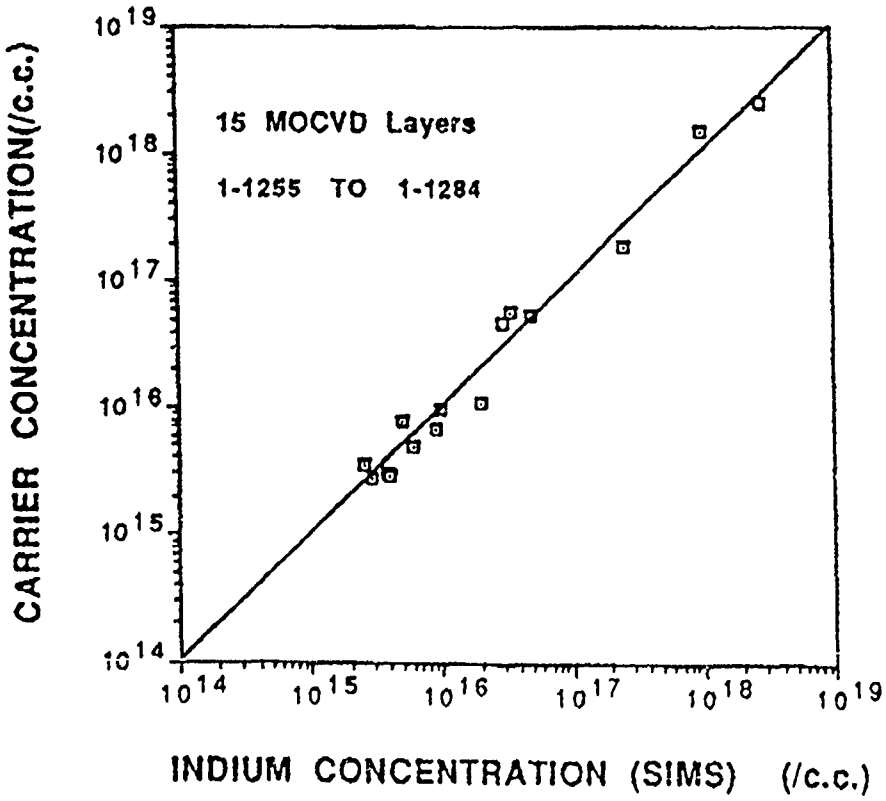

Characteristics of Arsenic Doped MOCVD MCT

Sample No.	Dopant Source	Growth Temp.	X Value	77K Hall Na cm^{-3}	Mobility cm^2/V-sec	77K Lifetime, ns	SIMS As level cm^{-3}
I-1285	DEAs	370	0.30	6.1×10^{16}	353	N/A	1×10^{17}
I-1287	DEAs	370	0.32	1.4×10^{16}	501	N/A	2×10^{16}
I-1302	DEAs	370	0.26	2.7×10^{16}	351	N/A	4×10^{16}
I-1316	DEAs	370	0.28	4.0×10^{15}	320	800	N/A
I-1322	DEAs	370	0.25	1.6×10^{16}	346	80	N/A

Growth and Properties of In Doped MOVPE (IMP) HgCdTe

J S Gough, M R Houlton, S J C Irvine, N S Shaw, M L Young and M G Astles
RSRE, St Andrews Road, Malvern, Worcerstershire, UK

The materials technologies for future generation of $Hg_{1-x}Cd_xTe$ infrared detectors need to be able to produce large areas of uniform composition MCT with good structural and electrical properties. Recently several groups[1,2,3] have demonstrated this can be achieved with metal organic vapour phase epitaxy (MOVPE) grown by the interdiffusion multilayer process (IMP) at 350°C with di-isopropyltelluride (DIPT), the required device thickness and compositional uniformity being obtained together with reproducible p-type background hole concentration due to native Hg vacancies. However for further development of this technology impurity doping is required for contacts and growth of p-n junction structures, and in this context we have investigated the behaviour of In doping with trimethyl indium (TMIn). The work has resulted in n-type layers with reproducible carrier concentration between 1-3 x $10^{17}cm^{-3}$ and the growth of n-type (In) - p-type (Hg vacancy) layer structures which appear suitable for IR detection.

Epilayers were grown on (100)CdTe substrates at 350°C the by IMP process with DIPT, after growth of a thin CdTe buffer layer. The MCT layers were capped with CdTe to prevent Hg in-diffusion after growth and give controllable electrical properties. Layer thickness and x values were varied between 5-20μmand 0.22 - 0.30 respectively by adjusting the growth conditions. In doping, which is found to be well controlled for the first time was carried out on the CdTe part of the IMP cycle with TMIn, (from a bubbler source). By varying the vapour flows and the bubbler temperature, In concentrations between 3x 10^{16} - 1 x $10^{18}cm^{-3}$ were obtained. The In concentrations were determined by SIMS and the electrical properties by 77K variable magnetic field Hall as a function of layer thickness. From an analysis of the Hall data, 77K differential carrier concentration profiles were obtained which could be directly compared with the SIMS profiles. Layers were assessed before and after a low temperature isothermal anneal to remove the native Hg vacancies. Results show that at In concentrations $> 10^{17}cm^{-3}$, only 50% of In is apparently electrically active in as grown layers, and this which increases to 100% upon annealing. The detailed electrical results suggest In doping introduces compensation, possibly through an increase in Hg vacancy concentration. A problem with an In memory effect was encountered which limited the growth of junction structures to n on p-type. However, the SIMS profiles of these junctions were well defined. Detailed electrical and In profile results on these structures will be presented.

References

(1) J Thompson, P Hackett, L M Smith, D J Cole-Hamilton and D V Shenai-Khatkhate
J.Crystal Growth 86, 233 (1988)

(2) S J C Irvine, J B Mullin, J Giess, J S Gough and A Royle
J.Crystal Growth 93, 732 (1988)

(3) D D Edwall, J J Bajaj and E R Gertner
J.Vac.Sci. Technol. A8(2), 1045 (1990)

CONTROL OF CARRIER TYPE AND CONCENTRATION IN MOCVD GROWN HgCdTe

D.D. Edwall and L.O. Bubulac
Rockwell International Science Center
Thousand Oaks, CA 91360

The rationale for developing MOCVD grown HgCdTe (MCT) is based on MOCVD's dual capability in high throughput and sophisticated material/device engineering. Early results of MOCVD MCT have confirmed the throughput capabilities by demonstrating large area uniformity[1] and material quality compatible with device fabrication.[2] Considerations for higher performance, process simplification and producibility are leading to device structures based on in-situ grown junction or diffused junction from in-situ deposited diffusion sources which requires the incorporation and activation of extrinsic dopants during the MOCVD growth cycle. Reported here are the initial results of an effort of in-situ control of the electrical properties of MOCVD MCT.

We have used arsenic and indium for p- and n-type doping, respectively, using the alkyl sources tertiary-butyl-arsine (TBAs) and ethyl-dimethyl-indium (EDMIn). HgCdTe layers were grown by the interdiffused method on (100) GaAs and GaAs/Si substrates in a commercial (CSI) reactor. For p-type doping, TBAs was introduced on the CdTe growth cycles under metal-rich conditions to promote As acceptor behavior, in agreement with previously published data.[3-4] A 77K carrier concentration of $2 \times 10^{17} cm^{-3}$ was measured for a layer with Cd concentration x=0.31 (all carrier concentrations quoted are obtained after low temperature Hg annealing to remove Hg vacancies); the corresponding hole mobility was 200 $cm^2/v\text{-}s$. These values were unchanged for three different conditions of the layer: as-grown, after 20h Hg vapor annealing at 250C, and after 400C (2h)/250C (20h) Hg vapor annealing, demonstrating thermal stability of the As acceptors. An As concentration of 2×10^{17} cm^{-3} was also measured for this layer by SIMS. Work is currently in progress to establish the relationship between dopant partial pressure, incorporation and activation and will be reported at the conference.

Doping with EDMIn, levels of low-10^{14} (near background) up to 10^{18} cm^{-3} have been measured by SIMS. With EDMIn doping, two phenomena occur as

yet not observed with TBAs doping: memory and threshold effects. In the memory effect, use of high EDMIn fluxes produces In doping in subsequent growths. For example, following a doped growth with a 77K electron concentration of low-10^{17} cm^{-3}, the next growth without intentional doping resulted in an n-type layer with a low-10^{15} cm^{-3} concentration. Subsequent growth of one or two more undoped layers results in a p-type background with In levels near background detection levels in SIMS analysis (low 10^{14} cm^{-3}). For the desired doping levels in the low 10^{15} cm^{-3} range, the memory effect is insignificant although we are currently investigating its source (or sources) for enhanced process control.

The threshold effect with EDMIn doping presents greater difficulty. Over a certain range of alkyl partial pressures no doping effect (as indicated by electric properties) is observed. Beyond a specific concentration, the electron concentration increases rapidly with increasing alkyl flux. The threshold effect is illustrated in Fig. 1(a) where 77K electron concentration is plotted against alkyl flux on a linear scale. Figure 1(b) shows that an excellent fit to the data is obtained using an equation of the form:

$$\text{carrier concentration} \propto \text{Exp}\left(\frac{-K}{F-Fo}\right),$$

where K is a constant >0, F is the EDMIn flux, and Fo is the threshold flux. An identical threshold effect was evident for both carrier concentration and In concentration measured by SIMS. Experiments are in progress to determine the nature of the threshold effect (potential sources: physical adsorption of EDMIn on tube walls between alkyl source and reactor, prereaction with other alkyls, upstream pyrolysis). The physical layout of the reactor apparently also plays a role. No threshold effects are observed in a second prototype MOCVD growth system with a different gas manifold arrangement.

We have also observed that the EDMIn is incorporated more efficiently downstream than upstream. Both the electrical and SIMS analysis results confirm this, as shown in Table I. The distance between upstream and downstream is approximately 5 cm. As the layer is sampled from upstream to downstream, the SIMS In level increases as well as the relative quality of the 77K electron mobility, taking into consideration the variation in composition x.

Work funded by SDIO/TNS, sponsored by AFSTC/SWS, managed by WRDC/MLPO, contract No. F33615-89-C-5557, Robert Hickmott, Technical Monitor.

1. D.D. Edwall, J. Bajaj, and E.R. Gertner, J. Vac. Sci. Technol., A8, 1045 (1990).

2. L.O. Bubulac, D.D. Edwall, D. McConnell, R.E. DeWames, E.R. Blazejewski, and E.R. Gertner, to be published in Semicon. Sci. Technol.

3. C.D. Maxey, P. Capper, P.A.C. Whiffin, B.C. Easton, I. Gale, and J.B. Clegg, Mat. Lett. 8, 190 (1989).

4. J.M. Arias, S.H. Shin, D.E. Cooper, M. Zandian, J.G. Pasko, E.R. Gertner, R.E. DeWames, and J. Singh, J.Vac. Sci. Technol., A8, 1025 (1990).

Table 1

Hall Results at 77K and In Levels as a Function of Position Using EDMIn Doping

Position	x	n,cm^{-3}	μ,cm^2/V-s	approx. μ expected for good n-type material with this x,cm^2/V-s	μ quality factor $\mu_{meas.}/\mu_{expected}$	In level, cm^{-3}
upstream	0.266	7×10^{14}	5,958	40,000	0.15	$(1\text{-}2) \times 10^{15}$
center	0.218	2.2×10^{15}	42,119	100,000	0.42	4×10^{15}
downstream	0.17	8.5×10^{15}	350,112	350,000	1.0	5×10^{15}

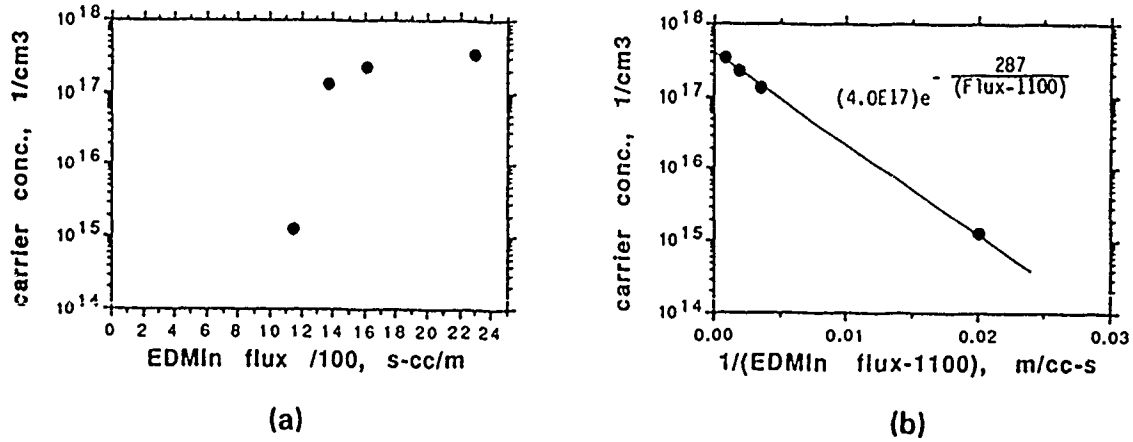

Fig. 1 Relationship between EDMIn flux into reactor and MCT carrier concentration at 77K, showing threshold effect.

DYNAMICS OF ARSENIC DIFFUSION IN OMVPE HgCdTe ON Si SUBSTRATES

L.O. Bubulac, C.R. Viswanathan, L.D. Edwall

Rockwell International Science Center
1049 Camino Dos Rios
Thousand Oaks CA 91360

Abstract:

Diffusion mechanisms of arsenic in layers grown by organometallic vapor phase epitaxy (OMVPE) on Si substrate following implant and post-implant thermal treatments have been studied from chemical analysis (secondary ion mass spectroscopy - SIMS) and from theoretical modeling. The results obtained for two temperatures, 400°C and 450°C, demonstrated that a classical gaussian depth redistribution of arsenic in both thermal treatments from the implanted sources has been obtained. Diffusion coefficients of $D_{(400°C)} = (2.5 - 2.8) \times 10^{-14}$ cm^2/sec and $D_{(450°C)} \sim 2 \times 10^{-13}$ cm^2/sec have been measured. These values are in the range of diffusion coefficients obtained in LPE - HgCdTe on CdTe substrates ($D_{(400°C)} = 1.25 \times 10^{-14}$ cm^2/sec and $D_{(450°C} = (0.9 - 1.7) \times 10^{-13}$ cm^2/sec). A series of experiments have been performed, varying the time in the post-implant thermal treatment performed at 450°C. By using both experimental results from SIMS analysis and theoretical modeling, we have shown that the diffusion length of arsenic varies linearly with the square root of time, thus confirming the classical depth distribution of arsenic from the implanted source. The dependence of the diffusion mechanism on the defect structure of the material will be discussed. The results obtained in this study are essential in controlling the junction electrical profile of p-on-n devices.

EXTRINSIC p-DOPED HgCdTe GROWN BY ALLOY GROWTH ORGANOMETALLIC EPITAXY†

N.R. Taskar, I.B. Bhat, K.K. Parat and S.K. Ghandhi

Rensselaer Polytechnic Institute
Troy, New York 12180

We report on the properties of p-HgCdTe grown by OMVPE, using the Alloy Growth Process. Arsenic was used as the dopant, with arsine gas as the dopant source. The growth procedure has been outlined previously [1, 2]. Layers described here were 7 μm thick and had a Cd fraction of 0.27-0.31. A 1 μm cap layer of undoped CdTe was grown on the HgCdTe as a passivant layer.

Figure 1 shows the acceptor concentration measured as a function of arsine flow, for arsenic doped layers grown lattice matched on CdZnTe substrates.The measured doping concentration is seen to increase from 8×10^{15} cm^{-3} to 9×10^{16} cm^{-3} as the arsine flow was increased from 10 to 250 sccm. Increasing the arsine flow beyond 250 sccm did not increase the doping concentration. Also shown is the doping characteristic when GaAs substrates were used, with a 2 μm thick CdTe buffer layer. Consistently, a factor of 2 to 4 higher doping level was achieved when lattice matched CdZnTe was used as the substrate. We believe HgCdTe grown on GaAs has more defects than material grown on lattice matched substrates, and that As segregation in its defect sites is the main reason for this difference.

Arsenic in HgCdTe was found to be very stable, after low temperature isothermal annealing in a Hg-rich ambient. Measurements of the Hall coefficient were made as a function of temperature for pairs of samples, grown side by side, during the same run. One was an as grown layer, while the other was annealed under Hg overpressure at 270°C for 16 hours, followed by 220°C for 10 hours. In each case, both samples showed almost identical behavior, which suggests that arsenic is stable under this heat treatment process.

Secondary Ion Mass Spectrometric (SIMS) measurements were made in order to

†This research was supported by the Defense Advanced Research Projects Agency (Contract No. N-00014-85-K-0151) and by a grant from the Raytheon Corp.

establish the presence of As in the layer. Figure 2 shows a typical SIMS profile of a HgCdTe layer grown with 50 sccm of arsine flow. The measured carrier concentration is 4.5×10^{16} cm^{-3}, and shows clearly the presence of incorporated arsenic.

Arsenic doped layers were analyzed after a two-step anneal (270°C for 16 hours, followed by 220°C for 10 hours) under Hg-rich conditions, so that the net acceptor concentration due to As could be determined. Experiments on samples grown at varying Hg pressures have shown that the total acceptor concentration increased roughly in proportion to P_{Hg}. For the samples grown with 125 sccm arsine flow, a factor of 3.75 increase in P_{Hg} resulted in an increase in N_A by a factor of 3.94. Roughly comparable results hold for samples grown with 25 sccm arsine, given the uncertainty in the measurement of low doped samples. This suggests [3] that there is negligible compensation in the As doped samples.

Figure 3 shows the low temperature (40K) for layers as a function of the arsine flow. The mobility values shown here are comparable to values obtained in bulk p-type layers with similar doping concentration and composition dependence. The high mobility of layers grown in the saturated region of the doping characteristic of Fig. 1 can be explained by Fig. 4, which shows the measured SIMS count as a function of the net acceptor concentration in the layers. The linear correspondence between the SIMS count and the net acceptor concentration indicates that saturation of the doping characteristic is related to a saturation of dopant surface coverage as the arsine flow is increased, and not to increasing incorporation of arsenic into inactive or compensating sites.

References

1. S.K. Ghandhi, I.B. Bhat and H. Fardi, Appl. Phys. Lett., 52, 392 (1988).
2. N.R. Taskar, I.B. Bhat, K.K. Parat, D. Terry, H. Ehsani and S.K. Ghandhi, J. Vac. Sci. Technol., A7, 281 (1989).
3. H.R. Vydyanath, J. Electrochem. Soc., 128, 2610 (1981).

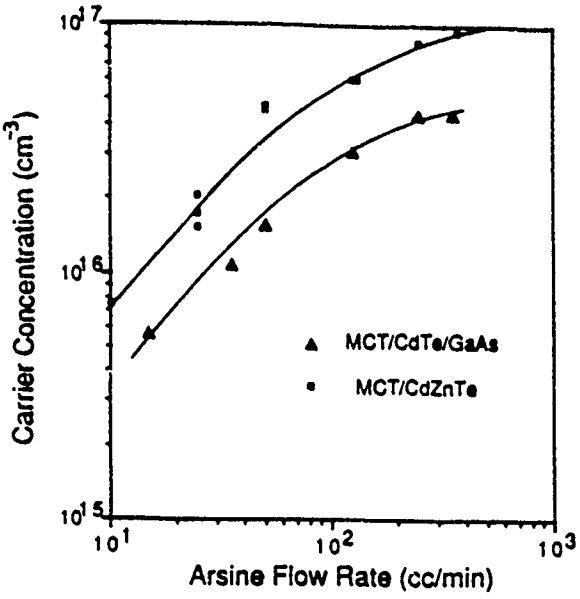

Figure 1 Net acceptor concentration as a function of arsine flow (■) CdZnTe substrates (▲) GaAs substrates.

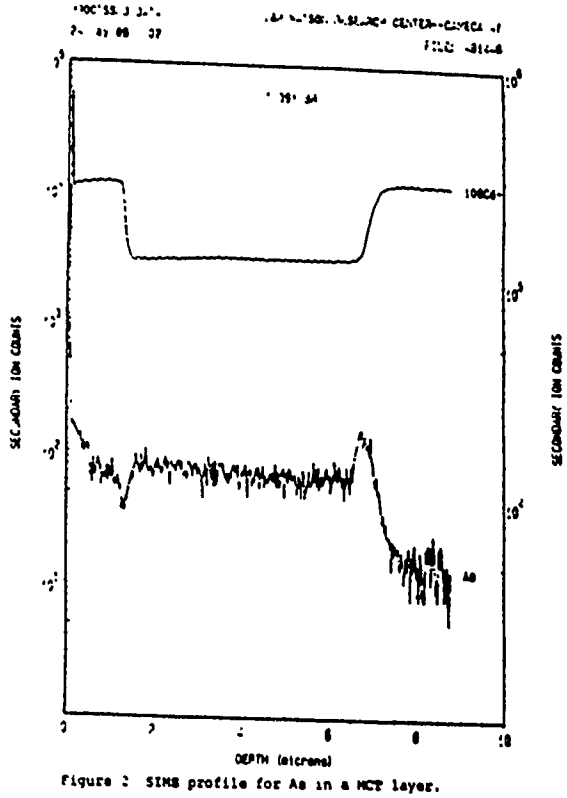

Figure 2 SIMS profile for As in a MCT layer.

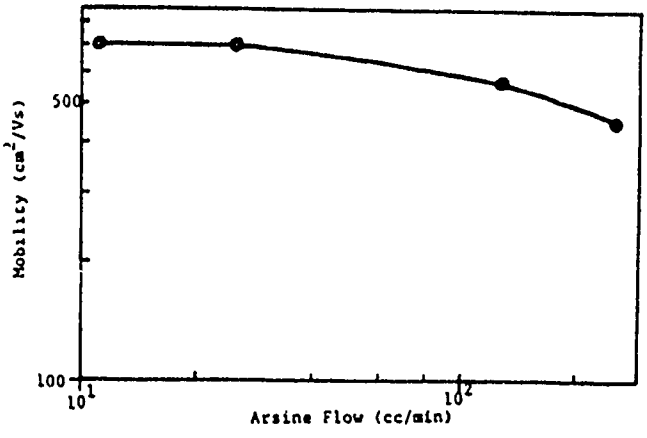

Figure 3 Low temperature (40K) mobility of HgCdTe layers as a function of arsine flow.

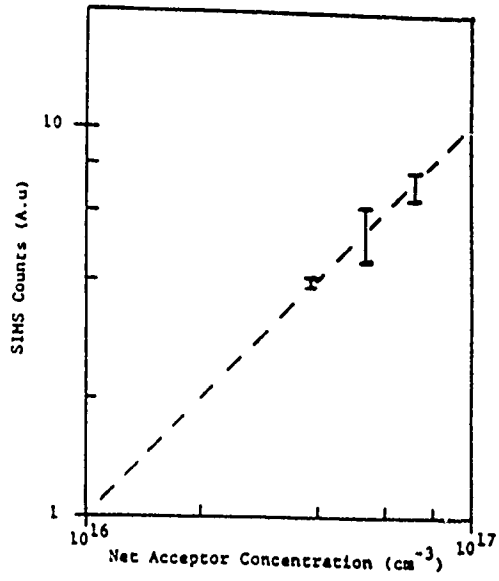

Figure 4 Arsenic SIMS count vs. net acceptor concentration.

HgCdTe Heterostructures Grown By MBE

Owen K. Wu*, Doug M. Jamba & G. Sanjiv Kamath
Hughes Research Laboratory
3011 Malibu Canyon Road, Malibu, California 90265

W. Radford, K. Gorton, D. Walsh, J. Myrosznyk and P. Bratt
Santa Barbara Research Center, 75 Coromar Drive, Goleta, CA 93117

ABSTRACT

In this paper, We will report on the MBE growth and characterization of HgCdTe Heterostructures. MBE growth of n- and p-type doped HgCdTe alloys has been achieved in the range of 10^{15} to $10^{18}/cm^3$. The ability to control both n-type and p-type doping using indium and arsenic has led to the growth of a variety of heterostructures including hybrid MBE/LPE, MBE/bulk and all MBE grown junctions. Surface morphology and crystallinity have been characterized by scanning electron microscopy, electron channeling pattern and x-ray techniques. Doping concentrations and interface charcteristics at the heterojunction are analyzed by secondary ion mass spectroscopy and Auger electron spectroscopy. Good i-v characteristics, photocurrent and spectral responses at MWIR and LWIR were observed. Fig.1 shows the SIMS profile of an MBE/LPE grown n-p-n triple layer heterojunction structure. Dual color detection was demonstrated on this n-p-n structure by alternating bias voltage. Fig.2 shows the 300K IR transmission spectrum of an all MBE grown double layer heterojunction structure for MWIR applications. We will discuss the MBE growth, heterojunction characteristics and diode fabrication results of a variety of HgCdTe heterostructures and their applications in 3-5μm and 8-12μm regions.

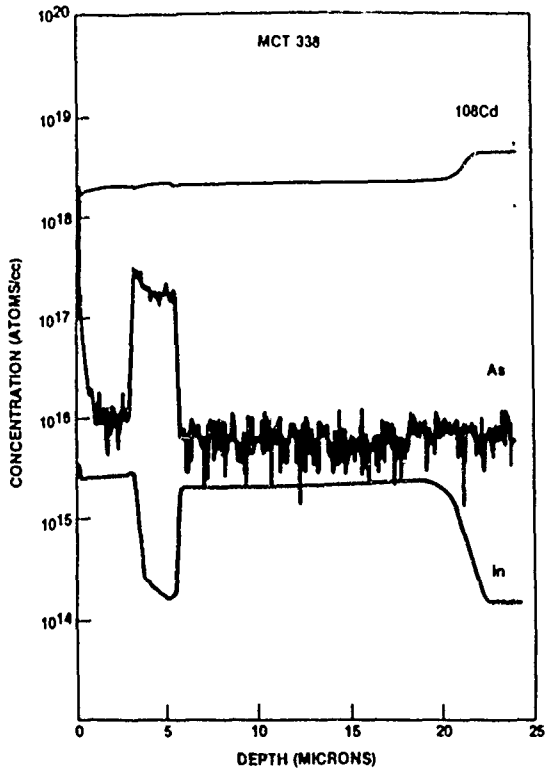

Fig.1 SIMS profile of an MBE/LPE grown n-p-n triple layer heterojunction structure

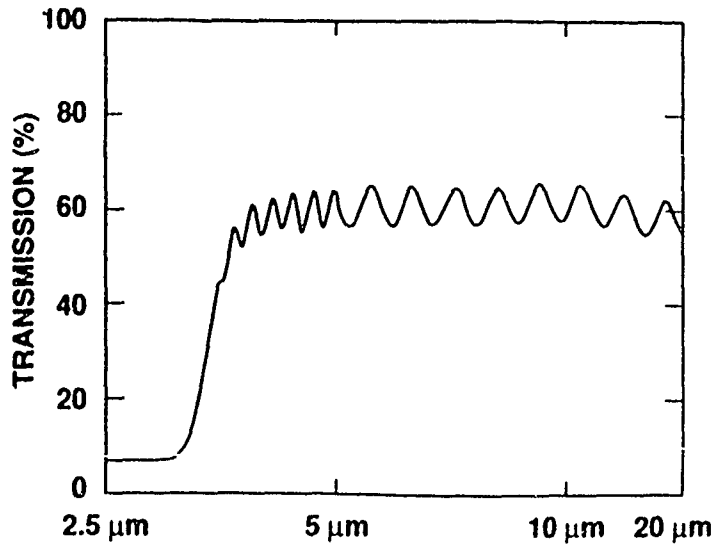

Fig.2 300K IR transmission spectrum of an MBE grown double layer heterojunction structure

DETERMINATION OF ACCEPTOR DENSITIES IN P-TYPE $Hg_{1-x}Cd_xTe$ BY THERMOELECTRIC MEASUREMENTS*

J. Baars, D. Brink, and J. Ziegler†

Fraunhofer-Institut für Angewandte Festkörperphysik
Eckerstr. 4, D-7800 Freiburg, Fed. Rep. Germany
†AEG, D-7100 Heilbronn, Fed. Rep. Germany

There is an urgent need for reliable techniques to characterize p-type $Hg_{1-x}Cd_xTe$ (MCT) of CdTe mole fractions $0.2<x<0.25$. The determination of acceptor densities and compensation in p-MCT by Hall-effect requires a considerable effort in measurement and evaluation. Moreover, the interpretation of the measured data often is complicated due to surface inversion layers obscuring the bulk properties. In particular, this applies to epitaxial layers.

In this study we measured the differential thermoelectric voltage (DTV) of p-type bulk samples and epitaxial layers of MCT ($0.2<x<0.25$) in the temperature range from 20 to 300 K using two different experimental techniques, the thermoelectric probing, well known as "hot point" method, and the "lateral gradient" method (Fig. 1). The samples were also examined by Hall-effect and conductivity measurements. In addition we calculated the Seebeck-coefficient of p-MCT for acceptor densities $10^{14}<N_A<10^{17}cm^{-3}$ employing empirical relations for the energy gap, the intrinsic carrier density[1], the carrier mobilities, and the LO phonon frequencies[2]. By fitting the calculated temperature dependence of the thermoelectric voltage to the experimental one, the "lateral gradient" method proved to be an adequate tool for determining the effective acceptor density in p-type MCT including surface inversion.

Fig. 2 presents the DTV vs. temperature calculated for $0.2<x<0.24$ and obtained from thermoelectric measurements of a MCT epitaxial layer in the "lateral gradient" configuration. The calculation is based on the effective

*This research was supported by the Bundesminister der Verteidigung, Federal Republic of Germany.

acceptor density and the activation energy of the specimen determined by Hall-effect measurements. The best fit is obtained for x = 0.225 which is close to the mole fraction x = 0.226 found by transmission measurements. Prior to the thermoelectric and Hall-effect measurements the specimen was subjected to a special electro-chemical etch treatment to avoid surface inversion.

The "hot point" method was found to be insensitive to surface inversion. It may be used for determining the temperature of zero thermoelectric power, which directly yields an estimate of the acceptor density (Fig. 3).

References

1. G. L. Hansen and J. L. Schmit, J. Appl. Phys. 54, 1639 (1983).
2. J. Baars and F. Sorger, Solid State Commun. 10, 875 (1972).

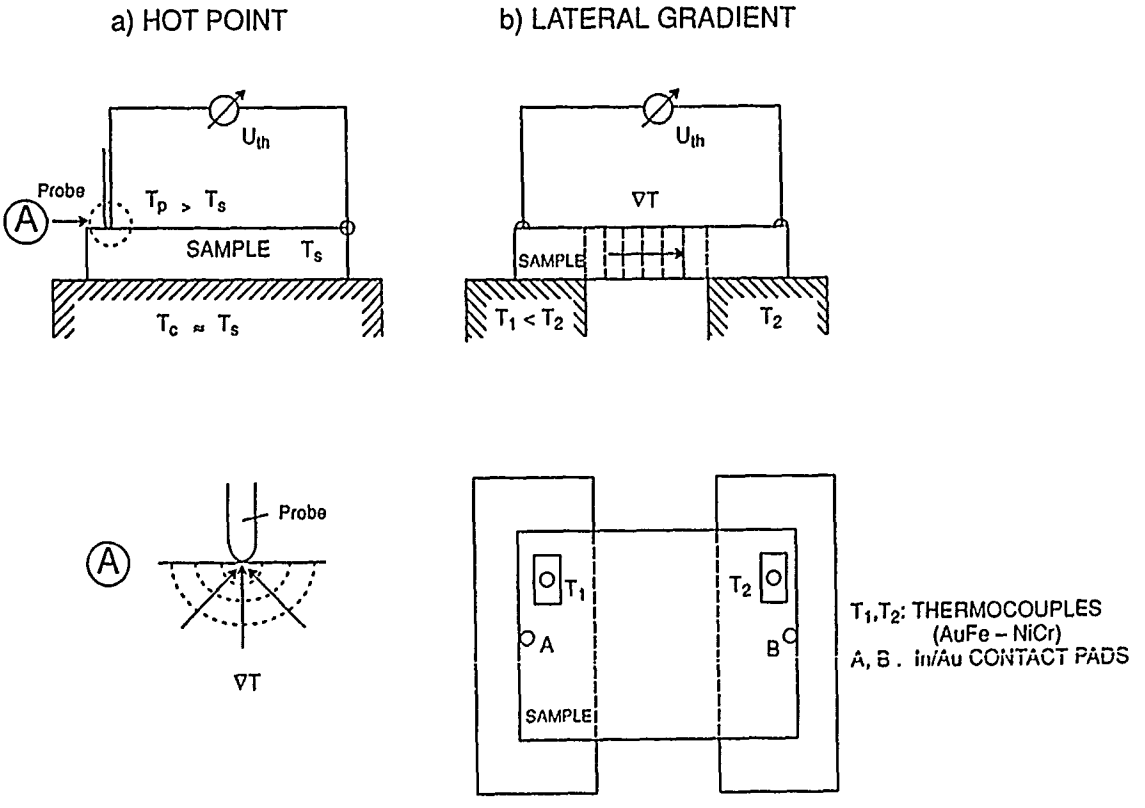

Figure 1. Schematic arrangement for measuring the thermoelectric power of MCT by a) the "hot point" technique and b) the "lateral gradient" technique. In contrast to the "lateral gradient" technique, the temperature gradient produced by the "hot probe" is almost perpendicular to the surface of the specimen (A).

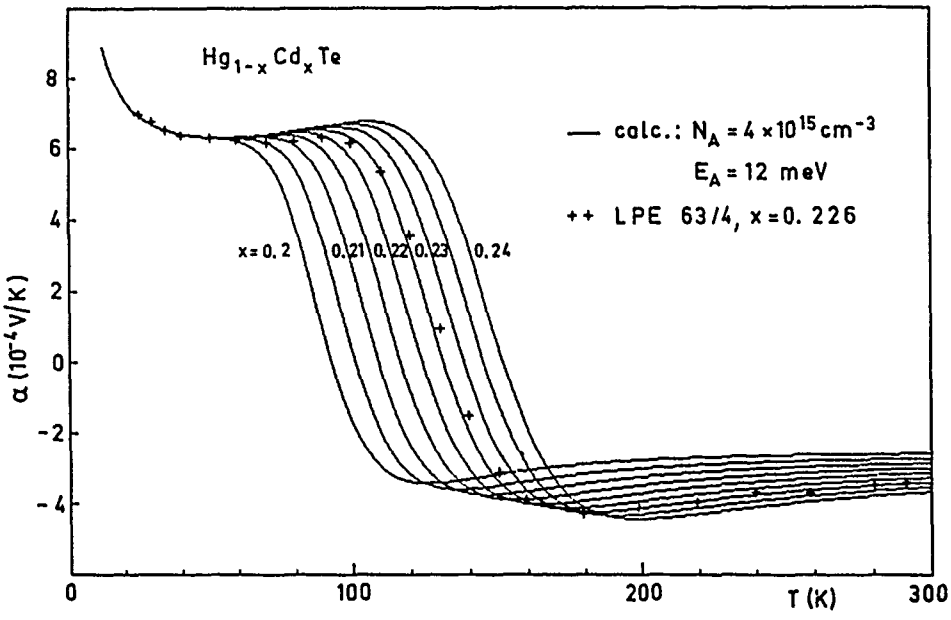

Figure 2. Seebeck-coefficient vs. temperature calculated for MCT 0.2<x<0.24 and determined from measurements of the thermoelectric power of a MCT epitaxial layer using the "lateral gradient" technique (+).

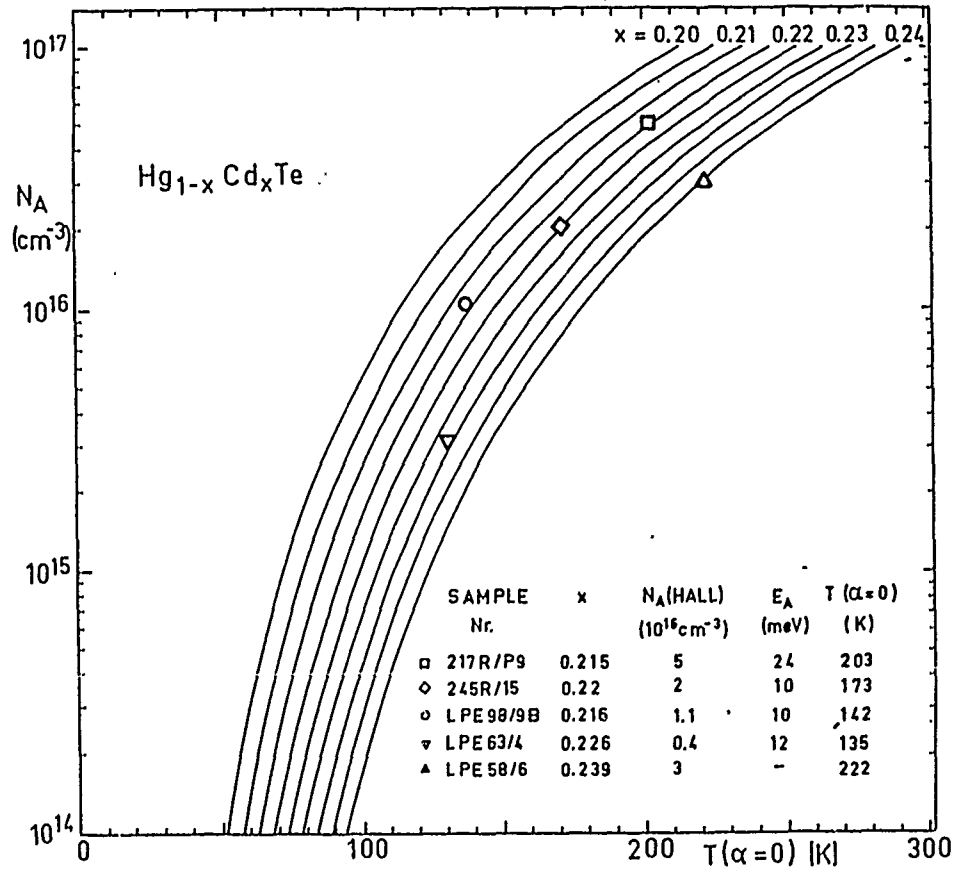

Figure 3. Effective acceptor density vs. temperature of sign reversal of the thermoelectric voltage calculated for MCT 0.2<x<0.24, and obtained from thermoelectric measurements using both the "hot point" and the "lateral gradient" techniques.

MECHANISMS OF INCORPORATION OF ACCEPTOR DOPANTS IN MCT ALLOYS

H. R. VYDYANATH
AEROJET ELECTROSYSTEMS
1100 W. HOLLYVALE STREET
AZUSA, CALIFORNIA 91702

ABSTRACT

The behavior of dopants which act as acceptors on metal lattice sites will be compared with that of dopants which act as acceptors on tellurium lattice sites and in interstitial lattice sites. The way in which the mode of incorporation of the dopants varies with the conditions of preparation of the crystals will be reviewed in detail. Experimental incorporation data in material grown from different growth techniques will be compared with thermodynamic defect model predictions.

The amphoteric behavior of Group V dopants will be discussed in detail along with implications on device fabrication aspects.

Growth and characterization of P-on-n Heterojunction material for 8 μm to 18 μm applications.

G. N. Pultz, P. W. Norton, E. E. Krueger
Loral Infrared and Imaging Systems, Inc.
2 Forbes Road (MS #146)
Lexington, MA 02173
(617) 863-3091

A variety of applications for infrared detection (particularly space-borne) require information at wavelengths greater than 15 μm. This paper will discuss the growth and characterization of P-on-n heterojunction material with photodiode performance at the theoretical Auger lifetime diffusion limit for cutoffs as long as 18.8 μm at 80K.[1] The growth process capitalizes upon the ability of horizontal slider, Te-rich growth to provide thick (≈12 μm), spatially uniform, n-type (In doped) absorbing layers, complemented by thin (≈1 μm) p-type (As doped) junction layers produced by infinite melt, vertical Hg-rich growth. The combined growth process yields very high material composition and thickness reproducibility from growth to growth, with excellent compositional (x = ± .001) and thickness (± 10%) uniformity within 10.5 cm^2 films. The paper will present a discussion of the practical aspects of achieving such control and uniformity including system design, materials analysis, and growth parameters. This material was processed into test structures which were analyzed to determine the characteristics of the grown p-n junction. The measured RoA data follow a 1-dimensional Auger lifetime diffusion limited model (Figure 1), placing these detectors/material at performance levels far abc · anything previously reported in the literature at the extended wavelengths. Finally, measured material properties such as carrier concentration, Hall mobility, majority and minority carrier lifetime, thickness, and etch pit density of the material will be discussed with respect to the measured test structure characteristics.

---

[1] We believe this is the first report of such performance at this extended wavelength.

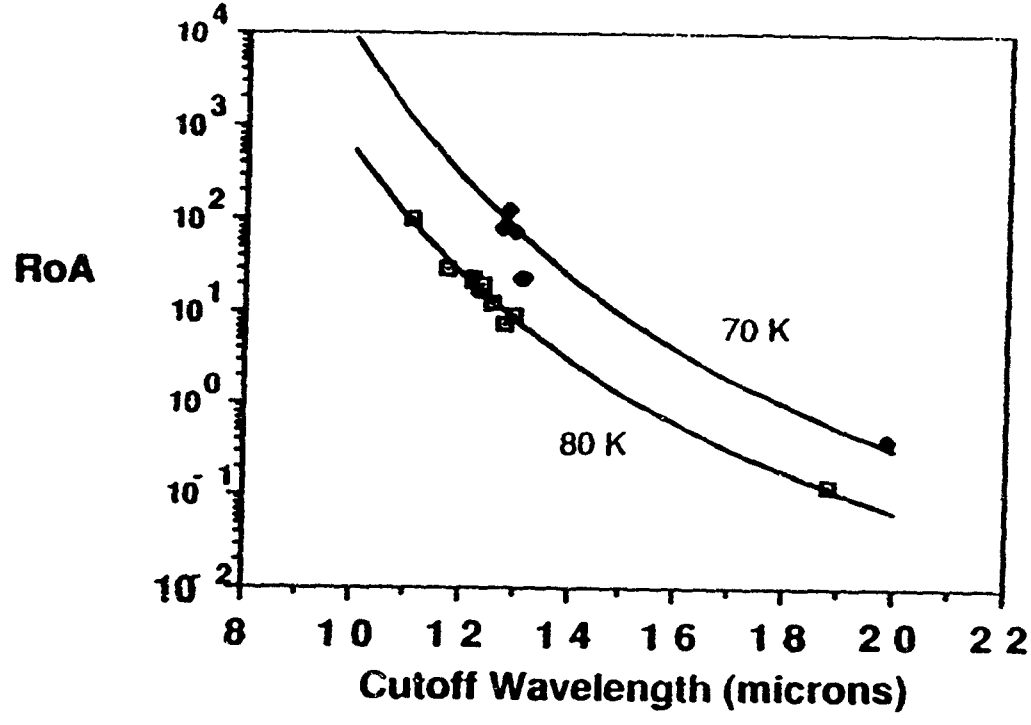

Figure 1. 70 & 80 K RoA vs cutoff wavelength. Solid line represents a one dimensional model of RoA of large area diodes and Auger lifetimes. Input parameters of model were diode thickness, base layer doping level and cutoff wavelength.

IMPROVED BREAKDOWN VOLTAGE IN MBE HgCdTe HETEROSTRUCTURES

R.J.KOESTNER, M.W.GOODWIN and H.F.SCHAAKE
Texas Instruments, Inc., Central Research Laboratories, Dallas, Tx 75265

HgCdTe heterostructures consisting of a thin n-type widegap (250 meV or 5 μm cutoff) layer deposited on an n-type narrowgap (100-125 meV or 10-13 μm cutoff) layer offer the promise of very high performance metal-insulator-semiconductor (MIS) photocapacitors for long wavelength infrared (LWIR) detection. To date, HgCdTe(001) heterostructures grown by molecular beam epitaxy (MBE) have not achieved the predicted MIS performance due to premature breakdown in the widegap layer. In this paper, we examine the improved breakdown voltages measured in widegap HgCdTe(112)Te relative to HgCdTe(001) layers.

Figure 1(a) shows the MIS breakdown voltages measured for MBE grown HgCdTe (001) layers with a cutoff wavelength varying from 4 to 11 μm. A breakdown voltage of $\sim$0.2 V is found which does not improve with increasing bandgap. In contrast, Figure 1(b) shows the net donor density and breakdown voltage for a set of MIS test structures fabricated on MBE grown HgCdTe(112)Te. In this case, breakdown voltages of 0.8 V are observed in medium wavelength infrared (MWIR) films.

The premature breakdown in MBE HgCdTe(001) epilayers may be due (1) to the presence of highly defective pyramidal hillocks under the MIS gate, (2) to any compositional or dopant non-uniformity on a 1000 Å scale, or (3) to the possible presence of Te antisites within the HgCdTe(001) film. As shown in Figure 2, we have recently reduced the pyramidal hilock density in MBE grown HgCdTe(001) layers to 2×10^3 cm^{-2}. At this density, only 1 of every 3 MIS gates with a 5 x 5 mil^2 geometry would have a pyramidal hillock underneath it. Nonetheless, the measured breakdown voltage in MWIR MBE HgCdTe(001) did not improve.

At this point, we believe the autodoping behavior that is unique to MBE grown HgCdTe(001) films is responsible for the measured premature breakdown. Any compositional or dopant non-uniformity due to facetting of the growth surface is expected to be equally likely for HgCdTe(001) and (112)Te growth. However a distinct difference is found in the point defect densities for these two growth orientations.

MBE HgCdTe(001) layers are n-type as-grown and do not show any metal vacancy concentration. In contrast, MBE HgCdTe(112)Te layers are usually p-type as grown with a metal vacancy concentration near 1×10^{16} cm^{-3}. After a Hg saturated post-growth anneal at 200 °C, the HgCdTe(112)Te film converts n-type with a residual donor density range given in Figure 2(b). It appears that the probable formation of Te antisites on the metal sublattice in HgCdTe(001) films causes the premature breakdown observed in MWIR MBE HgCdTe(001) layers.

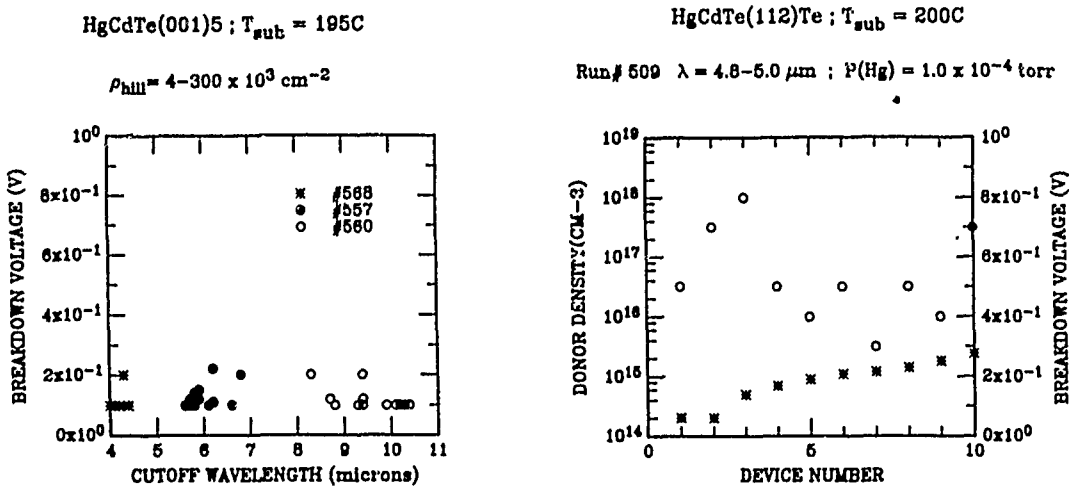

Figure 1: A comparison of MIS breakdown voltages is illustrated for MBE grown (a) HgCdTe(001) and (b) HgCdTe(112)Te films.

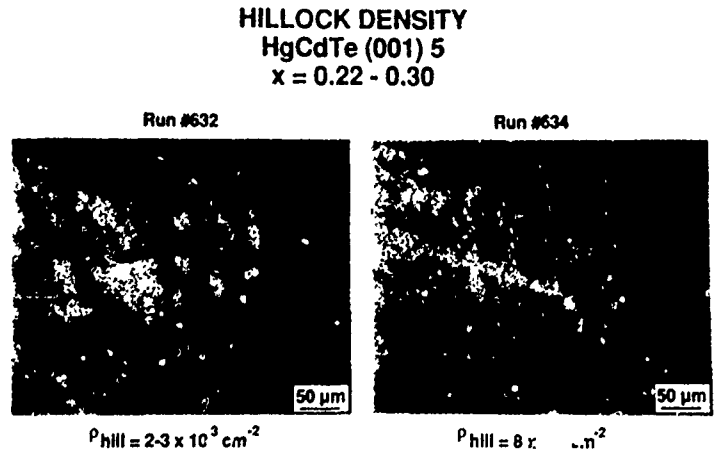

Figure 2: The reduction in pyramidal hillock density for HgCdTe(001) layers grown by MBE is shown. The two films illustrated were grown with different Hg effusion cells.

AN INTEGRATED MULTISPECTRAL IR DETECTOR STRUCTURE

T. N. Casselman, D. T. Walsh, J. M. Myrosznyk, K. Kosai, W. A. Radford, E. F. Schulte
Santa Barbara Research Center, Goleta CA
and
O. K. Wu, Hughes Research Laboratories, Malibu CA

Multispectral infrared sensors are an important component of the SBRC/Hughes LANDSAT earth resources system. They also have considerable potential for atmospheric physics instruments such as used in NASA's Earth Observation System. We report here on the development of a unique material structure that affords multispectral IR detection within each detector pixel. This integrated multicolor (IMC) device structure can reduce cost and complexity as well as enhance reliability and performance of the IR sensor.

In this paper, we describe a two color IMC detector where a specific spectral band is selected by the choice of bias voltage. As shown schematically in Figure 1, the detector is a three layer structure with two *p-n* junctions, one for each pectral band (color). The top and bottom layers are the IR absorbers with the middle layer transparent. For a given bias polarity one of the junctions will be reverse biased, producing a signal for the color associated with that junction.The junction associated with the second color is forward biased, producing no signal. Reversing the bias polarity activates the other junction yielding at the contact, the signal for the other color. Note that the architecture only requires a single contact within the unit cell.

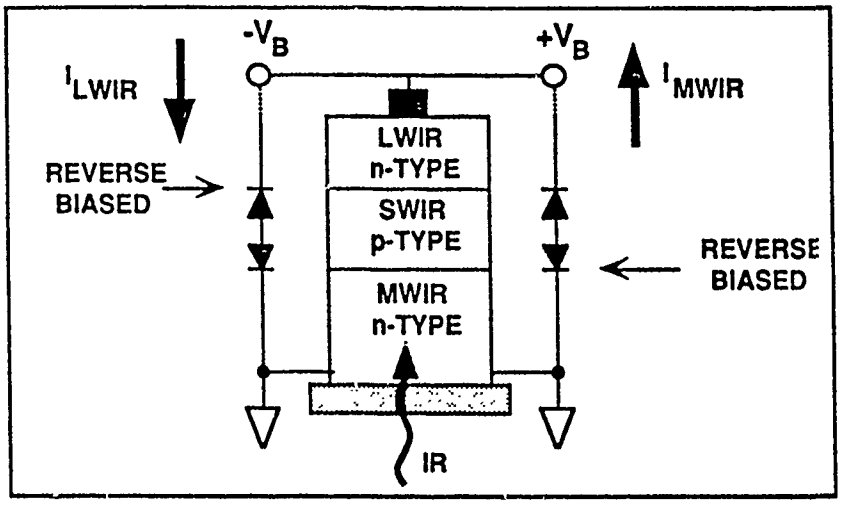

Figure 1. Schematic of Bias-Selectable Two Color IM Detector Structure

We have fabricated this bias-selectable two color detector structure by first growing a *LPE* HgCdTe MWIR *p-on-n* double layer heterojunction on top of which is grown, by *molecular beam epitaxy* (MBE), a *n*-type LWIR layer. The structure forms a *n-p-n* triple layer graded heterojunction (TLHJ) with the middle layer being more heavily doped than the top or bottom layers. The measured relative spectral response per photon at 77K for both colors is shown in Figure 2 for a typical backside illuminated IM TLHJ detector with cutoff wavelengths of 5.1 μm and 8.2 μm. The layer thicknesses are: top (LWIR) ~ 3 μm and bottom (MWIR) ~ 13 μm. It can be seen that, depending on the choice of bias polarity, the IM device detects two separate and distinct spectral bands.

In the paper, we will describe the geometry and the material properties of the structure as well as some of the growth issues. In addition, we will show I-V and spectral data from several devices and relate the results to the properties of the material structure.

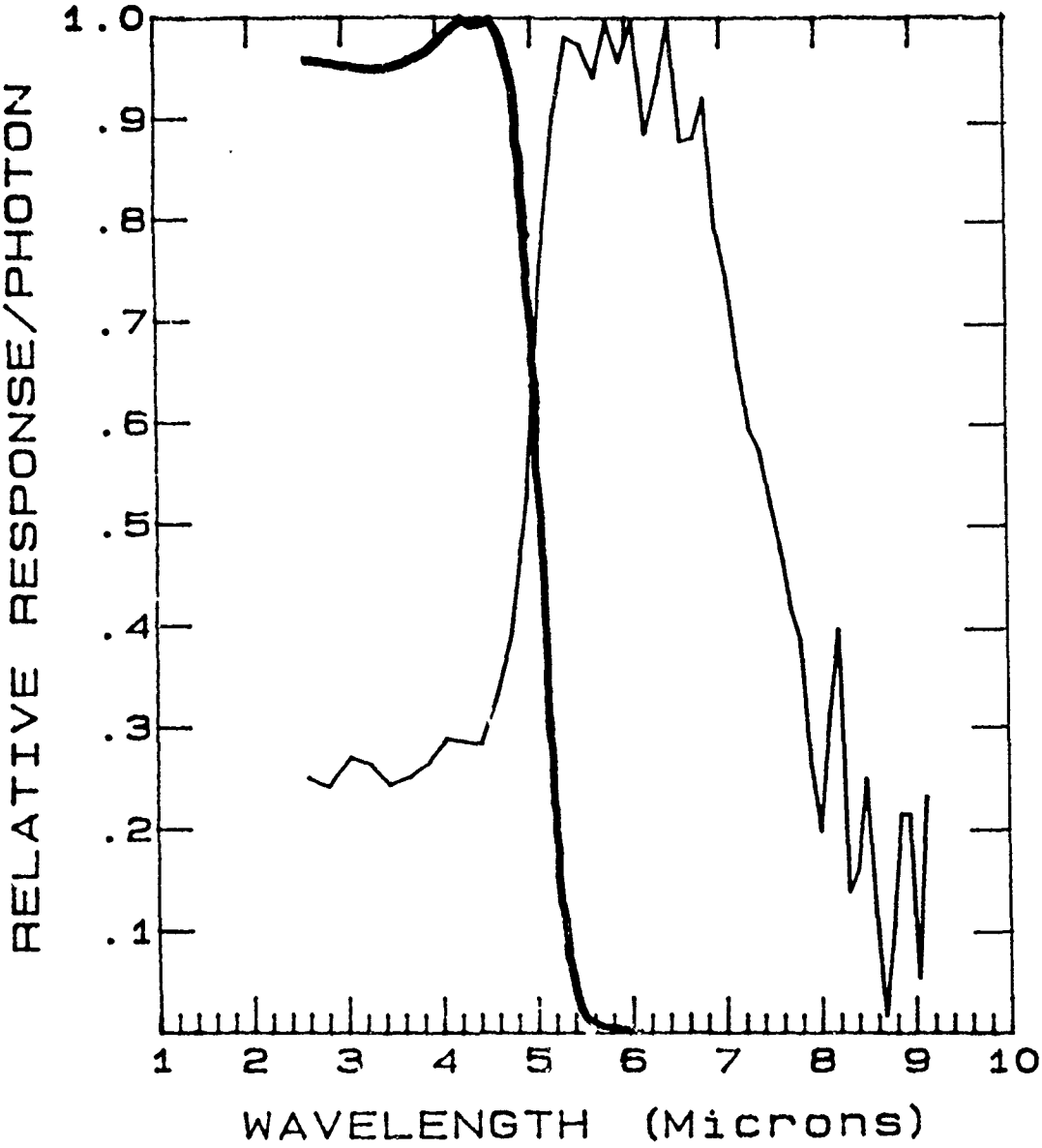

Figure 2. Relative spectral response /photon of the two color ™M detector. The heavy and light lines are the MWIR response and the LWIR response, respectively.

MERCURY CADMIUM TELLURIDE EPITAXIALLY GROWN JUNCTIONS

C.C. Wang and M. Chu
Fermionics Corporation
Simi Valley, CA 93063

Y.Lu and D.S. Pan
Electrical Engineering Department
University of California
Los Angeles, CA 90024

This paper reports the advancement of HgCdTe epitaxial technology. Specifically, we will discuss the grown p-n junctions using liquid phase epitaxy (LPE). The feasibility of multilayer growth for the purpose of achieving advanced device structures will also be highlighted.

In our LPE approach, ZnCdTe lattice-matched to HgCdTe is used as the substrate. Two types of LPE technology are studied, namely, the interrupted growth and the sequential growth. In the first development, an HgCdTe active layer was first grown with a desired composition. After growth is terminated, the furnace is cooled down to room temperature. The HgCdTe layer is then characterized before reinserting into the furnace for the second layer growth. Both p-on-n and n-on-p type of heterostructures are obtained by controlling dopants in each layer properly. For the p-on-n type, the first layer is either un-doped or doped with In and the second layer is doped with column V species. For the n-on-p type, the first layer is undoped and the second layer is doped with either In or I together with Cu. In either case, the location of the p-n junction can be well controlled. Fig. 1 shows the SIMS profile of I in an HgCdTe layer. In the second development, the multilayers are grown sequentially in Te solutions in a slider. The doping of each layer is less controllable but the potential of achieving advanced device structures exists. Fig. 2 shows the cross section of a triple layer.

The basic modelling of HgCdTe heterojunctions have been established before.[1,2,3] In this work, we use the same approach with typical electrical properties and composition profiles found in our p-on-n heterojunctions. Fig. 3 is an approximation of the actual Auger profiles of a typical heterojunction. The doping level of the p-type and n-type regions are $1x10^{16}cm^{-3}$

and $1x10^{15}cm^{-3}$, respectively. To construct a band-edge diagram from such a structure, one solves the Poisson's equation[1]

$$(1/q)d(\varepsilon(d\Psi/dz))/dz = N_A - N_D + n - p \qquad (1)$$

with

$$\varepsilon = (20 - 9.4x)\varepsilon_o.$$

where x is the composition of Cd in HgCdTe. Using the "common anion rule", the conduction and valence band-edges are given by[1,2]

$$E_c(z) = -q\Psi(z) - \chi(z) \qquad (2)$$

$$E_v(z) = -q\psi(z) - \chi(z) - E_g(z) \qquad (3)$$

where $\chi(z)$ is the electron affinity. The results show that when the electrical junction is located at 0.7 micron from the surface, the depletion edges are at 0.64 and 1.07 micron, respectively, with a built-in potential of 78 mV. Under this condition, there is no barrier effect and the interband tunneling is reduced. The schematic of a band diagram corresponding to this special case is shown in Fig. 4.

Diode R_oA and other parameters have also been calculated. Based on the calculation, it is evident that in the diffusion-limited region, p^+-n are superior to n^+-p heterojunction diodes.

REFERENCES

1. M.A. Herman and M. Pessa, J. Appl. Phys. 57, 2671 (1985)

2. P.R. Bratt and T.N. Casselman. J. Vac. Sci Technol. A3, 238 d(1983)

3. K. Kosai and W.A. Radford, J. Vac. Sci. Technol. A8, 1254 (1990)

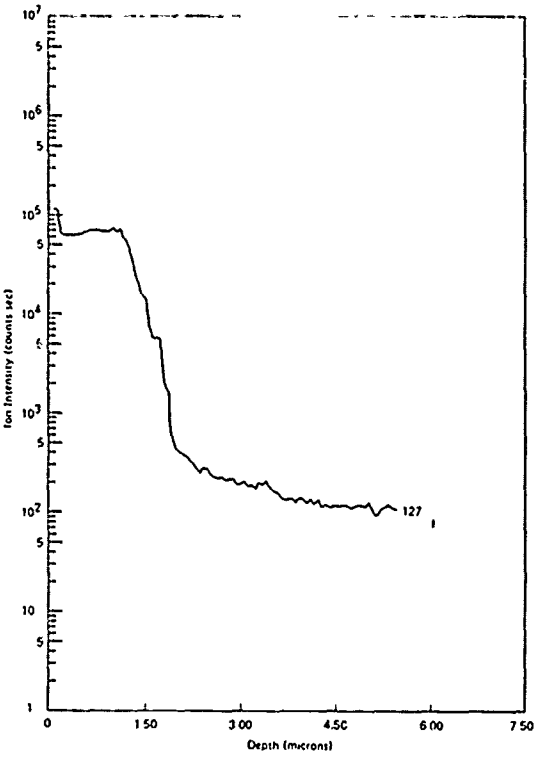

Fig. 1 SIMS profile of I in HgCdTe

Fig. 2 HgCdTe triple-layer structure

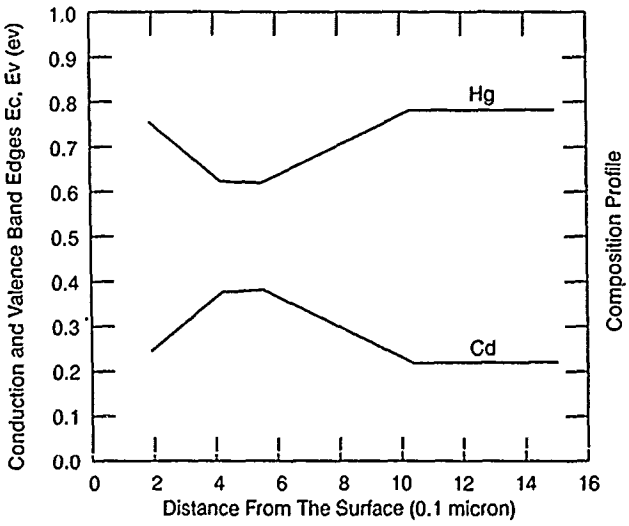

Fig. 3 Piece-wise linear approximation of Cd composition

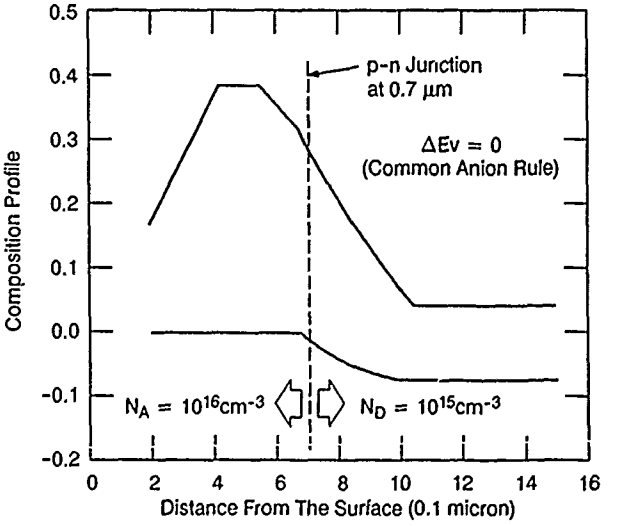

Fig. 4 Calculated energy band diagram

HgZnTe for VLWIR NASA Applications

Elizabeth A. Patten and Murray H. Kalisher
Santa Barbara Research Center, 75 Coromar Drive, Goleta, CA. 93117

HgZnTe has been of considerable interest in the last few years as an alternative IR detector material to HgCdTe because of HgZnTe's greater mechanical hardness, higher Hg vacancy formation energies, and other desirable properties which may lead to greater producibility (yield) and reliability (operation life). We are developing VLWIR (17 μm at ≥ 65K) detectors for longterm Eos (Earth Observing System) NASA missions (hence the need for detector stability and reliability). Last year we reported on the growth of high quality LPE HgZnTe on lattice-mismatched substrates ($Cd_{0.96}Zn_{0.04}Te$). In recent months we have been able to achieve outstanding quality HgZnTe on lattice matched substrates ($Cd_{0.80}Zn_{0.20}Te$) by careful substrate quality screening and reduction of growth system oxygen. X-ray rocking curve widths (full width at half maximum) as low as 28 arc-sec (1 x 8 mm spot) have been achieved. In addition, we have, for the first time, fabricated and demonstrated high performance VLWIR (λ_{co} > 18 μm at 80K) photoconductors made from LPE HgZnTe.

We have fabricated common module configuration arrays of HgZnTe photoconductors with cutoffs ranging from 10 - 18+ μm at 80K and have measured blackbody D*, responsivity, noise and spectral response at 30K and 80K. Shown in the figure is an 80K spectral of a HgZnTe photoconductor with a cutoff of 19 μm and peak response at about 17 μm. Peak D* of 6×10^{10} cm√Hz/W were achieved for the best detectors at 30K with a background of 9×10^{16} ph/cm²/sec placing peak D* within a factor of two of BLIP. These results represent a very significant achievement in that such high performance was achieved with this first lot of HgZnTe photoconductors and that this lot was fabricated using our HgCdTe process sequence showing that HgCdTe processing is largely compatible with HgZnTe. A second lot with more optimized materials parameters will be processed by this meeting date and test results from that lot will be reported. Ultimately, bake stability measurements on the highest performing HgZnTe arrays will be performed and compared with analogous data on HgCdTe devices to assess the potential of greater reliability of HgZnTe-based detectors.

This work was supported by NASA/Langley on NASA Contract NAS1-18232 with William E. Miller as the NASA technical monitor.

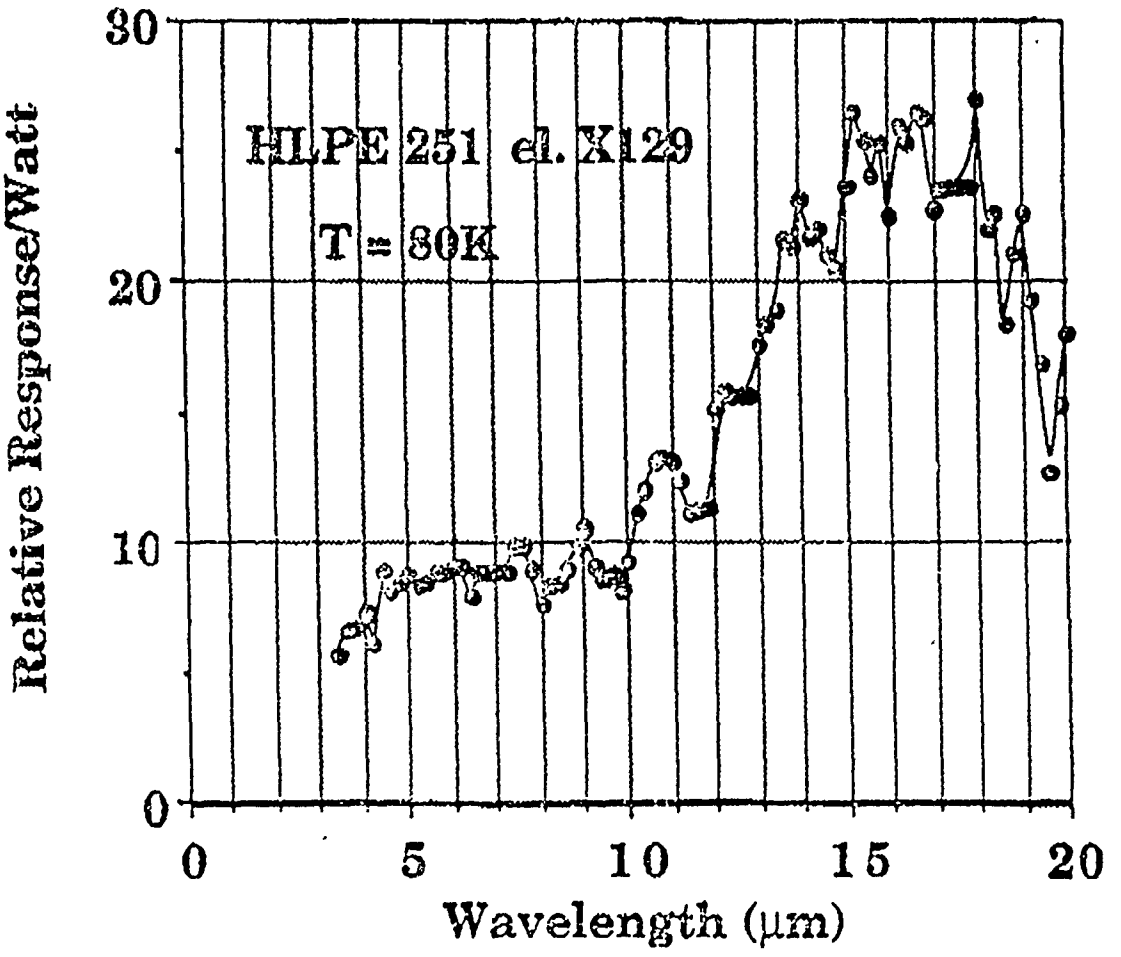

Figure 1. 80K spectral of a HgZnTe photoconductor (2x2 mil) reveals a cutoff of 19 μm and a peak response at about 17 μm.

High Quantum Efficiency HgTe-CdTe Superlattice Device Structures Grown by Photo-assisted Molecular Beam Epitaxy

T.H. Myers, R.W. Yanka, L.M. Mohnkern, K.A. Harris, D.W. Dietz, S.C.H. Wang, G.K. Dudoff, and K.M. Girouard

Electronics Laboratory, General Electric Company
Syracuse, New York 13221

In 1979, the use of HgTe-CdTe superlattices (SL) in IR detector structures was theoretically shown to be the material of choice for long wavelength infrared detectors (LWIR).[1] The calculations showed that SLs in IR detector structures will allow better control over cutoff wavelength, minimize diffusion currents, and greatly lower band-to-band tunneling currents over that of the alloy. Since that initial report, a few HgTe-CdTe SL-based detectors have been fabricated. In this paper we report the first high quantum efficiency IR detectors based on HgTe-CdTe SLs. This experimental breakthrough is significant because it represents experimental verification that SL detectors can in fact be fabricated for practical use.

The wafer used to fabricate the detectors was grown in one of GE's Photo-assisted Molecular Beam Epitaxy (PAMBE) machines that has been previously described.[2] The layer consisted of a p (As) on n (In) SL homojunction 4 μm in total thickness grown on a CdTe substrate. Detectors were fabricated using GE's mesa diode process. Figure 1 shows a representative spectral response curve. The MWIR detectors exhibited quantum efficiencies (QE) as large as 66% (140 K) at the peak wavelength and an average over waveband of 55%. Note that this high quantum efficiency was achieved using a very thin detector. Measured QE was lower at 78 K, with a peak QE of 45-50% and λ_c of 4.9 μm. Spot scans show a very uniform response across the devices at 78 K as illustrated in Figure 2. A representative I-V curve, shown in Figure 3, reveals that the resistances and breakdown voltages are reasonable for this wavelength device and are comparable to that which has been achieved from the corresponding alloy.

The superlattice architecture of the devices was confirmed in three ways. First, differential etching was observed as rings at the mesa base. This occurs due to the different etch rates of the SL constituents during the mesa delineation step. Second, the detector cutoff varied 0.27 meV/K from 40 K to 140 K which is characteristic of SL behavior. Last, the x-value significantly shifted to larger x after a standard interdiffusion (see Figure 4); this verifies that the structure tested was indeed a SL. Additional measurements and further discussion will be presented at the meeting.

[1]J.N. Schulman and T.C. McGill, Appl. Phys. Lett. 34(10), 663 (1979).
[2]T.H. Myers, R.W. Yanka, K.A. Harris, A.R. Reisinger, et.al., J. Vac. Sci. Technol. A 7(2), 300 (1989).

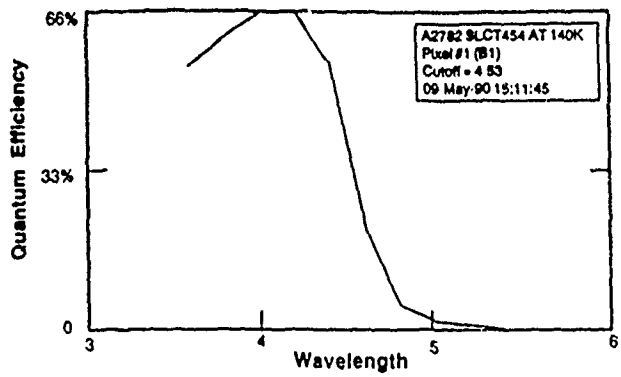

Figure 1 Representative spectral response of a SL detector with λ_c = 4.48 um @ 140 K illustrating a sharp profile The peak response corresponds to 66% quantum efficiency.

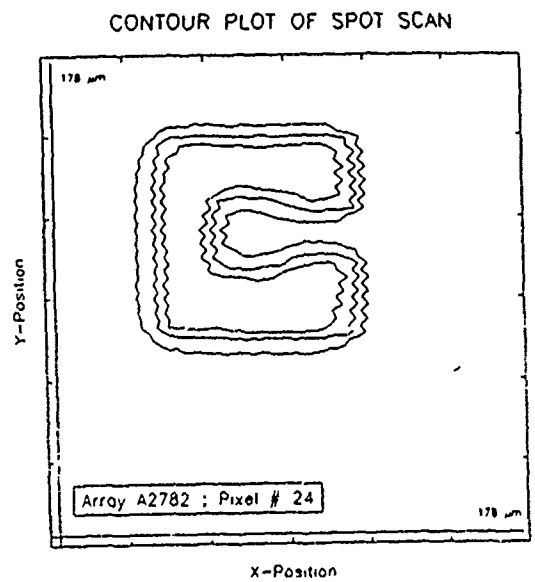

Figure 2 Representative spot scan contour plot of a SL detector The isoresponse lines, corresponding to 25, 50, and 75% of maximum response, illustrate uniform response across the detector except over the region of the contact.

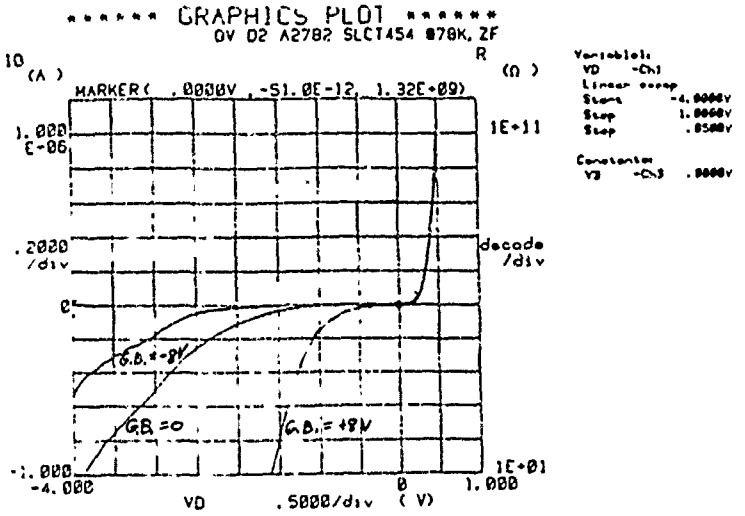

Figure 3. I-V trace of a representative SL diode (gated test device) illustrating breakdown voltages comparable to that typically observed for devices fabricated from the alloy. The diode dark current is drastically reduced by reverse biasing the guard gate, which is indicative of surface limited passivation.

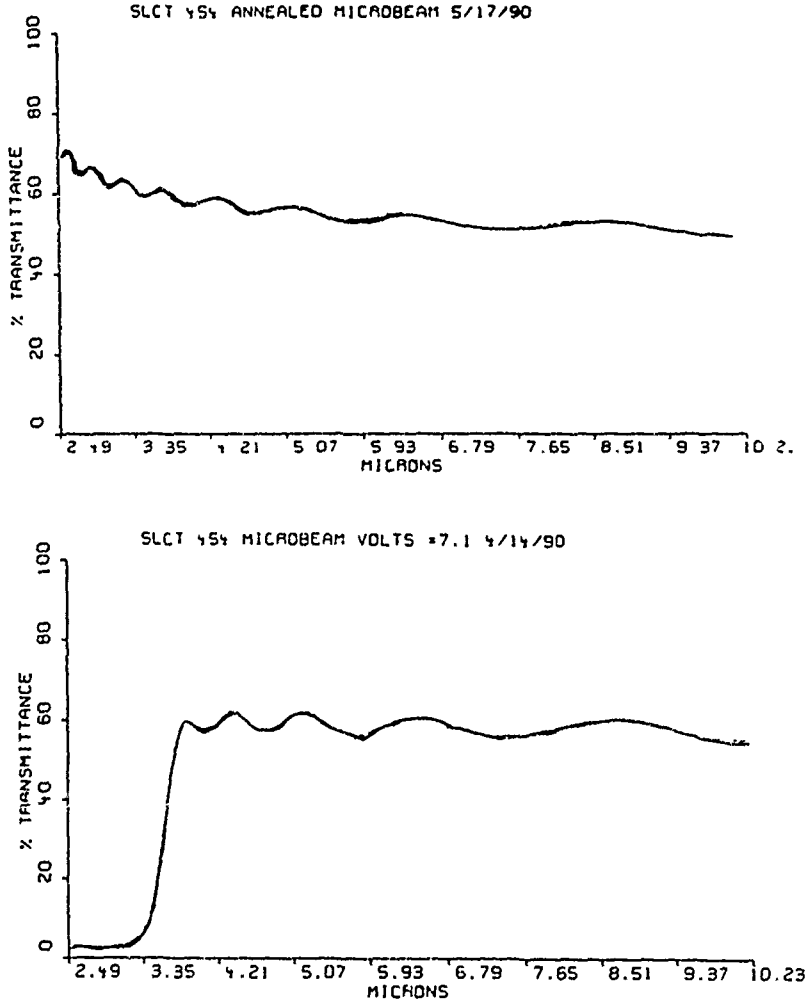

Figure 4. (a) IR microbeam transmission of the SL having undergone an interdiffusion anneal. The cutoff wavelength is below the range of the spectrometer and is estimated from atomic density calculations to be 1.5 μm. (b) IR microbeam transmission of the SL structure. The shift to longer cutoff wavelength is indicative of quantum size effects associated with carrier confinement of a periodic layered structure.

STEADY STATE MEASUREMENT OF DARK CURRENT AND INVERSION LAYER PROPERTIES IN MIS STRUCTURES

R. A. Schiebel

Texas Instruments Incorporated

Dallas, Texas 75265

The MIS structure is widely used for HgCdTe materials characterization and study of inversion layer properties. Its high impedance frustrates direct measurement of material properties through steady state measurements (such as current-voltage) and neccssitates pulsed or ac techniques. Stray capacitance and resistance and speed limitations of pulsed techniques limit analysis to relatively large area devices with low dark currents. Low field dark current measurements are limited by signal/noise limitations of pulsed techniques. These factors limit the sensitivity of MIS devices to material non-uniformities, and restrict characterization to relatively low-doped material, particularly for narrow band gap HgCdTe.

In this work we demonstrate a novel technique that circumvents these limitations and allows steady state current-voltage measurements on the MIS device in strong inversion. To do so we use the familiar gated diode structure shown in Figure 1. We make direct, ohmic contact to the inversion layer through an adjacent metallurgical diode and use it to monitor the current through the induced junction under the MIS gate. Diode bias determines quasi-Fermi level splitting in the induced junction and together with gate bias determines the field. We have successfully made current vs. gate and diode voltage measurements on small (1 mil by 1 mil) MIS devices, with quasi-Fermi level splittings as low as 2 mV, at doping levels in excess of 10^{16} cm^{-3}. These are all beyond the limits of conventional MIS measurement techniques.

Figure 2 shows a measurement of the diode current vs. gate bias. Three regimes are noted:

- At the most negative biases, the surface under the MIS gate is accumulated, producing a substantial tunnel current at the periphery of the metallurgical diode.

• At moderate biases the region under the MIS gate is depleted, and the measured current is dominated by the leakage current of the metallurgical diode. Due to the low test temperatures, high quality interfaces, and predominance of tunneling, no surface generation-recombination currents are observed in this regime.

• At more positive biases, the region under the MIS gate is inverted and the current from the induced junction, by virtue of its much larger area, predominates.

Figure 3 shows the current-diode voltage curves of the metallurgical junction and the induced junction, obtained by proper choice of gate bias.

We apply this technique to the study of inversion layer properties. In general, direct observation of sub-band structure in semiconductors by current-voltage measurements has required special device features such as thin insulators [1] or tunnel junctions [2]. In HgCdTe, inversion layer quantization has been manifested in MIS devices as oscillations in measured capacitance or conductance vs. gate bias [3,4]. In Figure 4 we observe oscillations in measured MIS tunnel current, corresponding to the Fermi level passing through quantized levels, that show excellent agreement with capacitance oscillations on an MIS device on the same film.

By measuring these current-voltage characteristics vs. temperature we may identify dark current mechanisms and demonstrate how the nature of the tunneling transition to the quantized levels changes with temperature and the degree of quasi-Fermi level splitting.

To summarize, we have demonstrated a technique that extends the measurement capabilities of HgCdTe MIS devices and consequently adds to the understanding of dark current mechanisms and inversion layer properties in HgCdTe.

[1] D. C. Tsui, Phys. Rev. Lett. **24**, 303 (1970).

[2] U. Kunze, J. Phys. C, **17**, 5677 (1984).

[3] M. A. Finch, J. D. Beck, and W. T. Zwirble, IEDM Technical Digest, 508 (1980).

[4] M. J. Yang, C. H. Yang, and J. D. Beck, Semicond. Sci. Technol. **5**, S118 (1990).

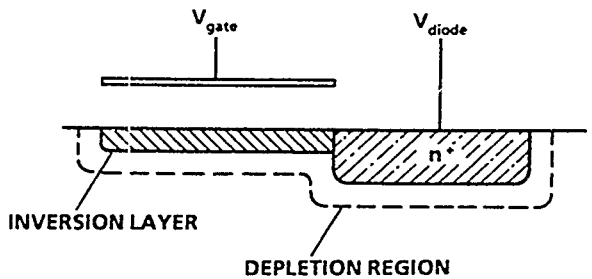

Figure 1 Crosssection of diode-MIS structure used for this study.

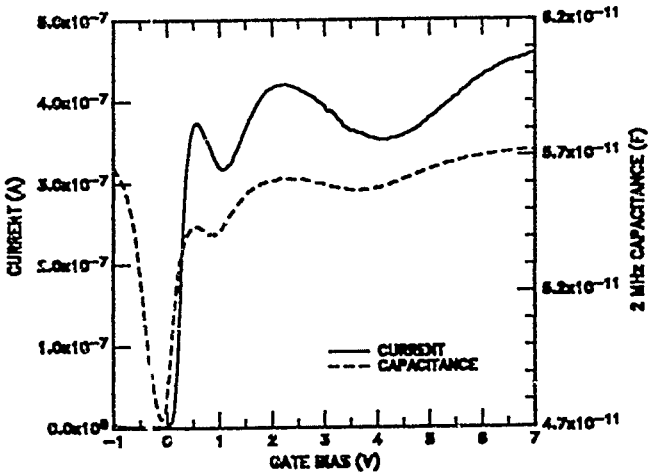

Figure 4 Current-voltage and capacitance-voltage curves showing oscillations due to inversion layer quantization. Capacitance data is from a 24 by 8 mil MIS device; the current from a 2 by 2 mil device. T = 40 K. V_{diode} = 2 mV. λ_C = 9.3 μm at 77 K.

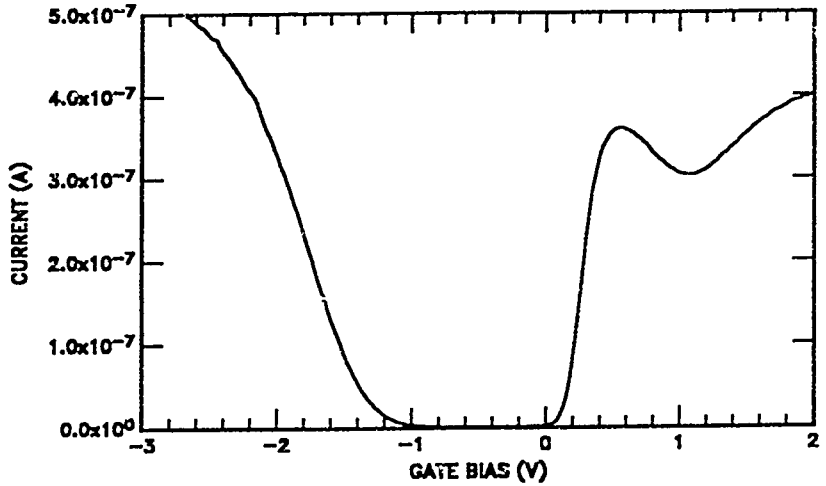

Figure 2 Diode current vs. gate bias showing accumulation, depletion, and inversion regimes. T = 40 K. V_{diode} = 2 mV. λ_C = 9.3 μm at 77 K. MIS area = 4 mil^2.

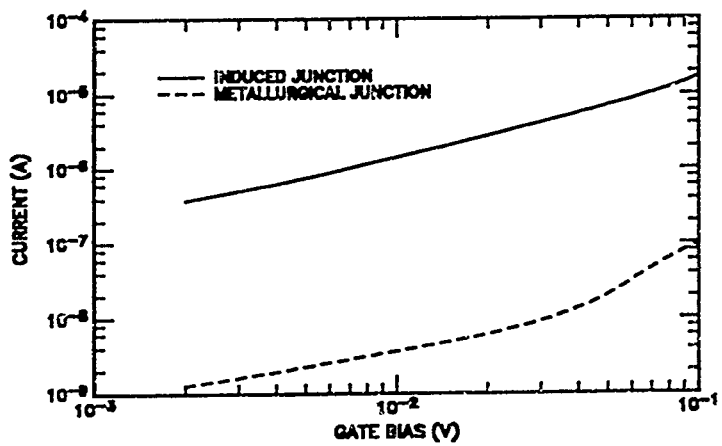

Figure 3 Current-voltage characteristics for the metallurgical junction and the induced junction. T = 40 K. V_{gate} = -0.5 V and 2.0 V. Same device as Figure 2.

DARK CURRENT PROCESSES IN THINNED P-TYPE HgCdTe

D.K. Blanks

Texas Instruments Incorporated

Dallas, Texas 75265

Previous studies of p-type HgCdTe indicate that diffusion is the dominant dark current mechanism for material in the the 10 μm spectral cutoff range (x=.225) at 77 K [1]. A significant reduction in dark current is expected for material thinned below the diffusion length [2]. In this paper, we demonstrate the reduction of diffusion current in 10 μm thick p-type HgCdTe. Voltage and charge transient techniques applied to metal-insulator-semiconductor (MIS) structures were used to compare dark currents over a temperature range of 40-100 K and electric fields of 0.4-1.4 V/μm for thick/thin pairs of p-type HgCdTe slices.

To characterize dark current in an MIS device, the charge or voltage on the gate is monitored as the device is pulsed into deep depletion. The time τ_s required to come to equilibrium is referred to as the storage time of the MIS device and is related to the dark current J_d via the expression

$$\tau_s \cong \frac{C_i \Delta V}{< J_d >} \tag{1}$$

where C_i is the insulator capacitance and ΔV is the voltage on the gate with respect to the threshold of inversion. The maximum storage time is determined by the ΔV at tunnel breakdown and the average dark current over the course of the transient.

The high electron mobility in narrow-gap HgCdTe results in minority-carrier diffusion lengths on the order of 250 μm in p-type HgCdTe. Hence, lower diffusion current and enhanced storage times should result upon thinning below the diffusion length. To demonstrate this, a single slice of p-type HgCdTe was sawed in half and processed with MIS devices on both sides. One slice was thinned to 10 μm thickness prior to device fabrication. While the storage times varied across each slice, the general trend shows a 3X increase in storage times for the thinned slice compared to its thick sister slice (Fig. 1). One device in particular has a storage time of 480 μsecs compared to 60 μsecs for the best

device on the thick sister slice.

The storage transient for the control thick device is shown in Fig. 2. The large initial curvature from 0-10 μsecs is associated with tunnelling across the depletion region. The tunnel current decreases rapidly as the depletion region collapses until diffusion current becomes the dominant dark current source. The slope of the transient becomes almost constant after $\sim$10 μsecs, reflecting the constant diffusion of minority carriers from the bulk.

In contrast, the thinned device charge transient has a steady curvature (Fig. 3) indicating dark current dominated by tunnelling throughout the transient with no significant diffusion current. To illustrate this point more clearly, the transient data for both devices is translated into dark current vs electric field in Fig. 4. The thick device has a constant dark current plateau over the E=0.7-1.0 V/μm range followed by the onset of tunneling around 1.0 V/μm. The dark current for the thinned device ranges over the 0.5-0.9 V/μm range. Over the common range between 0.7-0.9 V/μm, the thinned device demonstrates dark current with smaller magnitude but greater field sensitivity compared to the thick device.

In addition to transient data taken at 77 K, transient scans were taken as a function of temperature to clarify the nature of the dark current sources. Various dark current processes, including direct tunneling, trap-assisted tunneling, depletion, and diffusion currents will be examined to quantify changes in dark current mechanisms with material thickness, temperature, and electric field.

[1] D.K. Blanks, J.D. Beck, M.A. Kinch, and L. Colombo, J. Vac. Sci. Technol. A, **6**, 2790 (1988).

[2] J.P. Omaggio, IEEE Trans. Electron Devices, **37**, 141 (1990).

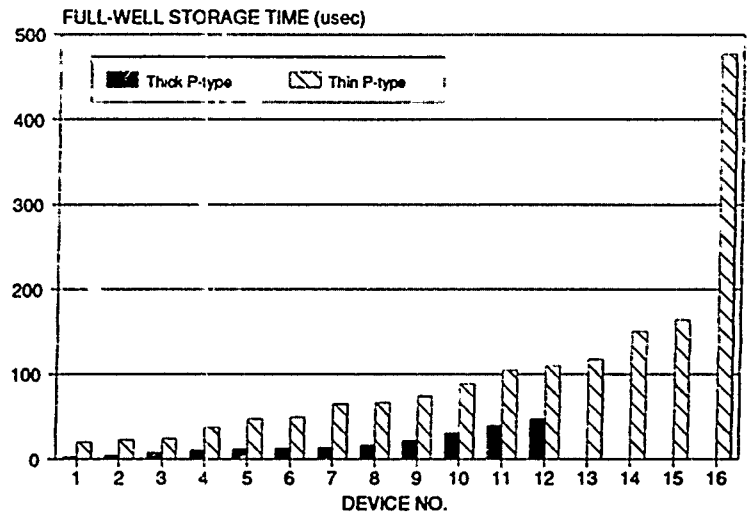

Fig. 1. Storage times for MIS devices fabricated on p-type $Hg_{1-x}Cd_xTe$ with 10 μm cutoff (x=0.225) for a thick slice and a sister slice thinned to 10 μm thickness. Reduced diffusion current in the thinned slice results in a 3X increase in average storage times.

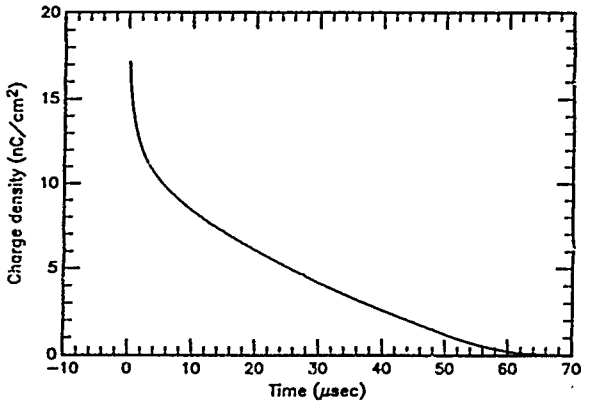

Fig. 2. Charge transient for an MIS device on a thick p-type HgCdTe slice with a spectral cutoff of 10 μm at 77 K. The storage time is approximately 60 μsecs.

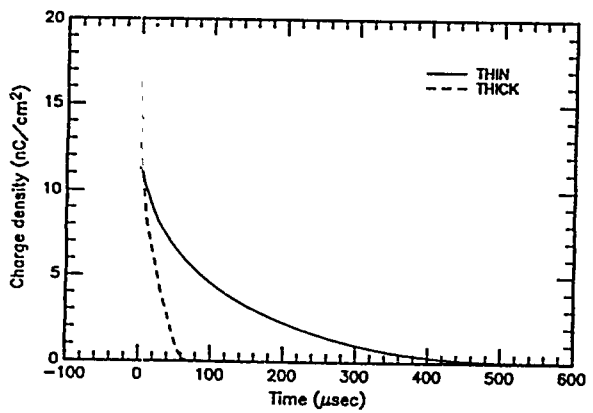

Fig. 3. A comparison of the charge transient from Fig. 1 with a transient for an MIS device a sister slice thinned to 10 μm thickness. The reduced diffusion current results in a 450 μsec storage time for the thinned device.

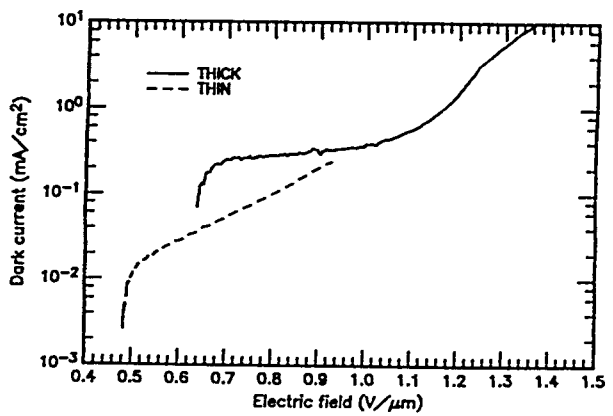

Fig. 4. Dark current vs electric field data derived from the charge transients in Figs. 1 and 2 illustrating the reduced dark current in the thinned p-type HgCdTe.

PROPERTIES OF SCHOTTKY DIODES ON n-TYPE $Hg_{1-x}Cd_xTe$

P.W.Leech and M.H.Kibel

Telecom Australia Research Laboratories,

Clayton, Victoria, Australia.

The ability to form Schottky barrier diodes on n-type $Hg_{1-x}Cd_xTe$ enables fabrication of the gate metal-semiconductor field effect transistor (MESFET)[1] and the interdigitated metal-semiconductor-metal (MSM) detector, these devices having importance in monolithic integrated circuits for 1.5μm optical communications. But while the formation of Schottky barriers at metal:n-$Hg_{1-x}Cd_xTe$ contacts in the stoichiometric range $x > 0.4$ has been predicted in theory[2], little published data exists on the electrical contact properties. We report studies of the electrical and interfacial characteristics of Ag, Au, Cu, Pd, Pt, Sb and Ti metals on n-$Hg_{1-x}Cd_xTe$ for x=0.6-0.7, using both liquid phase epitaxy (LPE) and metalorganic chemical vapor deposition (MOCVD) grown epitaxial layers. Metal contacts were deposited under conditions of negligible substrate heating. For Pt/n-$Hg_{0.3}Cd_{0.7}Te$, barrier heights measured by current-voltage and capacitance-voltage techniques were $\Phi_b = 0.69 \pm 0.01$ eV with n=1.25 for Br:HBr etched surfaces and n=1.30 for air exposed (Fig.1). Significant changes in the diode parameters were found with variation in x (Fig.2) but not substrate doping. Auger sputter profiles of the Pt/n-$Hg_{1-x}Cd_xTe$ interface (Fig.3) showed intermixing of the Pt overlayer and loss of surface Hg, consistent with the Pt-cation alloying observed in p-$Hg_{0.7}Cd_{0.3}Te$[3]. In contrast, for Au/$Hg_{0.3}Cd_{0.7}Te$ contacts, $\Phi_b = 0.79 \pm 0.03$eV with value of n strongly dependent on surface pre-treatment (Fig.1). Auger sputter profiles exhibited an indiffusion of Au (Fig.3). However, the inability of the Au to reduce TeO_2 at air

exposed surfaces or to react with the Cd/Hg depleted region[4,5] at chemically etched surfaces correlates with an effect of these interfacial layers on the diode characteristics. In general, the barrier heights produced by unreactive and intermediate reactivity metals were in the range Φb=0.74 to 0.79V, while for the more reactive metals Pd and Pt, Φb=0.69$\pm$0.01V. The current-voltage characteristics of contacts formed on chemically etched surfaces have been described by a thermionic emission-recombination model.

The permission of the Executive General Manager, Telecom Australia Research Laboratories to publish this work is acknowledged.

REFERENCES

1. P.W.Leech, P.Gwynn, G.Pain, N.Petkovic and J.Thompson, Electronics Letters, 26, (4), 221, (1990).
2. W.E.Spicer, D.J.Friedman and G.P.Carey, J.Vac.Sci.Technol., A6(4), 2746., (1988).
3. D.J.Friedman, G.P.Carey, I.Lindau and W.E.Spicer, Phys.Rev.B, B5, (3), 1188, (1987).
4. P.W.Leech, P.J.Gwynn and M.H.Kibel, App.Surf.Sc., 37, 291, (1989).
5. P.W.Leech, M.H.Kibel and P.J.Gwynn, J.Electr.Soc., 137, (2), 705, (1990).

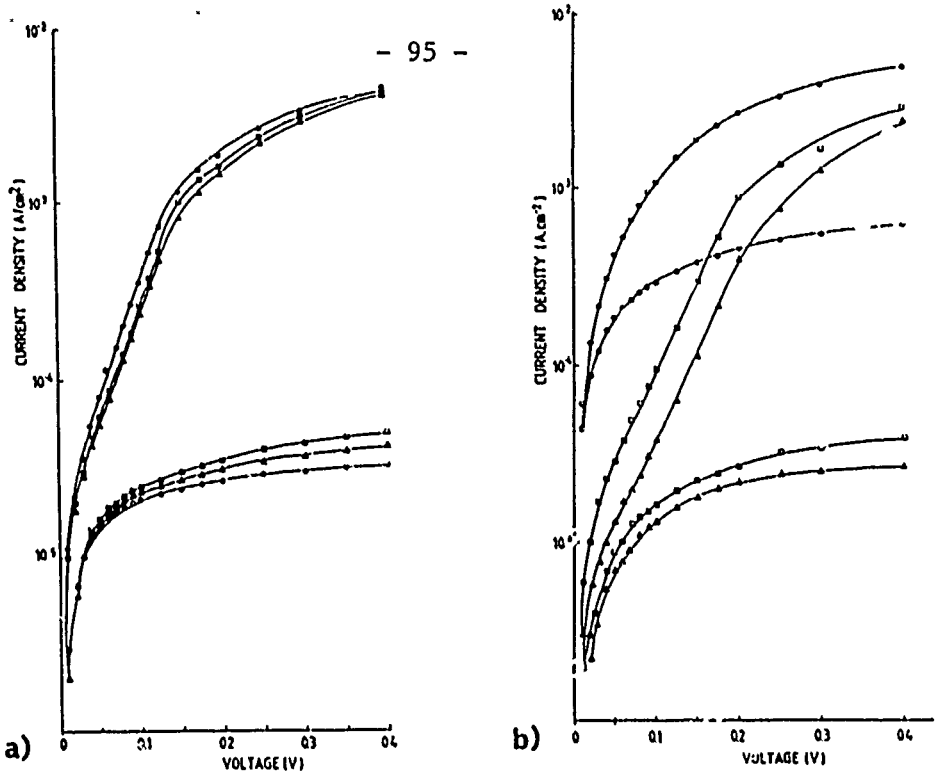

Fig. 1 Typical lnJ-V curves at 293K for a) Pt/n-$Hg_{0.3}Cd_{0.7}Te$ and b) Au/n-$Hg_{0.3}Cd_{0.7}Te$ diodes formed on (111) surfaces : ○ Air exposed, □ I:KI:HBr etched, △ Br:HBr etched.

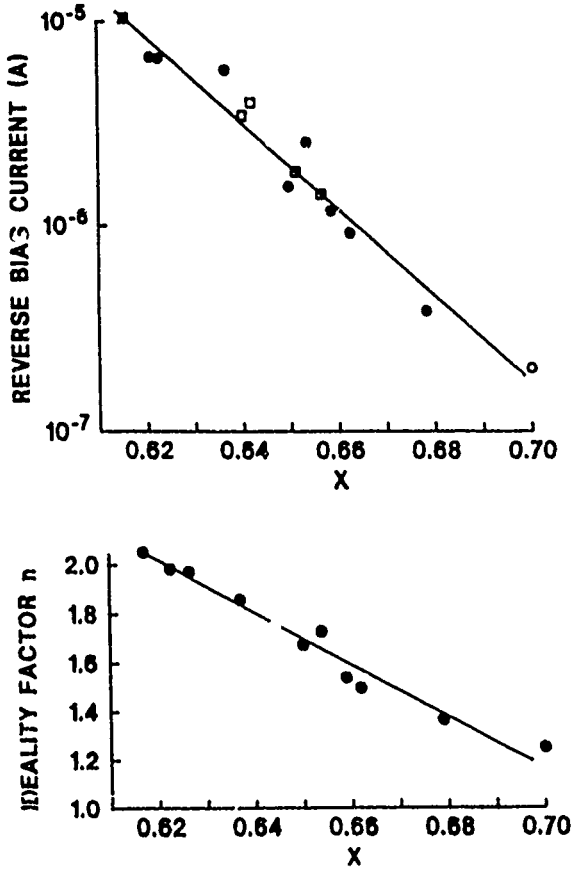

Fig. 2 Reverse leakage current and ideality factor n as a function of x for ● Pt and □ Au diodes on MOCVD $Hg_{1-x}Cd_xTe$(2° off 100).

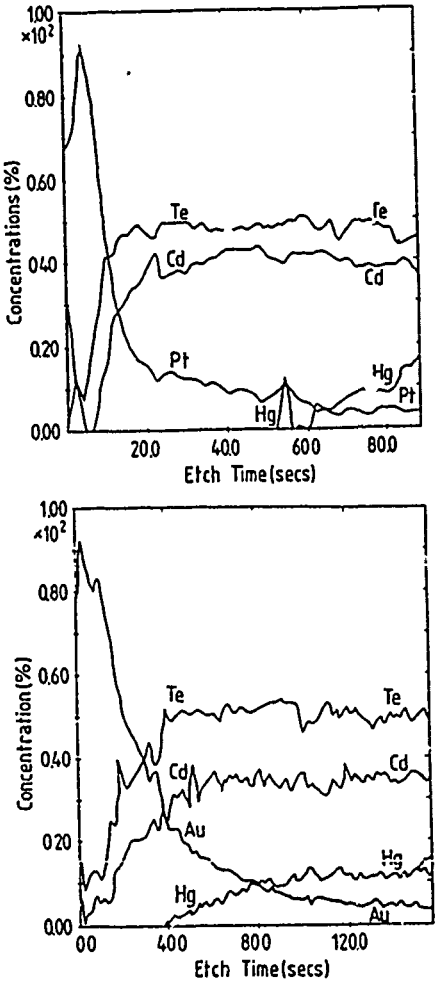

Fig. 3 Sputter depth profiles of a) Pt/$Hg_{0.3}Cd_{0.7}Te$ and b) Au/$Hg_{0.3}Cd_{0.7}Te$ interfaces.

UNCOOLED 10.6 μm MERCURY MANGANESE TELLURIDE PHOTOELECTROMAGNETIC IR DETECTORS

P. Becla
Massachusetts Institute of Technology
Cambridge, MA 02139

and

N. Grudzien* and J. Piotrowski*
Boston Optronics Corporation
Brookline, MA 02146

Introduction

$Hg_{1-x}Cd_xTe$ has long been the material of choice for fabrication of various infrared devices. Currently, $Hg_{1-x}Mn_xTe$ with comparable electronic properties, may be a potential competitor. In this communication we report the preparation and performance of the uncool photoelectromagnetic (PEM) detectors for 10.6 μm wavelength range utilizing $Hg_{0.92}Mn_{0.08}Te$ single crystals grown by the traveling solvent method (TSM) (1). The work consists of theoretical and experimental components. Lile's (2) generalized model was used to calculate the voltage responsivity R_v and the resistivity R_o of the PEM detectors. Detectivity was calculated from the standard photoelectric equation as described in paper (3), assuming that the noice of PEM detectors is limited by the thermal Johnson–Nyquist noise. The experimental part primarily focuses on material preparation and various (electrical, optical and photoelectrical) characterizations. Both the experimental and modeling results are anticipated to establish the maximum performance of MMT/PEM detectors.

Experimental Procedures

The bulk crystals of $Hg_{0.92}Mn_{0.08}Te$ have been grown by the TSM method (1). The native acceptor concentration has been adjusted at a level of about 1×10^{17} cm^{-3} by the post–grown annealing of the wafers in mercury saturated atmosphere. The wafers have been epoxied to silicon substrates, thinned to final thickness of about 5 μm and cut into bars of about 1 mm by 2 mm. Electrical

*On leave from Vigo LTD, Warsaw 00-908, Poland.

contacts were made by gold electroplating to the end of the HgMnTe bars to which the fold wires were attached. The typical size of active areas was 1 mm^2. The sensitive elements were then mounted in the narrow slot of the miniature permanent magnet having a magnetic field strength of about 1.5 Tesla. Spectral characteristics were measured in a standard set-up with an infrared monochromator and black body source.

Results and Discussion

According to Lile and Genzow et al equations (2,3), the voltage responsivity of PEM detector depends on several technological parameters, ie surface recombination velocities at the front and back sides, S_1 and S_2; reflectivities at the front and back sides, R_1 and R_2; sample thickness, d; and the ratio of concentration p/n_i, the optimization of which allows us to maximize R_v. Other parameters such as E_g, μ_n, μ_p, and τ are materials properties or limited for experimental reasons (as B and T).

Figure 1 shows typical calculated data [normalized resistivity (R_o), responsivity (R_v), detectivity (D*), and photoresponse (τ_r)] of an uncooled 10.6 μm MMT PEM detector as a function of acceptor doping. The maximum sensitivity ($R_v \simeq 0.3$ V/W) and detectivity ($D^* \simeq 2.3 \times 10^7$ cm $Hz^{1/2}$/W) occur at the acceptor concentration of about 3×10^{17} cm^{-3} and 2×10^{17} cm^{-3} respectively. Of interest is the region where the time constant τ_r decreases with the acceptor concentration and is shorter than the bulk recombination time (3).

Figure 2 shows the typical experimental spectral responses (R_v and D*) of 10.6 μm PEM detectors. The maximum performance of 10.6 μm optimized devices is shifted toward a shorter wavelength to about 7-8 μm wavelength. At 10.6 μm wavelength, the voltage responsivity R_v and detectivity D* achieve the level of about 0.1 V/W and 1×10^{17} cm $Hz^{1/2}$/W respectively, which is by a factor of 3 below the calculated values. Typical response time of the MMT/PEM detector with the SMA connector and about 3 ft standard 50Ω cable is in the range of 100 psec to 50 psec.

Summary

Single crystals of $Hg_{1-x}Mn_xTe$ solid solution of well controlled composition, purity and morphology were obtained by the TSM method. Uncooled PEM detectors for the 10.6 μm wavelength range were designed and constructed. Lile's model was used to optimize the spectral characteristics (R_v, D*) and response time, τ_r. The measured photoelectric characteristics confirmed the expectations given in Lile's theroetical model.

References

1. P. Becla, to be published.

2. D.L. Lile, Phys. REv. B8, 4708 (1973).

3. D. Genzow, M. Grudzien and J. Piotrowski, Infrared Phys. V20, 133 (1980).

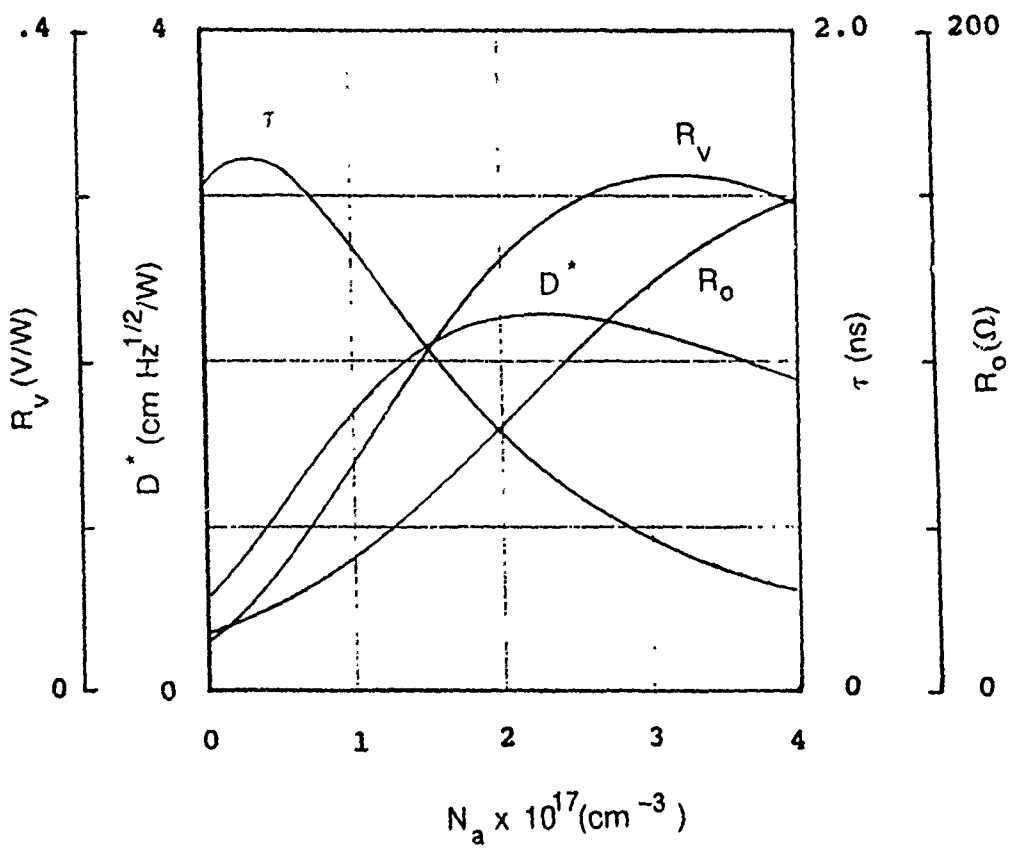

Fig. 1 Normalized resistivity, responsivity, detectivity and response time of uncooled 10.6 μm MMT/PEM detectors as a function of acceptor concentration.

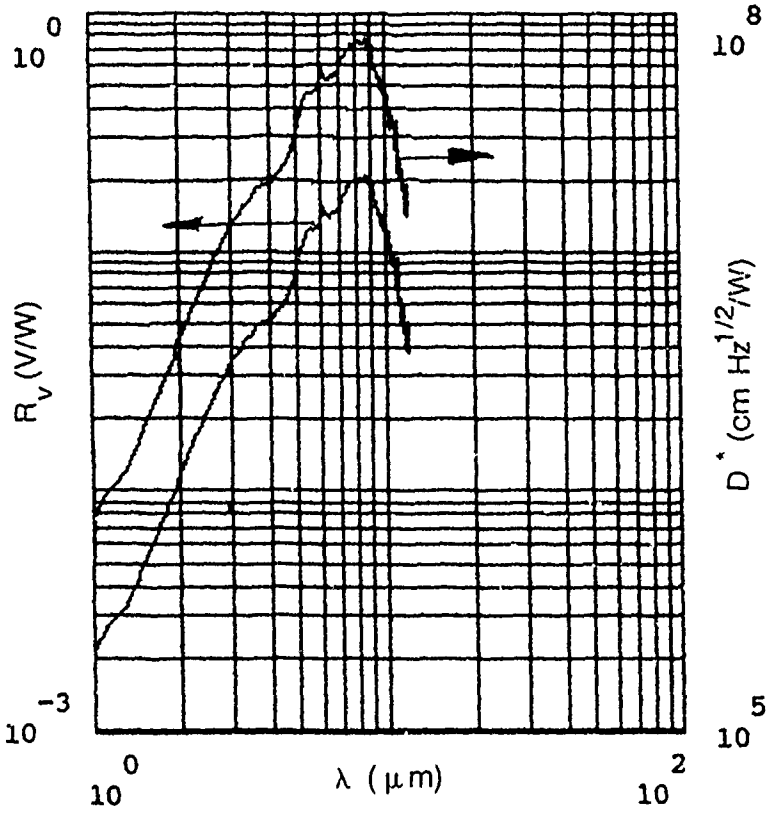

Fig. 2 Measured spectral responsivity and detectivity of uncooled 10.6 μm MMT/PEM detectors.

NOVEL DEVICE CONCEPT FOR SILICON BASED INFRARED DETECTORS

G. Scott, D. E. Mercer, C. R. Helms

Stanford Electronics Laboratories, Department of Electrical Engineering, Stanford University, Stanford, California 94305

Infrared focal plane arrays utilizing PtSi/p-Si Schottky barriers have several advantages over competing technologies in the areas of uniformity, ease of manufacture, and potential for integrating into monolithic circuits. However, these devices suffer from low quantum efficiency. One of the major factors which limits efficiency is the high density of states near the Fermi level of the PtSi. This affects both the optical absorption and hot carrier transport processes[1]. The majority of the incident photons are lost through excitations to states below threshold. Most of the hot carriers produced with sufficient energy to surmount the barrier are rapidly thermalized by carrier-carrier scattering, again a consequence of the high density of available final states near the Fermi level.

We propose a novel device concept for infrared detectors which utilizes a thin film of a narrow gap semiconductor (NGS) deposited on a p-type silicon substrate. The operation of the device would be similar to a Schottky barrier detector, in that carriers would be excited from the overlayer into the substrate. However, the presence of the bandgap in the overlayer should reduce the high density of undesired states near the Fermi level. This would lead to a considerably higher absorption efficiency, as most hot carriers produced by the incident photons would have energies above threshold. Hot carrier lifetimes in the NGS would be expected to be several orders of magnitude greater than in a metal, which would give a higher probability for a hot carriers to cross the barrier into the Si substrate. For the device to respond to light in the 3-5 μm range, it should have a threshold around 0.2 eV, which means that the valence band offset (threshold minus overlayer bandgap) should be around 0.1 eV. The overlayer material should have a high workfunction, as this is correlated with low valence band offset to Si. Calculations using a

recently developed diffusion model[1] for the behavior of Schottky barrier detectors indicate the potential for an order of magnitude improvement in quantum efficiency over Schottky barrier detectors at a wavelength of 4μm (fig. 1).

We have begun our investigation with materials that are easily deposited, namely PbTe, SnTe, and the ternary alloy. We have prepared structures by congruently evaporating films of PbTe and SnTe from single sources of the compounds onto <100> p-Si wafers which were chemically cleaned prior to deposition. These films are polycrystalline and may therefore be expected to lead to poor performance. However, as the devices are being operated in a mode similar to PtSi/p-Si Schottky barrier detectors, even polycrystalline films would be expected to give significant increases in performance. The density of states in the overlayer bandgap due to defects would be far less than the state density in the same energy range for a silicide film. Auger sputter profiles of the films indicate that both the PbTe and SnTe indicate that the films are stoichiometric. Current-voltage measurements indicated rectifying behavior with good ideality factor and low leakage down to 77°K for the case of SnTe/Si. High series resistance of the PbTe/Si structures made electrical characterization difficult, though they also showed rectifying behavior and low reverse leakage. Photoresponse measurements indicate a threshold of 0.35 eV for SnTe/p-Si and 0.3 eV for PbTe/p-Si. Measurements on the PbSnTe alloy, which has a narrower bandgap than either PbTe or SnTe, will also be discussed. Preliminary results show a lower energy photoresponse threshold on p-Si for the alloy.

REFERENCES

[1] D. E. Mercer, C. R. Helms, J. Appl. Phys. 65, 5035 (1989).

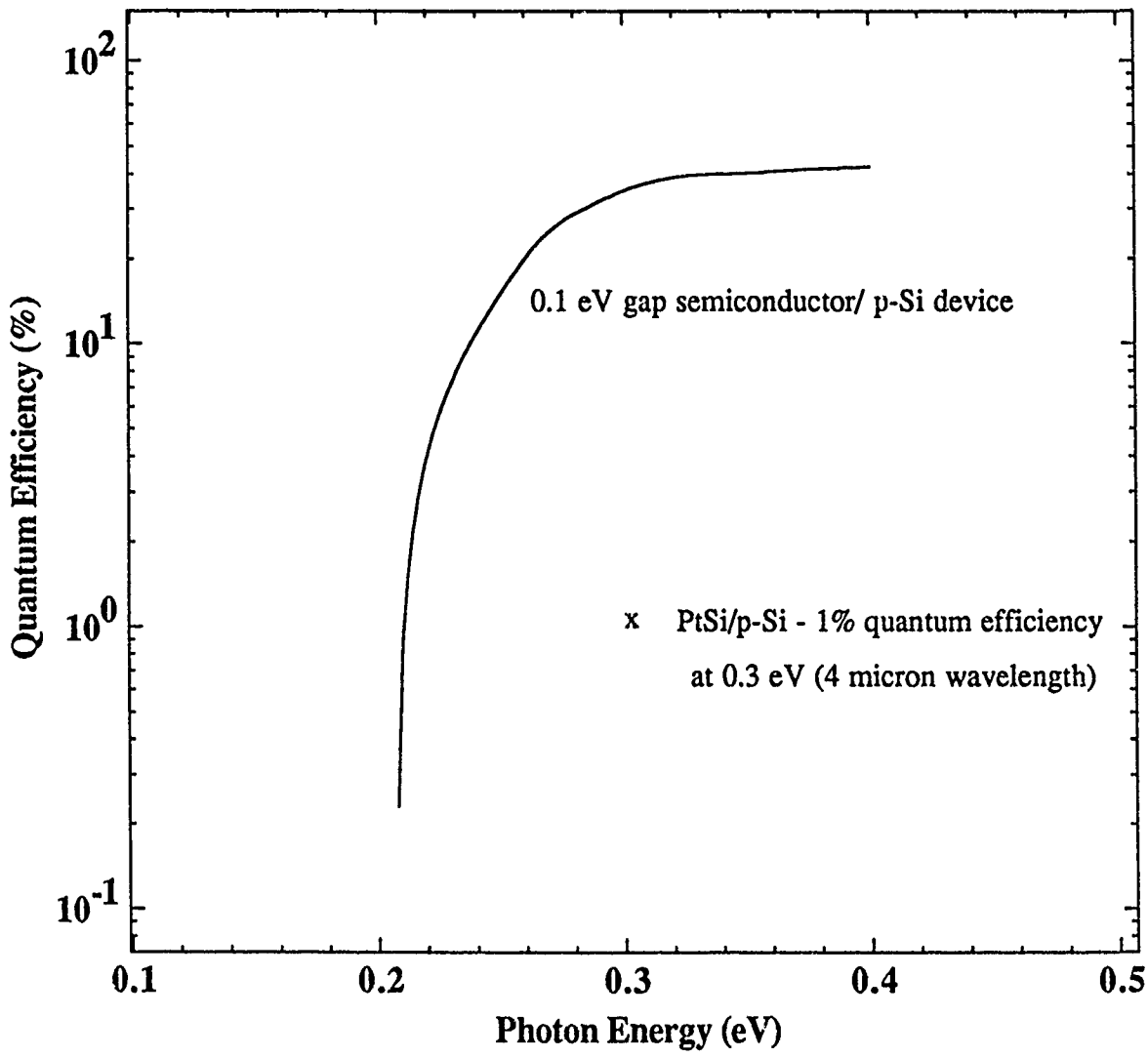

Figure 1. Comparison of the quantum efficiency of a PtSi/p-Si Schottky barrier to the theoretical efficiency of a heterostructure detector. The heterostructure is assumed to have a 0.1 eV bandgap in the overlayer and a 0.2 eV threshold. Both devices are modeled with an optical cavity to maximize quantum efficiency.

LONG-WAVELENGTH INFRARED DETECTION IN A PHOTOVOLTAIC-TYPE SUPERLATTICE STRUCTURE

Byungsung O, J.-W. Choe, M. H. Francombe, K. M. S. V. Bandara, and D. D. Coon

Microtronics Associates, Inc., Pittsburgh, PA 15213

and

Y. F. Lin and W. J. Takei

Westinghouse Science & Technology Center , Pittsburgh, PA 15235

Recent research on optical excitation of intersubband transitions in semiconductor quantum well structures has demonstrated that by careful engineering of quantum well and superlattice parameters in the GaAs-AlAs materials systems, tailored IR response at chosen wavelength can be achieved over a very wide spectral range extending to the LWIR band and beyond. [1] Multi-quantum well (MQW), photoconductive detector structures showing high performance at about 10 microns, e.g., have been reported [2] and we have published results indicating IR response with excellent detector uniformity at wavelengths out to 12 microns. [3].

Most of the MQW embodiments studied thus far have employed the photoconductive mode of operation, and although capable of high current responsivity, this mode involves high dark current and high levels of operating power. A low-power type of structure has been described by Kastalsky et al. [4] which involves photovoltaic IR detection in the optical range 3.6-6.2 micron. In the present work we have studied a Kastalsky-type of superlattice detector structure with quantum well parameters adjusted for IR response in the LWIR range. The structure, which was grown by MBE, consists of 50 periods of 73 Å GaAs quantum wells and 65 Å AlGaAs barriers (see Fig. 1). A 1000 Å $Al_xGa_{1-x}As$ layer graded from $x = 0$ to $x = 0.18$ was grown adjacent to the superlattice and the combination was sandwiched between doped contact layers. With the parameters shown, there are two minibands below the top of the barrier, with the energy of the graded

barrier at $x = 0.18$ being lower than the bottom of the first excited miniband, but much higher than the top of the ground state miniband to block the flow of the electrons (dark current) to the collector contact layer.[5]

Detector arrays, fabricated in the geometry of 4-mil square mesas, were illuminated from the backside via an array of etched grooves on the GaAs surface. Typical spectral photoresponse results are shown in Fig. 2(a) and display a peak value which agrees closely with that calculated from the superlattice parameters indicated in Fig. 1. The peak response was shown to vary both with bias voltage and with temperature, as illustrated in Fig. 2(b). We suggest that the rapid fall-off in response at bias values above 0.6 V can probably be attributed to progressive decoupling of the miniband structure depicted in Fig. 1. The measured dark current under -0.6 V bias at 24 K was approximately 10^{-8} A. From these measurement data the detectivity at 24 K was estimated to be about 2×10^{8} cm$\sqrt{\text{Hz}}$/W.

Our analysis of these detectors suggests that the performance can be greatly improved by optimization of design parameters. Specifically, we discuss the enhancement of photoresponse through special tailoring of termination layers at the ends of the superlattice. Formulas have been deduced which specify the properties of optimal superlattice layers without requiring that one perform quantum mechanical calculations for the composite structure consisting of the superlattice with the attached termination layer. A key formula for design of termination layer involves a non-linear mapping called a Möbius transformation, which represents the mathematical relationship between reflected Bloch wave amplitudes R' and reflected plane wave amplitudes R.

Methods for further limiting the dark current are also discussed. These include modifications to the blocking layer design and reduction of carrier concentration in the wells as a means of reducing thermionic emission. It is shown that with appropriate design changes D* values approaching 10^{11} cm$\sqrt{\text{Hz}}$/W at 40 K in the LWIR range.

References

[1] D. D. Coon and R. P. G. Karunasiri, Appl. Phys. Lett. **45**, 649 (1984), D. D. Coon, J. Vac. Sci. Technol. A **8**, 2950 (1990).

[2] B. F. Levine, C. G. Bethea, G. Hasnain, V. O. Shen, E. Pelve, R. R. Abbott and S. J. Hsieh, Appl. Phys. Lett. **56**, 851 (1990).

[3] Y. F. Lin, M. H. Francombe, D. D. Coon, Byungsung O, and K. M. S. V. Bandara, *Factors Influencing Performance and Uniformity in GaAs Quantum Well IR Detector*, in Proceedings of the IRIS Specialty Group on Infrared Materials 1989.

[4] A. Kastalsky, T. Duffield, S. J. Allen and J. Harbison, Appl. Phys. Lett. **52**, 1320 (1988).

[5] Byungsung O, J.-W. Choe, M. H. Francombe, K. M. S. V. Bandara, D. D. Coon, Y. F. Lin and W. J. Takei, Appl. Phys. Lett. **57**, 503 (1990).

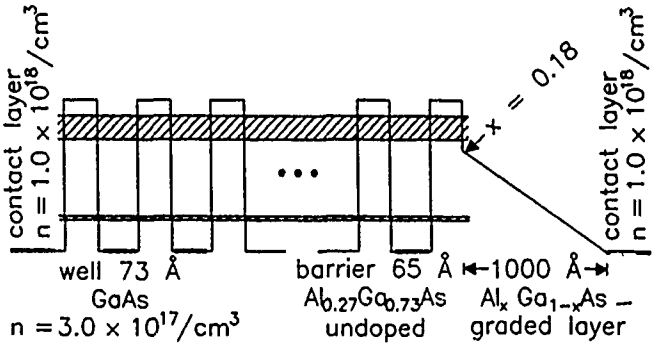

Figure 1: Structure of a multiple quantum well photovoltaic device.

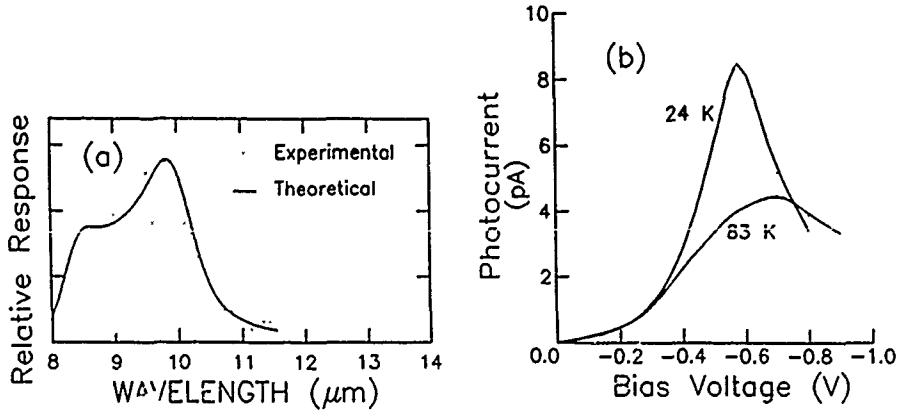

Figure 2: (a). Experimental and estimated spectral photoresponse at T = 24 K under a bias voltage of −0.58 V. (b). Photocurrent vs bias voltage at T = 24 K and 83 K.

PROPERTIES OF LASER DEVICES PREPARED FROM MCT AND MZT EPITAXIAL LAYERS

A. Ravid, A. Zussman, G. Cinader, A. Sher
Solid State Physics Department, Soreq Nuclear Center, Yavne Israel

Yoram Shapira.
Faculty of Engineering, Tel Aviv University, Ramat Aviv 9978, Israel.

We report the lasing properties of laser devices prepared from MCT and MZT single epitaxial layers grown by liquid phase epitaxy (LPE), and MCT layers structures grown by metallorganic vapor phase deposition (MOCVD). Lasing was observed in the wavelength range of 2.1 μm to 5.5 μm. The laser devices, with 1-10 μm thick active layer, were in the form of about 3 mm long, 400-500 μm wide bars and prepared by cleaving the wafer along two parallel (110) planes. Stimulated emission was obtained by optical pumping using a single GaAs diode laser emitting 200 ns long pulses.

Laser action was observed at temperatures as high as 160 K. This was obtained for a 1.5 μm thick MCT single active layer grown by MOCVD, which emitted at 2.8 μm. To the best of our knowledge, this the highest lasing temperature reported to date.

The threshold power densities were as low as 0.54 and 21.6 KW/cm² at 12 K and 160 K, respectively, obtained for the above mentioned laser. The temperature dependence of the threshold pump power for 4 laser devices is shown in Fig. 1. The corresponding characteristic temperatures, T_o, are indicated. The differential quantum efficiencies of two of these lasers, derived from the laser output power VS. the GaAs laser input power curves, are shown in Fig. 2. These figures, show that the LPE grown MCT layer yields higher efficiencies and T_o value than those grown by MOCVD. This may indicate a better crystalline quality for the LPE grown MCT layers. In several MOCVD grown devices, the laser properties degraded due to excited-carrier separation in p-n junctions that existed in the layers. The low quantum efficiency (0.17% at 12 K) and the lower maximum lasing temperature (50 K) of the MZT layer, can be partially accounted for by its longer lasing wavelength (≈5.4 μm), at which the Auger recombination process is expected to be stronger[1].

The far field patterns of the MCT and MZT layers which were grown by LPE, were typically about 4° perpendicular and parallel to the active layer. These narrow perpendicular angular distribution indicates that the lasing takes place over the entire ≈10 μm thick active layers[2].

Using excitation with high power GaAs laser array (100 W peak power), high peak output power of more than 20 mW (at 12 K) was achieved, as shown in Fig. 3.

Our preliminary results show that MCT and MZT are promising materials for the fabrication of efficient light emitting devices in the 2-5 μm wavelength range. The laser devices prepared from LPE grown MCT layers exhibited so far the lowest threshold power density and the highest quantum efficiency. However, the highest lasing temperature of 160 K (limited by the available GaAs pumping power) was obtained from MOCVD grown laser device. It is expected that by improving the quality and the layer structure of the MOCVD grown devices, better laser devices can be achieved.

References

1. T. N. Caddelman, J Appl. Phys., 52, 848 (1981).

2. A. Ravid and A. Zussman, J. Appl. Phys. 67, 4260 (1990).

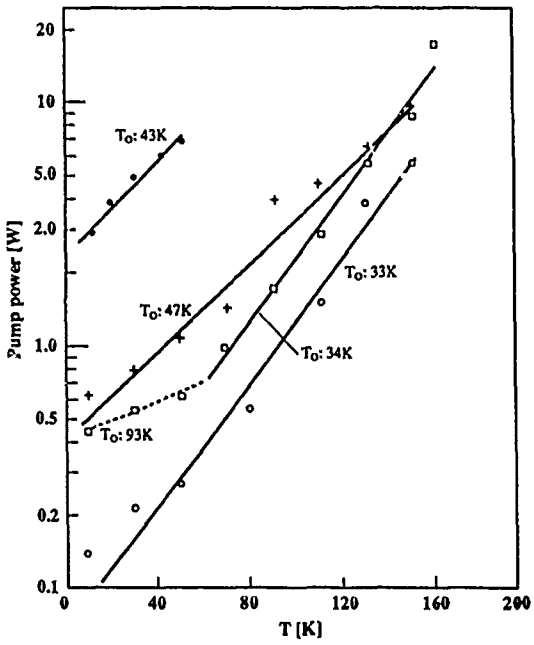

Figure 1: Threshold pump power as a function of temperature for 4 laser devices. •,+ LPE grown MZT and MCT devices with 10 μm thick active layer, λ ≈5.4 μm and λ≈2.1 μm respectively; ▫,o MOCVD grown MCT at λ≈2.8 and λ≈2.9 μm, with 1.5 μm and 3 μm active layers, respectively.

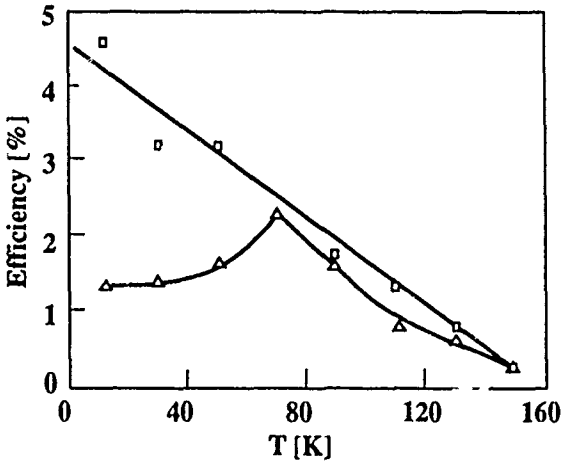

Figure 2: Temperature dependence of the differential quantum efficiency. ▫ LPE grown MCT with 10 μm thick active layer, λ≈2.1 μm; Δ MOCVD grown MCT with 1.5 μm thick layer, λ≈2.8 μm.

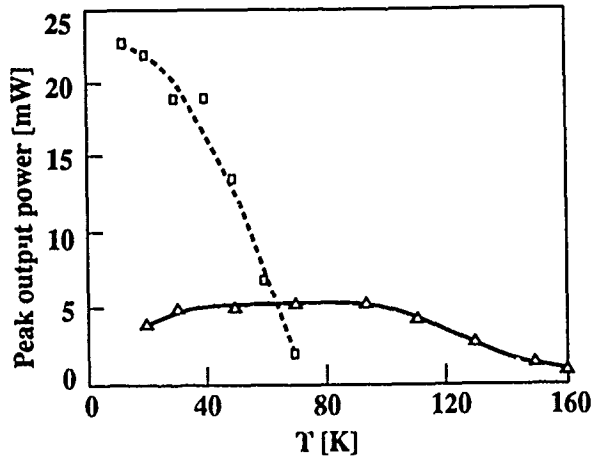

Figure 3: Maximum peak output power of two different laser devices as a function of temperature. ▫ MZT laser device (shown in Fig. 1), excited with 100 W GaAs laser array; Δ MOCVD grown MCT laser device with 1.5 μm thick active layer, excited with 19 W GaAs laser diode.

Title : High efficiency IR light emitting diodes made in LPE and MBE MCT layers *

Authors : P. BOUCHUT, G. DESTEFANIS, J.P. CHAMONAL
A. MILLION, J. PIAGUET, B. PELLICIARI

Affiliation : CEA - LETI - LIR
BP 85 X
38041 GRENOBLE - FRANCE

Abstract :

A huge effort has been devoted to MCT as the material for IR detection. Nevertheless, MCT can also find interest in IR emission. In this paper we present performances of light emitting diodes made in MCT epilayers grown either by LPE or MBE.

Diodes were made using our standard Ion Implantated technology, in epilayers with cut-off wavelength in the range 3.5 to 5 µm at 77 K, and thicknesses in the range 5 to 10 µm.

Devices are two dimensionnal LED arrays interconnected by hybridization. Backside emission was characterized through the CdZnTe substrate.

This paper will provide complete diode characterization such as electroluminescence spectrum versus temperature from 10 K to 300 K. Internal quantum efficiency as high as 25 % at 77 K and 5 % at 300 K were obtained for 4.3 µm and 3.6 µm λpic respectively.

As a conclusion, a comparison between devices made with MBE and LPE epilayers is given.

* Work sponsored by DRET (Minitry of Defence)

Properties of Modulation-doped HgTe-HgCdTe Superlattices and Quantum Well Structures Grown at Low Temperatures by Photoassisted Molecular Beam Epitaxy

Y. Lansari, S. Hwang, Z. Yang, J.W. Cook, Jr., and J.F. Schetzina, Physics Department, North Carolina State University, Raleigh, NC 27695-8202

Growth of HgTe-HgCdTe superlattices, both undoped and modulation doped, has been achieved at very low temperatures using photoassisted MBE. Growth temperatures in the range 140 - 100 °C and Hg fluxes with beam equivalent pressures of 1.5 to 0.5 x 10^{-4} Torr were employed. An argon-ion laser with output in the range 488 - 514 nm was used for substrate illumination during film growth, and power densities ranging from 35 mW/cm^2 to 70 mw/cm^2 were utilized. The layers were grown on (100) CdZnTe substrates, with the CdTe and Te fluxes adjusted to obtain 1 - 3 Å/sec growth rates.

X-ray diffraction and optical absorption coefficient measurements were obtained and analyzed for all of the multilayers studied. These measurements clearly illustrate the high degree of structural perfection obtained and the quantum nature that these new modulation-doped structures possess. Figures 1 and 2 show the absorption data for two of these multilayers, A30A (undoped) and A77A (As-doped).

Transport properties of the superlattices were investigated by means of variable magnetic field Hall effect measurements, using a mobility spectrum analysis [1]. The enclosed figure shows the mobility spectrum for sample A30A, whose well and barrier thicknesses are 96.0Å and 121.6Å, respectively. The spectrum is generated from magnetic-field-dependent Hall data taken at 102.6K with magnetic fields up to 2 tesla. Three distinct peaks, which correspond to one type of electrons and two types of holes, with comparable maximal values are clearly resolved in the spectrum. Very high mobility holes (~ 3.4x10^4 cm^2/Vs) are observed. For superlattices modulation-doped with As, the mobility spectrum (see figure 4) shows a single hole peak. The peak position and maximal value are in good agreement with conventional Hall data. This result demonstrates that modulation-doping has been successfully achieved for HgTe-HgCdTe superlattices.

1. W.A. Beck and J.R. Anderson, J. Appl. Phys. 62, 541 (1987).

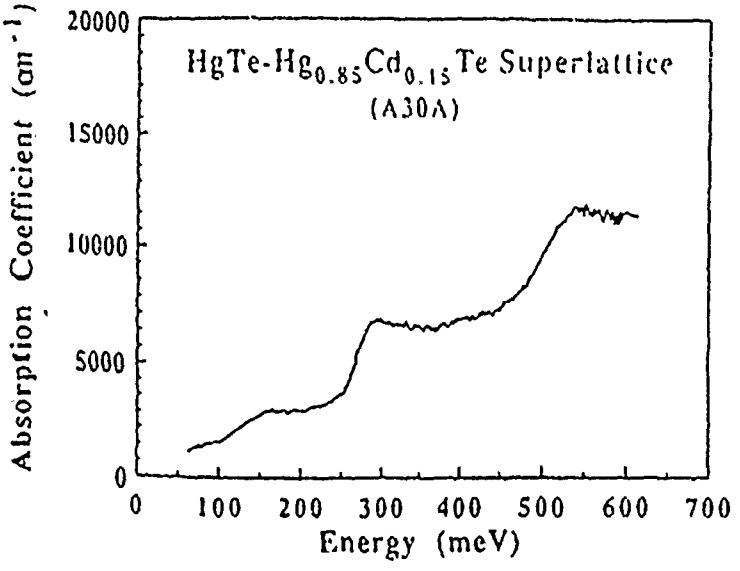

Fig 1 Absorption vs photon energy curve for an undoped HgTe-HgCdTe superlattice

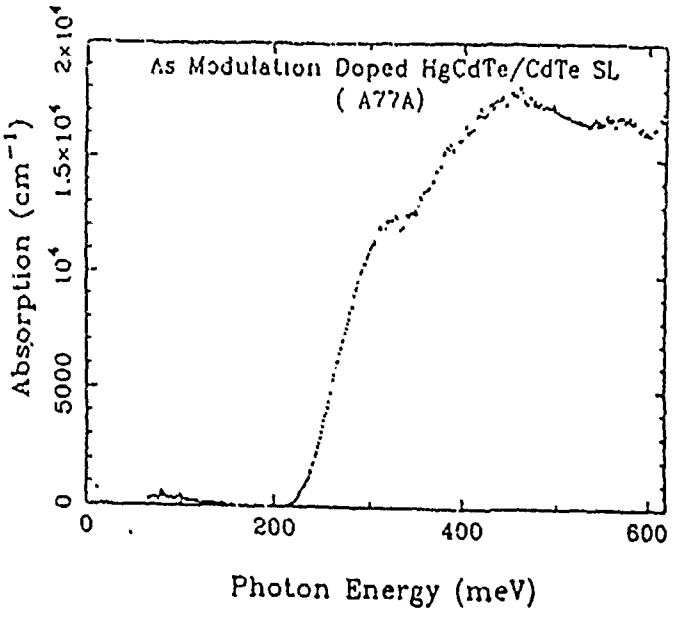

Fig.2 Absorption vs photon energy curve for an As modulation-doped HgTe-HgCdTe superlattice

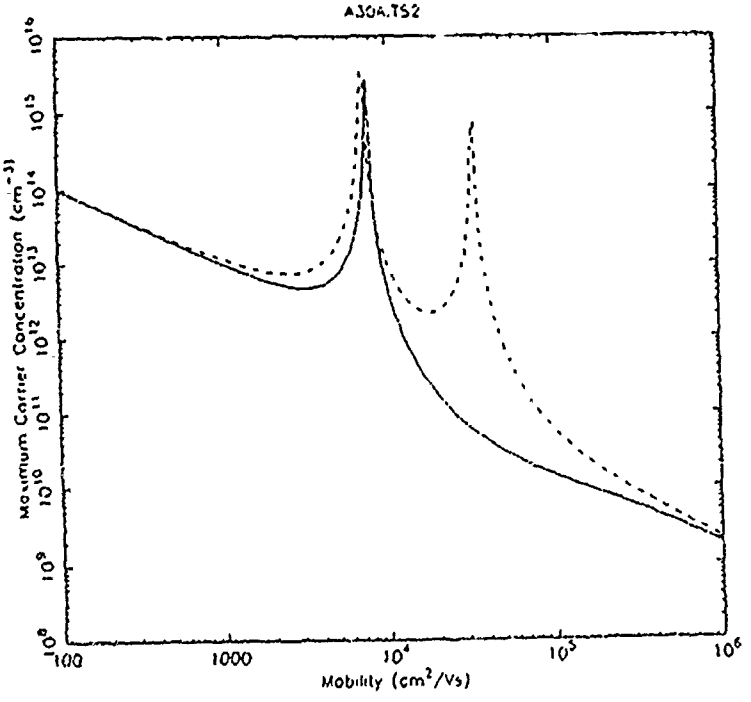

Fig. 3 Mobility spectrum for an undoped HgTe-HgCdTe superlattice The solid curve and dashed curve correspond to electrons and holes, respectively.

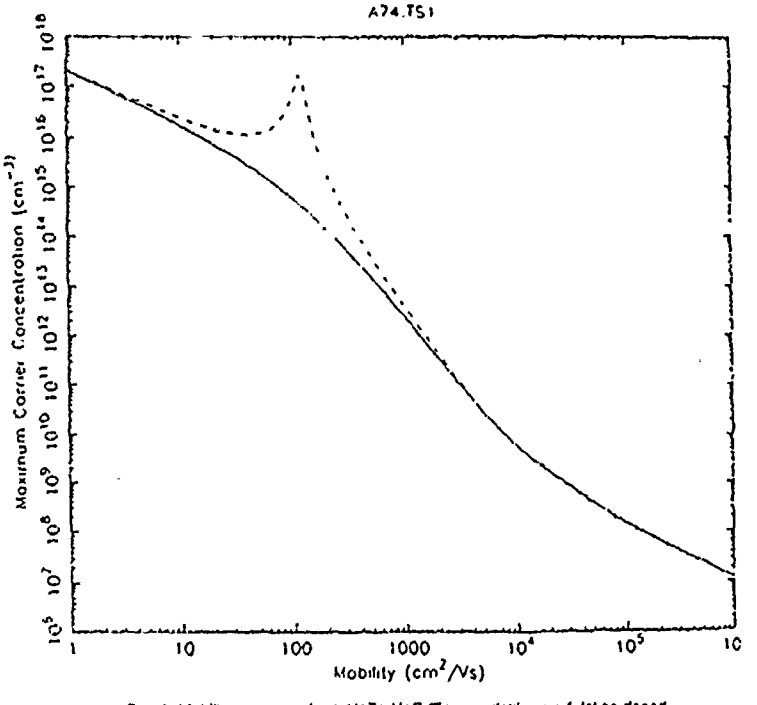

Fig 4 Mobility spectrum for a HgTe-HgCdTe superlattice modulation-doped with As. The solid curve and dashed curve correspond to electrons and holes, respectively.

INFRARED OPTICAL AND FAR-INFRARED MAGNETOOPTIC PROPERTIES OF HgTe/CdTe SUPERLATTICES AND MULTIPLE QUANTUM WELLS

Z. Yang, Z. Yu, Y. Lansari, J.W. Cook, Jr., and J. F. Schetzina
Department of Physics, North Carolina State University, Raleigh, NC. 27695-8202

HgTe/CdTe superlattices (SLs) and multiple quantum wells (MQWs) are alternatives to the HgCdTe alloy for infrared optoelectronic device applications. The electrical and optical properties of these new quantum structures are, however, still not well understood. Low temperature Infrared transmission and far-infrared magneto-transmission experiments have been completed on a series of HgTe/$Cd_{0.85}Hg_{0.15}Te$ SLs and MQWs to further understand these properties.

Infrared transmission spectra in the spectral region from 1 to 12 μm and in the temperature range from 4.2 to 300 K were obtained for five SLs and four MQWs. The well and barrier thicknesses for each sample are listed in Table 1. The five SLs all have positive band gaps, while the MQWs all have small negative band gaps. In the case of the SLs, the splitting of the first heavy hole subband and the first light hole subband was well seen in all of the transmission spectra. In the case of the MQWs, the light hole subband to the conduction subband transition was observed. Transitions to higher conduction subbands were also observed. All transition energies shift to lower energy when the temperature is lowered. An example is show in Fig. 1. Theoretical analysis of the results indicates that the valence band offset between HgTe and CdTe is 400 ± 100 meV and is temperature-independent.

Far-infrared magneto-transmission measurements were completed on the same SL and MQW samples in the photon energy range 4 - 13 meV, in the temperature range from 4.2 to 200 K, and in magnetic fields up to 7 Tesla. In the case of the MQWs, intraband electron cyclotron resonance was observed. Two resonance lines were observed for MQW samples A57B and A58B, while one broad line was observed for samples A59B and A60B. The electron effective masses obtained from the positions of the resonant lines in the transmission vs. magnetic field spectra are listed in Table 2. It is seen that the electron effective mass *increase* as the well width *increases.* This is because, for the MQWs, the band gap becomes more negative when the well layer thickness is increased; therefore the effective mass becomes larger. Detailed analysis of the data, using a six-band K·P model, will be presented. Results for additional SL and MQW samples, currently being studied, will also be reported.

Table 1

Sample	L_z(Å)	L_b(Å)
A17S	58.2	42.1
A18S	58.2	42.1
A19S	35.6	32.4
A20S	45.4	38.4
A21S	54.9	42.1
A57B	81.0	100.4
A58B	90.7	100.4
A59B	110.2	100.4
A60B	158.8	100.4

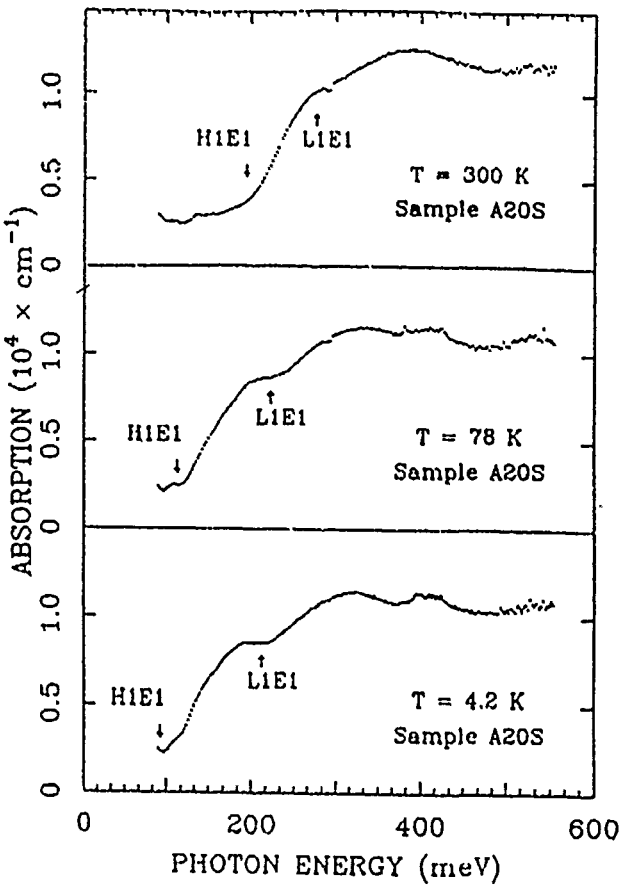

Figure 1

Table 2

Sample	Effective Mass (m_0)	
	E1	E2
A57B	0.0087	0.012
A58B	0.013	0.016
A59B	0.017	
A60B	0.025	

Magneto-optical Transitions Between Subbands with Different Quantum Numbers in Narrow Gap HgTe-CdTe Superlattices

H. Luo and J.K. Furdyna
Department of Physics, University of Notre Dame, Notre Dame, Indiana 46556
and
L.R. Rom-Mohan
Department of Physics, Worcester Polytechnic Institute, Worcester, Massachusetts 01609

Theoretical studies of magneto-optical spectra in HgTe-CdTe superlattices so far have focused on transitions involving $\Delta N = 0$, N being the subband quantum number. In the present study, we consider magneto-optical transitions in HgTe-CdTe superlattices involving $\Delta N = \pm 1$.

In a superlattice or a quantum well couplings between the conduction band and the valence bands lead to the mixing of subbands of different quantum number N.[1,2] The conduction band and valence band couplings via the momentum matrix element are particularly strong in narrow gap superlattices. Such mixing results in significant transitions involving $\Delta N \neq 0$, among which $\Delta N = \pm 1$ transitions are dominant. By considering the symmetries of the wave functions in the presence of an applied magnetic field parallel to the growth direction, the selection rules are[2]

$$\text{CRA (or } \sigma_L\text{): } a_n \rightarrow a_{n+1}, \quad b_n \rightarrow b_{n+1},$$
$$\text{CRI (or } \sigma_R\text{): } a_n \rightarrow a_{n-1}, \quad b_n \rightarrow b_{n-1},$$

for $\Delta N = 0$, and

$$\text{CRA: } a_n \rightarrow b_{n+1}, \quad b_n \rightarrow a_{n+1},$$
$$\text{CRI: } a_n \rightarrow b_{n-1}, \quad b_n \rightarrow a_{n-1},$$

for $\Delta N = \pm 1$, where a and b represent the two spin states[3] and n is the Landau level quantum number. Like the $\Delta N = 0$ case, transitions having $\Delta N = \pm 1$ are allowed when $\Delta n = \pm 1$ in the Faraday configuration. In contrast to the $\Delta N = 0$ transitions, however,

the $\Delta N = \pm 1$ transitions are between different spin states.

Numerical calculations in the $\mathbf{k}\cdot\mathbf{p}$ approximation of the transition probabilities were carried out for a superlattice of HgTe-CdTe (60Å-40Å), in a magnetic field parallel to the growth direction. Some of the Landau levels belonging to different subbands involved in the transitions of interest are shown in Figure 1, where the dashed lines (labeled by primes) and the solid lines correspond to the two different spin states b and a, respectively. The calculated probabilities are in agreement with the selection rules given above.

The ratio of the calculated transition probabilities (at $\mathbf{B}$ = 2 Tesla), involving Landau levels in E1, E2, LH1, HH1 and HH2 subbands, to the probability of the allowed -1(LH1) $\rightarrow$ 0(E1) transition are listed in Table 1. The Table shows that these transitions, which have been considered to be forbidden or weak, and which to our knowledge have not been studied in HgTe-CdTe superlattices, can in fact be observed. Since transitions from two heavy hole subbands (or two light hole subbands) to the same conduction subband can be observed, one can thus obtain direct information about the quantum confinement of the heavy hole (or light hole) band alone, providing important information on issues related to the band structure, such as the valence band offset.

Furthermore, in Table 1 one finds that transitions between LH1 and E2 subbands can also be strong. Therefore, by comparing transition energies of LH1 $\rightarrow$ E1 transitions and of LH1 $\rightarrow$ E2 transitions, one can study the conduction subbands without complications related to other bands.

References

1. J.N. Schulman and Y.C. Chang, Phys. Rev. B **24**, 4445 (1981).
2. H. Luo and J.K. Furdyna, Phys. Rev. B **41**, 5188 (1990).
3. C.R. Pidgeon and R.N. Brown, Phys. Rev. **146**, 575 (1966).

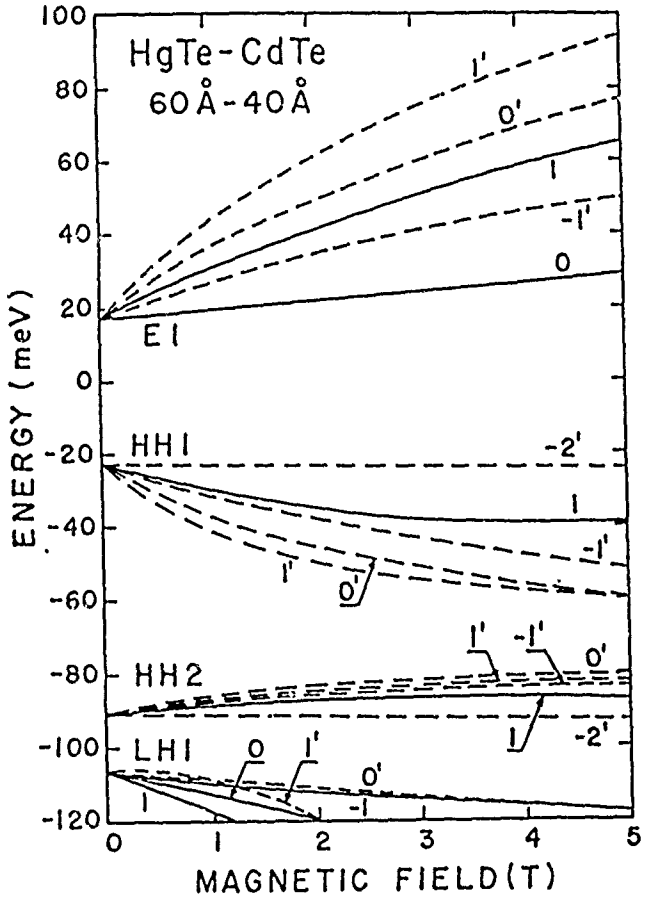

Figure 1. Landau levels at $q_z = 0$ as a function of applied magnetic field. The solid lines and the dashed lines represent the two spin states, a and b, repectively.

Table 1. The ratio of the transition probabilities to the probability of the allowed -1(LH1) → 0(E1) transition, and the polarizations needed to observe the transitions.

Transition	Probability	Polarization
1(HH2) → 0′(E1)	0.13	CRI/σ_R
−1′(HH2) → 0(E1)	0.53	CRA/σ_L
0′(HH2) → 1(E1)	0.44	CRA/σ_L
0(LH1) → 1′(E2)	0.94	CRA/σ_L
1′(LH1) → 0(E2)	0.51	CRI/σ_R
-1(LH1) → 0′(E2)	0.93	CRA/σ_L

Shubnikov-de Haas Oscillations and Quantum Hall Effect in Modulation-Doped HgTe-CdTe Superlattices

C. A. Hoffman, J. R. Meyer, D. J. Arnold, and F. J. Bartoli
Naval Research Laboratory, Washington, D. C. 20375

Y. Lansari, J. W. Cook, Jr., and J. F. Schetzina
North Carolina State University, Raleigh, NC 27695

We have investigated quantum oscillations in the magneto-transport properties of modulation-doped HgTe-CdTe superlattices grown by MBE. Indium donors or arsenic acceptors were incorporated into the CdTe barriers of the superlattices. Low-temperature electron mobilities remained above 4×10^4 cm^2/Vs at $N_D - N_A$ up to 8×10^{15} cm^{-3}, although the hole mobilities in p-type samples with $N_A - N_D$ up to 6×10^{16} cm^{-3} were found to be more strongly dependent on doping level. Some samples of both types displayed strong Shubnikov-de Haas oscillations in the magneto-conductivity at low temperatures.

Figure 1 illustrates the ratio of the oscillating and non-oscillating components of σ_{xx} as a function of inverse magnetic field. Up to 5 oscillations are observed at $T = 2$ K (solid curve), and a fit to the temperature decay of the magnitude (data at $T = 10$ K are shows by the dashed curve) yields an in-plane hole mass of $\approx 0.12 m_0$. This is a factor of 3 larger than the theoretical value of the superlattice hole for the appropriate well and barrier thicknesses.Furthermore, for the hole density determined from a mixed-conduction analysis of the non-oscillating magneto-transport data, holes uniformly distributed throughout the superlattice should all occupy the lowest Landau level at magnetic fields far below those at which the oscillations are observed. However, the mixed-conduction analysis also indicates the presence of a second hole species, apparently corresponding to quasi-2D carriers residing either at the interface of the superlattice with the substrate or at the top surface of the superlattice. The mobility and 2D density of this hole agree well with that of the carrier producing the Shubnikov-de Haas oscillations in Fig. 1. As further evidence, we plot in Fig. 2 the magnetic-field dependence of σ_{xy} in

units of $e^2/2\pi\hbar$. The quantum Hall plateaus evident in the figure occur at integer steps representing the number of conducting channels (i.e., i is the product of the number of occupied Landau levels and the number of participating superlattice wells). Since the step corresponding to $i = 3$ is quite well resolved, we must conclude that at most 3 wells contribute to the conduction, implying that the relevant holes do not reside in the interior of the 200-period superlattice. These data closely resemble the results of previous studies of low-order quantum Hall plateaus in HgTe-CdTe structures. Ong et al.[1] observed plateaus corresponding to $i = 2$ through 12 in a 12-period n-type superlattice, while Woo et al.,[2] observed $i = 9$ and $i = 18$ in a 100-period p-type superlattice. In both cases, the quantum effects occurred at magnetic fields well above those at which carriers in the interior of the superlattice should have reached the extreme quantum limit. As we have shown for the data in Fig. 2, it seems probable that previous observations of the quantum Hall effect in HgTe-CdTe superlattices were associated with quasi-2D carriers near the top or bottom surface of the superlattice.

We contrast this with the data shown in Figs. 3 and 4 for an n-type sample with $N_D - N_A \approx 8 \times 10^{15}$ cm^{-3}. Based on this density the electrons should all occupy the lowest Landau level whenever $B > 0.5$ T, and in fact a wide quantum Hall plateau in ρ_{xy} begins at $B \approx 0.7$ T. In the same field range, ρ_{xx} falls nearly to zero as expected when states near the Fermi level are localized. The plot of σ_{xy} vs B in Fig. 4 shows that the plateau occurs at $i \approx 140$, indicating that most of the 200 periods in the superlattice contribute to the conduction. We argue that this represents the first observation of the quantum Hall effect associated with carriers distributed throughout the interior of a HgTe-CdTe superlattice. For the GaAs-$Ga_{1-x}Al_xAs$ system, Stormer et al.[3] have shown that whereas the quantum Hall effect is a 2D phenomenon, it can be observed in 3D superlattices if the mini-band width is smaller than the Landau level spacing. Band structure calculations verify that this requirement is satisfied for the n-type superlattice discussed here.

1. N. P. Ong, J. K. Moyle, J. Bajaj, and J. T. Cheung, J. Vac. Sci. Technol. A 5, 3079 (1987).

2. K. C. Woo, S. Rafol, and J. P. Faurie, Phys. Rev. B 34, 5996 (1986).

3. H. L. Stormer, J. P. Eisenstein, A. C. Gossard, W. Wiegmann, and K. Baldwin, Phys. Rev. Lett. 56, 85 (1986).

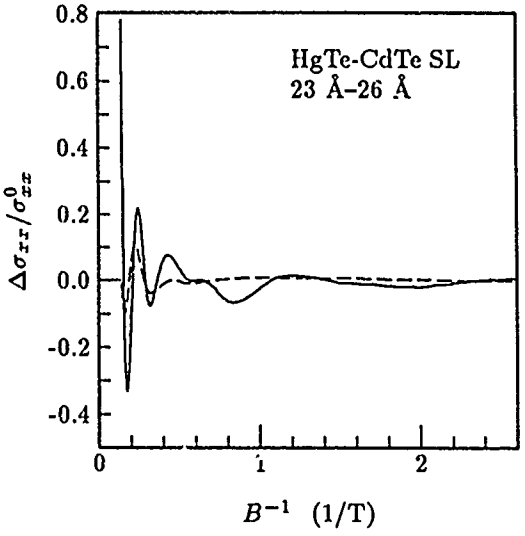

Figure 1. Ratio of the oscillatory and non-oscillatory components of the diagonal conductivity vs inverse magnetic field, for a p-type HgTe-CdTe superlattice with the indicated layer thicknesses. Two temperatures are shown, 2 K (solid curve) and 10 K (dashed curve).

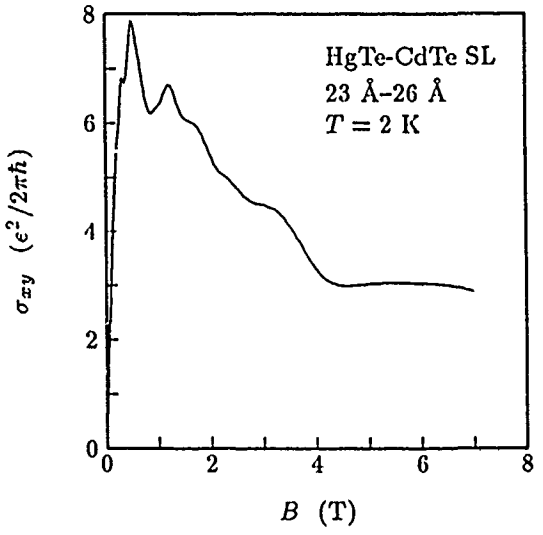

Figure 2. Hall conductivity vs magnetic field at $T = 2$ K, for the same superlattice as in Fig. 1. Lower-order quantum Hall plateaus are well resolved.

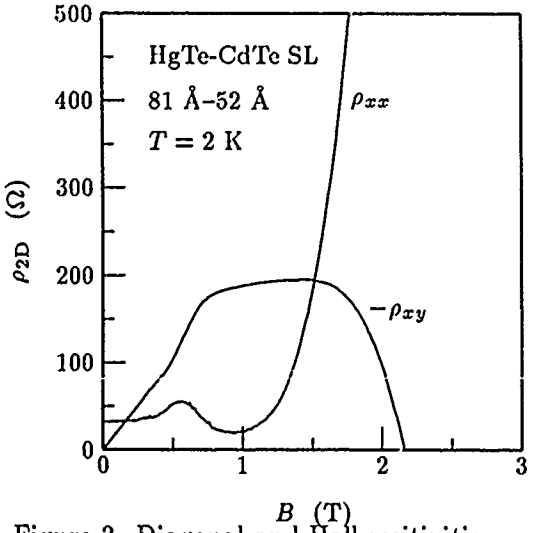

Figure 3. Diagonal and Hall resitivities vs magnetic field at $T = 2$ K, for an n-type HgTe-CdTe superlattice.

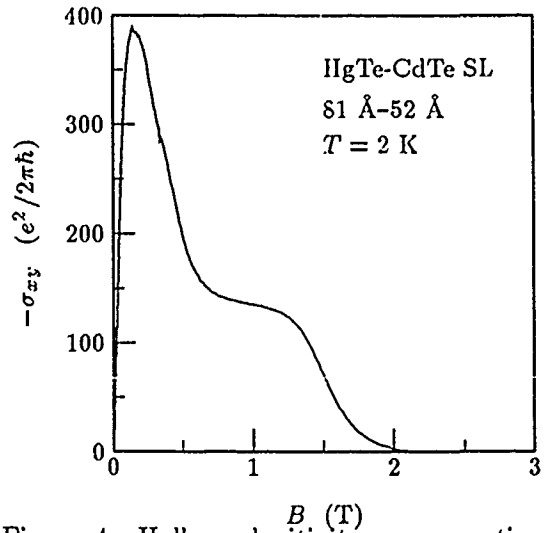

Figure 4. Hall conducitivity vs magnetic field at $T = 2$ K, from the same data as in Fig. 3. For this 200-period superlattice, the quantum Hall plateau occurs at $i \approx 140$.

Theory for Electron and Hole Transport in HgTe-CdTe Superlattices

J. R. Meyer, D. J. Arnold, C. A. Hoffman, and F. J. Bartoli
Naval Research Laboratory, Washington, D. C. 20375

L. R. Ram-Mohan
Worcester Polytechnic Institute, Worcester, MA 01609

Although extensive experimental results for electron and hole transport in HgTe-CdTe superlattices have been reported in recent years [e.g., C. A. Hoffman et al., Phys. Rev. B 39, 5208 (1989); J. Vac. Sci. Technol. A 8, 1200 (1990)], no previous attempt has been made to explain the data theoretically. This is primarily because none of the available formalisms could account for the highly-unusual band structure of the HgTe-CdTe system. Here we present the first calculation of electron and hole mobilities in HgTe-CdTe heterostructures, using a comprehensive new theory which not only incorporates the narrow-gap superlattice band structure but also includes important multi-well interactions in the scattering problem. Ionized impurity scattering is treated using a generalized potential which for the first time treats both scattering by remote impurities and screening by free carriers in neighboring wells. In contrast to the widely-studied problem of mobilities in a 2DEG at a III-V heterojunction such as $Ga_{1-x}Al_xAs$, the free carrier transport in Hg-based superlattices is shown to occupy a regime intermediate between the 2D and 3D limits considered previously. While the calculation yields nearly equal electron and hole mobilities at low temperatures, the extreme nonparabolicity of the valence band in conjunction with the onset of phonon scattering causes the mobility ratio to be well over an order of magnitude at somewhat higher temperatures. This correlates well with the experimental observation that the hole mobility drops dramatically with

increasing T. Comparison of theory and experiment demonstrates that not only is the ionized impurity scattering mechanism over an order of magnitude too weak to explain the experimental mobilities at low temperatures, the experimental temperature dependence is also different from that predicted for the impurity scattering mechanism. We consider the possibility that interface roughness scattering dominates the low-temperature transport, and correlation will be made with other evidence concerning the sharpness of the interfaces in HgTe-CdTe superlattices.

MINORITY CARRIER LIFETIMES OF MOCVD LWIR HgCdTe ON GaAs*

R. Zucca, D.D. Edwall, J.S. Chen, S.L. Johnston
Rockwell International Science Center
Thousand Oaks, CA 91360

and C.R. Younger
Rockwell International/Electro-Optical Center
Anaheim, CA 92803

MOCVD growth of HgCdTe on GaAs is a promising technique which overcomes the size and crystal quality limitations of CdTe substrates. An important material parameter is the minority carrier lifetime, which determines the ultimate zero bias impedance of a photodiode. We present the first systematic study of the temperature and carrier concentration dependence of minority carrier lifetimes on n-type and p-type layers of MOCVD LWIR HgCdTe grown on GaAs substrates.

Minority carrier lifetimes were measured from the decay of the photoconductive response to short laser pulses. All measurements were done as a function of temperature, from 20K or 78K to room temperature. The lifetime vs. 1/T data are compared with theoretical predictions based on Auger and radiative recombination, which represent the maximum attainable lifetime determined by fundamental properties. When the experimental lifetimes reach the Auger + radiative theoretical value, excellent fits are observed over the full temperature range (Fig. 1).

We will show that for both undoped and In doped n-type material the experimental lifetimes match the theoretical Auger + radiative prediction for carrier

* Work funded by SDIO/TNS, sponsored by AFSTC/SWS, managed by WRDC/MLPO, Contract No. F33615-89-C-5557.

concentrations higher than $2x10^{15}$ cm^{-3}. For lower carrier concentrations, the measured lifetimes are shorter than those predicted from Auger + radiative recombination. These deviations from the Auger + radiative lifetimes at low carrier concentration will be discussed in terms of Shockley-Reed recombination.

Plots of lifetime vs. carrier concentration (Fig. 2) show that the lifetimes of arsenic doped p-type material are one order of magnitude longer than those previously observed on vacancy doped LPE material,[1] and match the Auger + radiative theoretical values for carrier concentrations larger than $4x10^{15}$ cm^{-3}. Contrary to observations on LPE layers,[1] the minority carrier lifetimes of vacancy doped p-type MOCVD material also match the theoretical Auger + radiative prediction, and they are aligned with the arsenic doped lifetimes when plotted against carrier concentration.

---

1. J.S. Chen, J. Bajaj, W.E. Tennant, D.S. Lo, M. Brown and G. Bostrup, Proc. Mat. Res. Soc. Symp., v90, pp. 287-293, Dec. 1986.

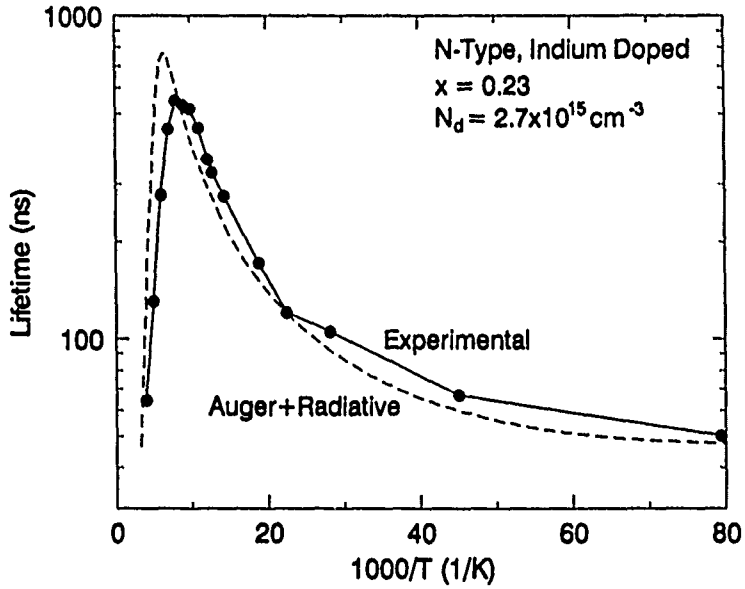

Fig.1. Example of temperature dependence of minority carrier lifetime for indium doped n-type MOCVD HgCdTe on GaAs. The experimental data match a theoretical prediction based on Auger and radiative recombination, without any adjustment of parameters.

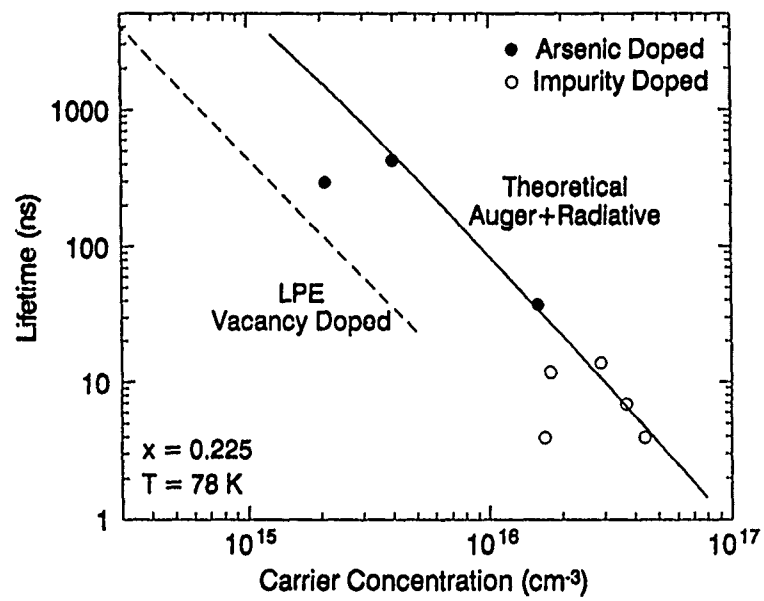

Fig.2. Dependence of minority carrier lifetime on carrier concentration for p-type MOCVD HgCdTe (x=0.225) on GaAs. The lifetimes of arsenic doped and vacancy doped material are compared with those of LPE material, and with theoretical values based on Auger and radiative recombination.

MECHANISMS FOR CARRIER CAPTURE AT POINT DEFECTS IN CADMIUM MERCURY TELLURIDE

R. S. Hall(*) and S. C. Barton(**)
(*) Royal Signals and Radar Establishment, Malvern, UK
(**) Philips Infrared Defence Components, Southampton, UK

High quality p-type cadmium mercury telluride (CMT) with a long carrier lifetime is required for improved performance photovoltaic infrared detectors. The low temperature (≤80K) carrier lifetime in CMT is limited by 'Shockley-Read' (SR) recombination through defects. The SR lifetime at a particular temperature depends on 4 defect parameters: defect density, the energy level position in the forbidden gap and the electron (σ_n) and hole (σ_n) capture cross sections. Only rarely has consideration been given to the mechanism of carrier capture[1,2]. The most likely energy loss mechanisms are (1) photon (radiative) emission (2) carrier-carrier collisions (defect Auger processes) or (3) phonon emission. Each of these processes is discussed briefly below in terms of an effective capture cross section.

Most cross section determinations in CMT have been either from fitting Shockley-Read formulae with temperature independent σ_n and σ_p to transient lifetime-temperature measurements, or from DLTS measurements on space charge regions in which a thermally activated cross section was assumed. Theory predicts very different magnitudes and temperature dependencies for the different processes, giving us the possibility of discriminating between mechanisms. The three energy loss mechanisms are briefly examined below.

Radiative Capture. The radiative capture rate and hence cross section is related to the radiative absorption rate by detailed balance and was calculated using a photoionisation cross section (σ^0) value of 10^{-16} cm^2, probably an overestimate for most traps. The value of σ^0 is not known for any defects in x=0.2-0.25 CMT. The resulting capture cross sections for electrons and holes are plotted in Fig. 1 against temperature. It is clear that $\sigma_n < 10^{-18}$ cm^2 at all temperatures. The values of σ_p are in the range 10^{-23}-10^{-20} cm^2. Radiative capture cross sections are almost temperature independent except at very low temperatures (<20K). Experimentally determined values of σ_n (typically 10^{-16}-10^{-14} cm^2) [1,3] are too large to be explained by radiative capture.

Auger Capture. Auger processes are important in CMT. The Auger-1 band-to-band process dominates the carrier lifetime at high temperatures. Two models describing Auger capture processes at traps[2,4] have been

considered. The model of Pines & Stafsudd[2] was developed specifically for narrow gap semiconductors including CMT. The Auger σ_n against temperature for x=0.22, 10^{16} cm^{-3} p-type CMT in zero FOV is shown in Fig. 2 for a hydrogenic defect and a highly localised defect. The very rapid rise of the cross section with temperature is due to the exponential behaviour of the electron density in p-type material at low temperature. The second model[4] predicts cross sections which differ essentially only by a factor of (10^{-7}/ defect wavefunction radius [cm]).

Phonon Emission Capture. There are two basic models for phonon emission capture. The first is commonly known as a Lax cascade[5] and the second is known as multi-phonon emission (MPE). Lax cascades, first used to explain 'giant' cross sections (>> 10^{-14} cm^2) in Si and Ge[5], involve the emission of either acoustic or longitudinal optical (LO) phonons. The cross sections have been calculated using the phonon mean free paths. The acoustic phonon mean free path was obtained from lattice force parameters and the LO- phonon mean free path from the electron mobility. The MPE cross section estimation in CMT is difficult; semi-classical expressions are not valid. The quantum approach of Ridley is more acceptable[4,6]. Calculations have been made in which one defect parameter, describing the defect localisation, is all that is needed to calculate cross sections for neutral point defects. The cross sections for shallow hydrogenic and highly localised midgap defects have been calculated and are shown in Fig. 3. The largest values of σ_n and σ_p occur for highly localised defects.

Discussion. Radiative capture is too slow to account for observed cross sections and lifetime results. Defect-Auger capture models give passable agreement with experimental lifetime data in n-type material and are certainly important in n-type and intrinsic material. Evidence for phonon emission is found in high field magnetic quantum oscillations in n-type material[7] in which 34meV and 50meV(2 and 3* LO phonon frequency) transitions to bandgap states have been observed. Phonon emission will dominate in extrinsic p-type material when there are many localised centres such as vacancies present. In conclusion, the nature of the dominant trap and the carrier concentrations determine whether an Auger or phonon emission process occurs during carrier capture at point defects in CMT.

References

[1] Polla D L & Jones C E J. Appl. Phys. 52, 5118 (1981)
[2] Pines M Y & Stafsudd O M Infrared Phys. 20, 73 (1980)
[3] Merilainen C A & Jones C E J. Vac. Sci. Technol. A 1, 1637 (1983)
[4] Ridley B K "Quantum processes in Semiconductors", 2nd. ed., Oxford University Press (1988)
[5] Lax M Phys. Rev. 119, 1502 (1960) [6] Ridley B K J. Phys. C 11, 2323 (1983)
[7] Ipposhi T, Takita K and Masuda K J. Phys. Soc. Japan 57, 1013 (1988)

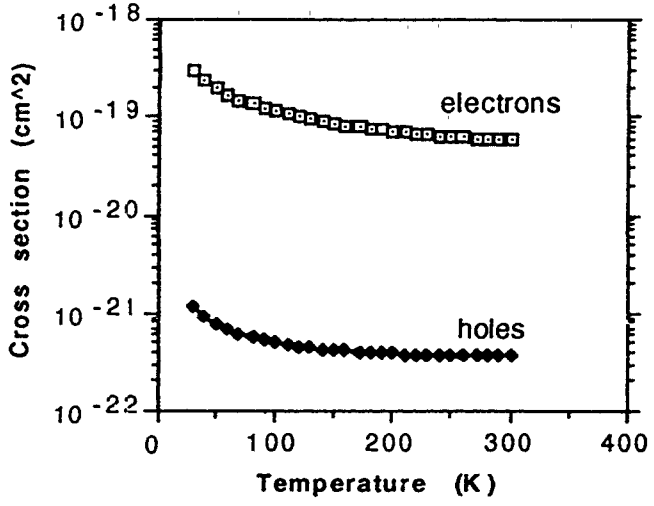

Fig. 1 High estimates of the radiative capture cross sections for electrons & holes in x=0.22 CMT as a function of temperature.

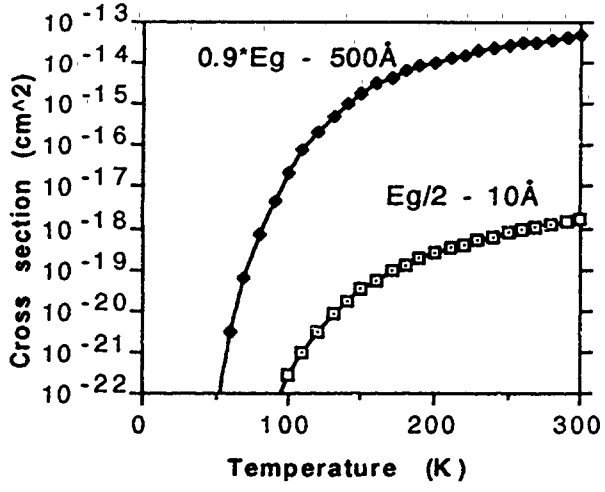

Fig 2. The Auger electron capture cross section temperation variation for x=0.22, 1.0*10^16 cm^-3 p-type CMT in the Pines & Stafsudd[2] model for the cases of a hydrogenic donor and a localised midgap centre.

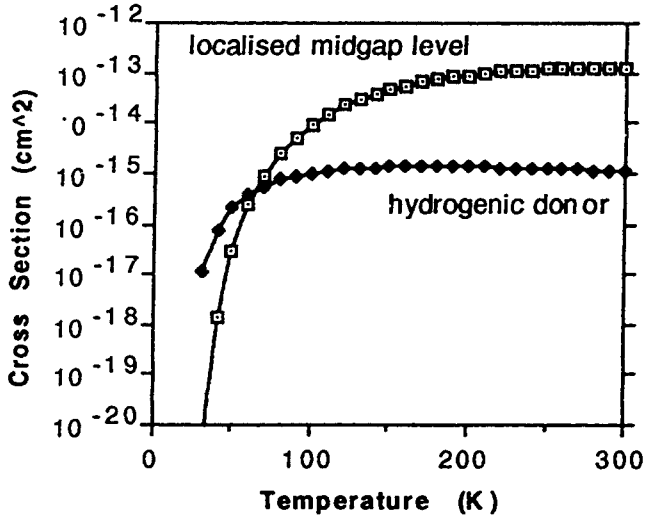

Fig. 3. The multiphonon emission electron capture cross section calculated for a shallow donor centre and a localised midgap centre.

TRAPPING EFFECTS IN HgCdTe

Y. Nemirovsky, R. Fastow, M. Meyassed and A. Unikovsky
Kidron Microelectronics Research Center, Dept. of Electr. Engineering
Technion - Israel Institute of Technology, Haifa 32000, Israel

ABSTRACT

Understanding the dynamics of trapping and the properties of traps in HgCdTe is required for characterizing material grown by various methods and obtained from different sources. The presence of traps affects the performance of all HgCdTe detectors regardless of their type or configuration.

In the past two decades, different techniques have been applied to identify traps and to determine their energy distribution and density, such as deep level transient spectroscopy (DLTS), [1,2] diode pulse recovery,[3,4] optical modulation absorption (OMA), and more recently the two-photon magneto-optical (TPMO) technique.[5] In addition, a number of theoretical approaches have been applied to estimate the properties of defects and traps in HgCdTe.[6-9]

This paper focuses on trapping phenomena that is directly related and extracted from current HgCdTe detectors (i.e. photoconductors and MIS as well as junction photodiodes).

Three topics are considered:

(a) Trap assisted tunneling in MIS and junction photodiodes.
(b) Trapping and recombination processes, as related to the excess carrier lifetime in steady state and transient measuremtns.
(c) Trapping as related to the noise current spectral density of devices.

(a) Trap Assisted Tunneling

At operating temperatures around 77 K, trap assisted tunneling is the dominant dark current mechanism over a wide range of biases in LWIR HgCdTe MIS diodes[10,11] as well as in junction photodiodes.[12,13]

Trap assisted tunneling exhibits a distinct temperature dependence that is remarkably different from band-to-band tunneling or thermally limited mechanisms.

In this study, we model the bias dependence as well as the temperature dependence of trap assisted tunneling. The model is based on two assumptions: that the dominant energy level in trap assisted tunneling coincides with the Fermi level, and that the tunneling proceeds via thermally excited bulk Shockley-Read centers. This model qualitatively fits previously measured data for MIS diodes fabricated on p-type material as well as the data for photodiodes.

(b) Trapping and the Excess Carrier Lifetime

Trapping is responsible for the large variation in reported "life times" in p-type material. In particular, in material dominated by Shockley-Read recombination, trapping is manifested by the large differences between steady state "lifetimes" and transient "lifetimes" measured on the same samples.[14,15]

A simple approach is presented which illuminates the role of trapping in transient experiments and correlates the transient "lifetime" with the properties of the trapping centers.

(c) Trapping and Noise

Traps contribute two types of excess noise in devices: 1/f noise which is correlated with the dark current associated with trap assisted tunneling, and generation-recombination noise.

Traps contribute to fluctuations in the density of carriers with a variance that is related to the concentration of the traps and a characteristic "knee" frequency that is determined by the "lifetime" of the trapped carriers.

The technique of noise spectroscopy is applied to obtain the trap energy distribution as well as the concentration and capture coefficients.

In summary, the unified approach to three major trapping phenomena in HgCdTe detectors illustrates the role of traps and suggests simple yet quantitative methods of characterizing trapping centers in HgCdTe material.

References

1. C.E. Jones, V. Noir, D.L. Polla, Appl.Phys.Lett., 39, 248 (1981).
2. D.L. Polla, S.G. Tobin, M.B. Reine and A.F. Good, J. Appl. Phys., 52, 5182 (1981).
3. C.E. Jones, V. Nair, J. Lindquest and D.L. Polla, J. Vac. Sci. Technol., 21, 1987 (1982).
4. D.L. Polla, C.G. Jones, J. Appl. Phys., 52, 5118 (1981).
5. C.L. Litter, MR. Loloee and D.G. Seiler, "Magneto-Optical Investigation of Impurity and Defect Levels in HgCdTe Alloys", J. Vac. Sci. Technology, March (1990).
6. D.T. Cheung, "An overview on defect studies in MCT", J. Vac. Sci. Technol. A3, 128 (1985).
7. C.E. Jones et al., "Status of point defects in HgCdTe", ibid, p.131.
8. C.W. Myles, "Charge state splitting of deep levels in HgCdTe", J. Vac. Sci. Technol. A6, p. 2675 (1988).
9. S. Goetting and C.G. Morgan-Pond, "Deep interstial levels in HgCdTe", ibid, p. 2690.
10. M.A. Kinch, in "Semiconductors and Semimetals", ed. by R.K. Willardson and A.C. Beer (Academic, N.Y., 1981), Vol. 18, p. 313.
11. D.K. Blanks, J.D. Beck, M.A. Kinch, and L. Colombo, "Band-to-band tunnel processes in HgCdTe: comparison of experimental and theoretical studies", J. Vac. Sci. A6, p. 2790 (1988).
12. R.E. DeWammes et al., "Dark current generation mechanisms and spectral noise current in long wavelength infrared photodiodes", ibid, p. 2655.
13. Y. Nemirovsky et al., "Tunneling and dark currents in HgCdTe photodiodes", J. Vac. Sci. Technol. A.7, p. 528 (1989).
14. R. Fastow and Y. Nemirovsky, "The excess carrier lifetime in vacancy and impurity doped HgCdTe", J. Vac. Sci. Technol., March (1990).
15. R. Fastow, D. Goren and Y. Nemirovsky, "Shockley-Read Recombination and Trapping in p-type HgCdTe", to be published in J. Appl. Phys. (1990).

Modelling of Deep -Level Trap Effects on Bulk Cadmium -Mercury -Telluride using Frequency Domain Transient Analysis

V.S. Veerasamy, B.D. Nener, L.Faraone
Department of Electrical and Electronic Engineering
The University of Western Australia
Nedlands, W.A. 6009, Australia

Abstract

The classic work of Rittner [1] in developing a continuity equation describing the behaviour of minority charge carriers under the effect of drift and diffusion in the bulk of semiconductors is well-known. However, it is difficult to include the effects of traps into this analysis. In this paper we analyse the effects of deep levels on the photoconductive response of a semiconductor. In steady state, the developed model predicts that the presence of deep levels has the effect of reducing the photoconductivity of the material when compared to the trap-free case. This effect is simulated for a range of temperatures relevant to the operation of CMT photodetectors. The above predictions correlate with experimental results concerning the variation of resistivity of bulk CMT with temperature [2]. Another outcome of the model is the sublinear variation of photoconductivity with light intensity. The transient response due to incident radiation is also dealt with in the presence of traps. Finally, the mathematical set-up for an alternative derivation of the continuity equation which includes the effects of traps is given together with simulations as applied to CMT photodetectors.

Frequency domain techniques have been found to be more complete in studying photocurrent transients in comparison to time-domain equivalents. The second part of this paper involves the use of the continuity equation in its frequency domain form to characterise deep-levels in bulk material. The Frequency -Domain Transient Analysis (FTDA) [3] allows the full transient response to be exploited instead of focusing on a particular part of the curve as is the case in time -domain measurements. This is done by taking the Fourier transform of the photocurrent transient and thus getting a relation between the input and output in the frequency domain. By using this technique it is possible to experimentally evaluate the trap density, minority carrier lifetime and diffusivity.

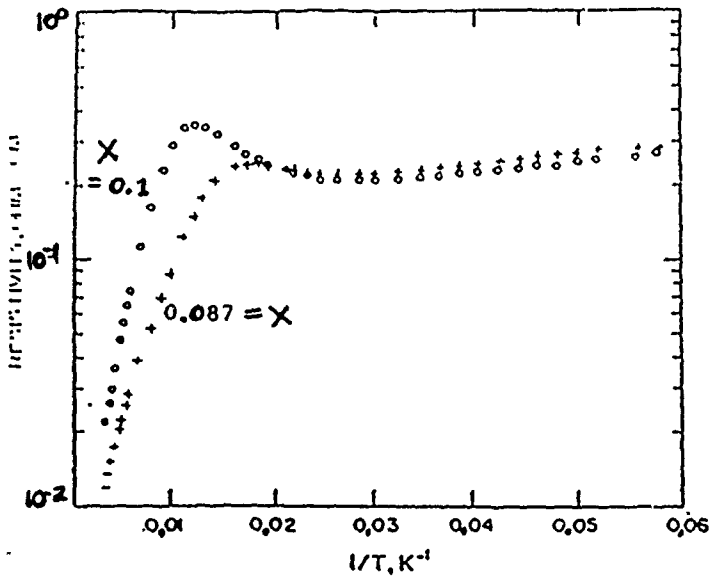

Figure 0.7: Variation of resistivity vs 1/Temperature [2]

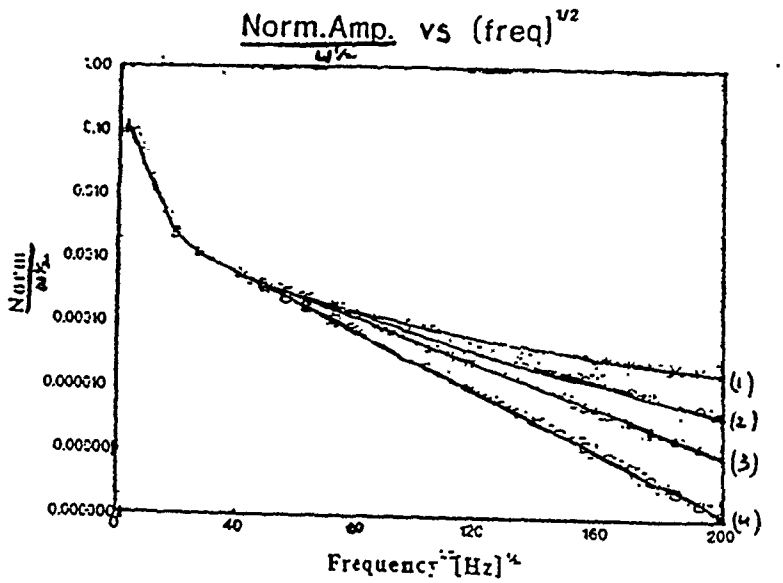

Calculated Amplitude response v/s $\sqrt{Freq}$ for different trap to majority carriers conc. ratio (1) $N_T/n_0 = 0$, (2) 0.5, (3) 0.1, (4) 0.01 for CMT (x =0.2)

References

1. E.S Rittner, "Electron Processes in Photoconductors",*Photoconductivity Conference*,edit. R. G. Breckenbridge , Nov. 1954, pp:215.

2. M.Y Pines *et al*, "Characteristics of n- type Mercury Cadmium Telluride", *Infrared Phys.*, vol 19 pp:633 (1979)

3. K.Misiakos *et al*, "Lifetime and diffusivity Determination from Frequency-Domain Transient Analysis", *IEEE Electron Devices*, vol EDL 8, pp:358, Aug 1987.

Correlation of HgCdTe Epilayer Defects with Underlying Substrate Defects By Synchrotron X-Ray Topography

B.E. Dean, C.J. Johnson, S.C. McDevitt, G.T. Neugebauer, and J. L. Sepich
II-VI Incorporated
Saxonburg, PA, 16056

R.C. Dobbyn and M. Kuriyama
National Institute of Standards and Technology
Gaithersburg, MD, 20899

J. Ellsworth and H.R. Vydyanath
Aerojet Electrosystems
Azusa, CA, 91702

J.J. Kennedy
US Army CECOM/CNVEO
Ft. Belvoir, VA, 22060

Synchrotron X-ray topography studies have been conducted at the National Synchrotron Light Source (NSLS) at Brookhaven National Laboratory to correlate defects in HgCdTe epilayers with those in CdTe family substrates. IR detectors are being fabricated on these epilayers to investigate the effect of specific defects on device performance. Images of substrates and epilayers are discussed and mapping of epilayer/substrate defects is demonstrated.

Figure 1, a topograph of a CdTe substrate (top) and the HgCdTe epilayer (below), shows significant lattice bending. The dark areas of the figure correspond to the areas of the substrate that didn't satisfy the Bragg condition. Despite significant strain, the single exposure coverage of the 2×3 cm^2 substrate and epilayer was almost complete. Several prominent substrate defects propogated into the epilayer. lattice bending, slip lines, a star-shaped precipitate near the surface, and localized lattice distortions. The extent of overall lattice bending in the substrate was on the order of 25 arc second. The magnitude of lattice bending was reduced in the epilayer.

The prominent CdZnTe substrate defects propogating into corresponding epilayers, as shown in Figure 2 are. lattice bending, subgrain boundaries, microtwins and cellular structure. The slip lines, prominent in the case of CdTe, were notably absent. The single exposure coverage the CdZnTe substrate was very poor, indicating that lattice bending was strong (on the order of 300 arc second).

Synchrotron X-ray topography is an effective means for non-destructively screening epilayers and substrates for defects that are not observable by common optical techniques. We found that defects near the epilayer/substrate interface always degrade epilayer quality. Lattice bending, which was present in all substrates, was reduced in epilayers. Growth by LPE reproduced all substrate defects in $Hg_{1-x}Cd_xTe$, $x = 0.2$, epilayers.

Figure 1

Synchrotron Reflection Typographs of a (111) A-face CdTe Substrate (top) and Corresponding HgCdTe Epilayer.

CdTe, 5277-17, $(444)_S$, 1 exposure.

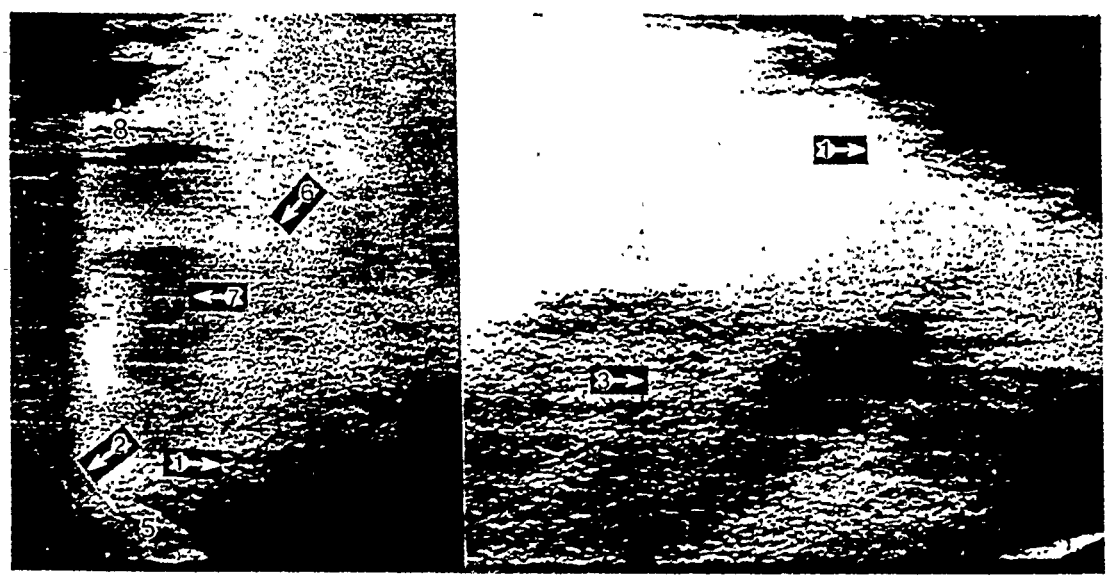

HgCdTe, 5277-17-734, $(444)_S$, 1 exposure.

Defect Key		Pre-topo Characterization	
1. Lattice bending	5 Subgrain boundary	IR transmission	> 50%
2. Microtwin	6 Te precipitate	EPD	$< 4 \times 10^5 cm^{-2}$
3. $[0\bar{1}1](1\bar{1}1)$ slip	7 Cross-hatching	DCRC	25 arcsec
4. $[10\bar{1}](\bar{1}11)$ slip	8 Localized distortion	Precipitates	One region &/or large linear $< 1\mu m$

Figure 2

Synchrotron Reflection Typographs of a $(\bar{1}\bar{1}\bar{1})$ B-face CdZnTe Substrate (top) and Corresponding HgCdTe Epilayer

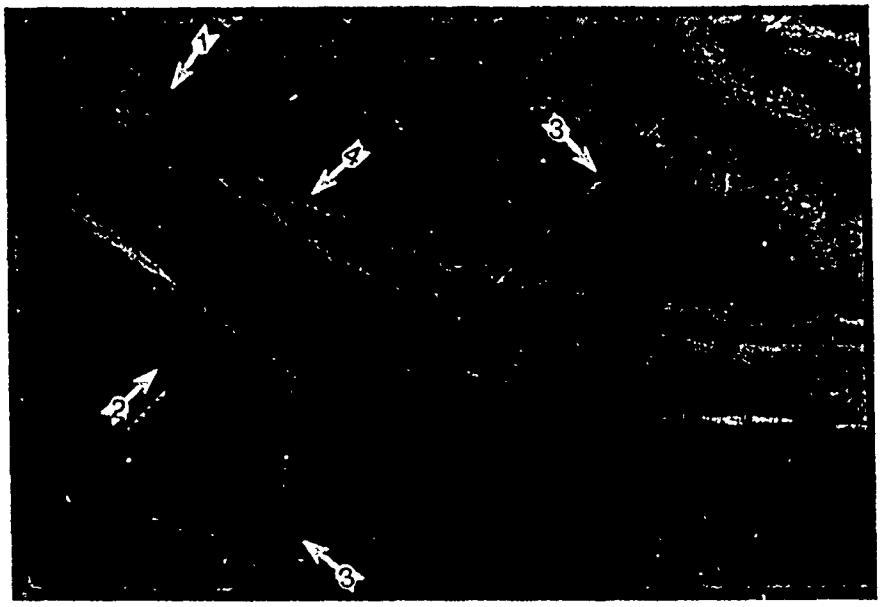

CdZnTe, 4899-20, $(444)_S$, 13 keV, 8 exposures $\Delta\theta \approx 0.01°$.

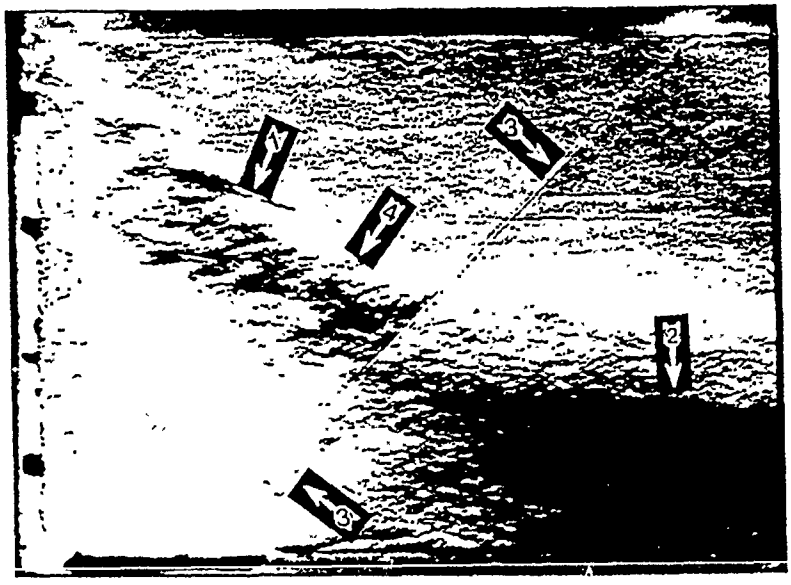

HgCdTe, 676-4899-20 $(444)_S$, 12 keV, 1 exposure.

Defect Key
1. Subgrain boundary
2. Lattice bending
3. Microtwins
4. Defect

Pre-topography Characterization

IR transmission	> 65%
EPD	$< 5 \times 10^4 cm^{-2}$
DCRC	20 arcsec
Precipitates	$16\mu m$

Photoexcited Hot Electron Relaxation Processes in n-HgCdTe Through Impact Ionization Into Traps*

D. G. Seiler and J. R. Lowney
Semiconductor Electronics Division
National Institute of Standards & Technology
Gaithersburg, MD 20899
and
C. L. Littler, I.T. Yoon, and M. R. Loloee
Department of Physics
University of North Texas
Denton, TX 76203

The interaction of optical radiation with semiconductors at near band gap photon energies has led to the observation of a number of novel optical effects including nonlinear absorption and transmission phenomena. In this paper we report on a new type of spectroscopy for impurity or defect levels in the energy gap of narrow gap semiconductors using near band-gap photon energies. This spectroscopy is done under the conditions of intense laser photoexcitation and is associated with the Auger relaxation processes of hot electrons involving impact ionization of valence electrons into impurity or defect levels.

Hot electrons were photoexcited into the conduction band by absorption of intense CO_2 laser radiation. Application of a magnetic field allows the formation of a nonequilibrium electron distribution. Grating tunable cw CO_2 laser pulses were obtained from a mechanical chopper with a low duty cycle to prevent lattice heating effects. The photoconductive (PC) response of the sample was monitored by either boxcar average techniques or magnetic field modulation and lock-in amplifier methods. Two sets of wavelength-independent oscillatory structure in the PC response versus magnetic field occur at high intensities. One set predominates at low fields and the other set at high fields. The amplitude of the structure is largest at the lower temperatures ($\approx$2 K).

The data correspond to intraconduction band energy relaxation of hot photoexcited electrons at liquid helium temperatures in several n-type samples of HgCdTe with $0.22 < x < 0.24$. The low field data was observed in a sample with $x \approx 0.22$. The conditions for which this is seen are that the LO phonon energy is larger than the Landau level separation $\hbar\omega_c$ and only a single photon absorption process is needed to establish the nonequilibrium distribution. The intraconduction band energy relaxation occurs through impact ionization of valence electrons into shallow acceptor levels with energies of 11.5 meV. High field oscillatory structure was observed in samples with $x = 0.22$ and 0.237. This structure arises from hot electrons photoexcited high into the conduction band by sequental absorption of the CO_2 radiation under conditions when the LO phonon energy is less than $\hbar\omega_c$. These hot electrons lose their energy by impact ionizing valence electrons into deep mid-gap levels.

This type of laser spectroscopy thus appears to be a rather simple means for observing and studying predominant impurity/defect levels in narrow gap semiconductors. This work also elucidates the predominant Auger processes occurring after high intensity laser photoexcitation.

*Work supported in part by the Center for Night Vision and Electro-Optics, Fort Belvoir, VA and a grant from Texas Instruments, Inc.

Dislocation Density Variations in HgCdTe Films Grown by Dipping Liquid Phase Epitaxy: Effects on Metal-Insulator-Semiconductor Properties.

D. Chandra, J.H. Tregilgas and M.W. Goodwin

P.O. Box 655936, MS 154, Texas Instruments, Inc.
Dallas, Texas 75265

The dislocation density variations in HgCdTe films grown by liquid phase epitaxy on CdTe and CdZnTe substrates in a dipping reactor from a tellurium rich melt were measured as functions of film thickness and substrate dislocation densities. For films ranging in thickness between 40 μm and 80 μm, the dislocation densities generally tracked the substrate dislocation densities immediately after growth and prior to any heat treatments. Following the stoichiometric adjustment anneals however, the dislocation density increased by degrees ranging between 300 and 1000% (Figure 1). This behavior is similar to the observations made on bulk materials and has been traced to a volume expansion during dissolution of Te precipitates present on existing dislocations by the advancing mercury front [1]. Interposition of a dislocation multiplication reduction annealing procedure prior to the stoichiometric adjustment anneal virtually eliminated the degree of dislocation multiplication. The dislocation density within the 'bulk' of the epifilm, i.e. in regions removed from the 'misfit' dislocation band, again tracked the substrate dislocation density levels approximately. For films with thicknesses less than 40 μm, the film dislocation density generally followed the substrate dislocation density level, both immediately after growth and after the stoichiometric adjustment anneal. No dislocation multiplication anneal procedure needed to be imposed.

For films with thicknesses greater than 80 μm, a progressive decrease in the film dislocation density to levels below the substrate dislocation density was noted. For distances greater than 120 μm from the substrate-film interface, film dislocation density decreased to less than 33% of the substrate dislocation density. A binary recombination mechanism similar to the model suggested by Kroemer et. al. [2] can be invoked to explain this behavior.

All the above results were obtained for films grown with moderate average growth rates: < 1 μm/min. For films grown with growth rates $> 1\mu$m/min, a wide high dislocation density band appears to cover a large part of the film. The pattern

of these dislocations appeared similar to threading dislocations. No evidence of dislocation multiplication similar to the observations described above was noted.

Metal-Insulator-Semiconductor (MIS) devices were fabricated on a number of these LPE films and their performances measured. Dislocation densities were measured on witness pieces sectioned from these films as well as by stripping the MIS devices and defect etching the mercury cadmium telluride active areas under respective devices. Correlations were established between the measured 'dark storage times' and the dislocation densities revealed by the defect etch (Figure 2).

References

1. H.F. Schaake and J.H. Tregilgas, J. Electron. Mater. 12, 931 (1983).

2. H. Kroemer, T.Y. Liu and P.M. Petroff, J. Crystal Growth, 95, 96 (1989).

The authors will only be interested in an oral presentation and publication.

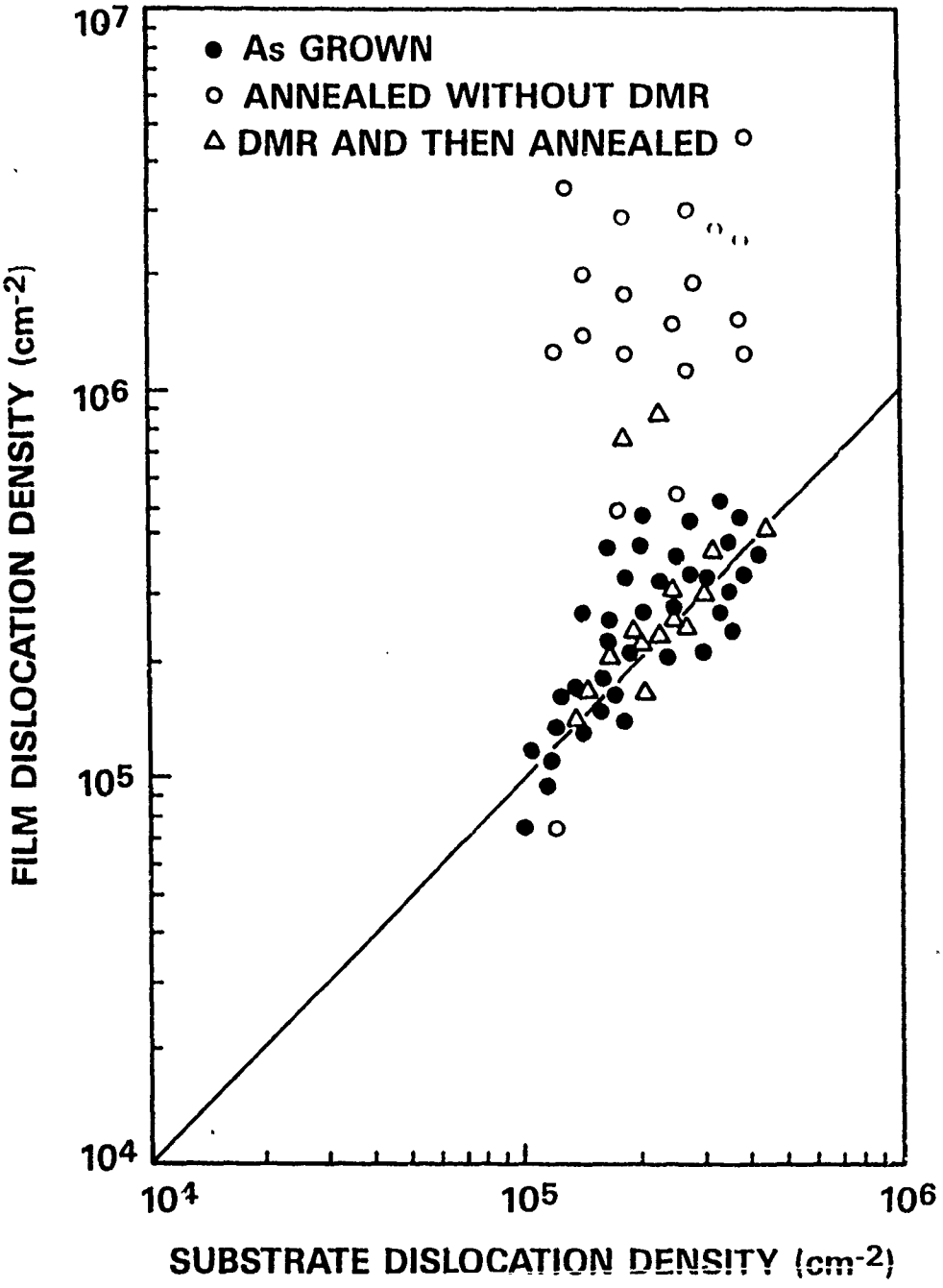

Figure 1. Dependence of the dislocation density within the 'bulk' of the mercury cadmium telluride epifilm (in regions well removed from the substrate-epi interface) on the CdZnTe substrate dislocation density. The respective symbols in the figure signify different heat treatments as indicated in the figure and described in the text. DMR refers to the Dislocation Multiplication Reduction annealing treatment.

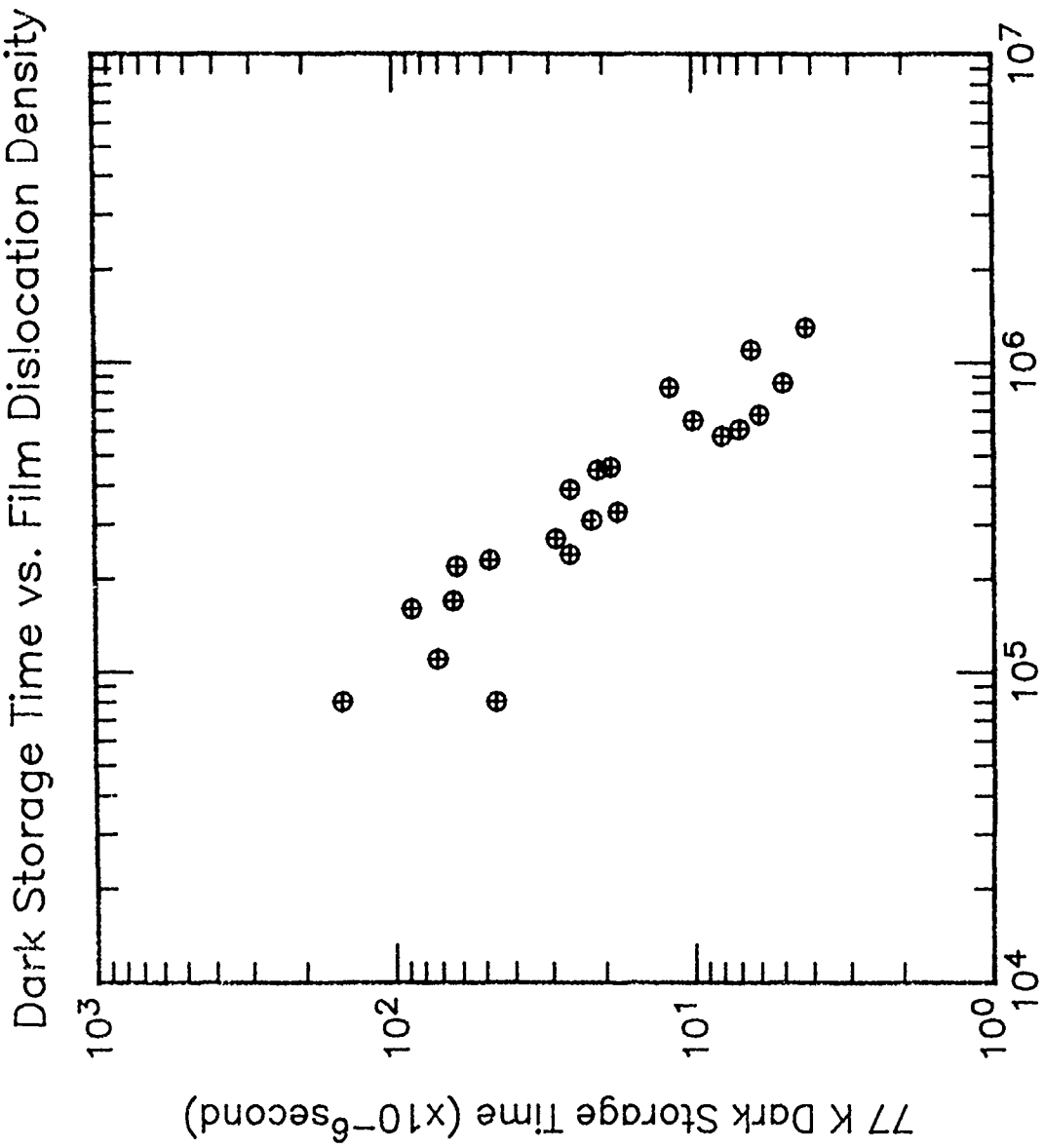

Figure 2. Dependence of the 'dark' storage time of MIS devices built on LWIR LPE films on the film dislocation density.

Surface sublimation energies for MBE growth of HgTe, CdTe, and ZnTe*

Marcy Berding, S. Krishnamurthy, and A. Sher
SRI International, 333 Ravenswood Ave., Menlo Park, CA 94025

We have recently calculated surface sublimation energies of constituent atoms from a completed surface layer (concentrated limit) and of isolated atoms (dilute limit) from ideal surfaces with (111)A, (111)B and (100) orientation [1]. From the dilute and concentrated surface energies, an effective surface pair interaction is deduced and used in a thermodynamic surface model. For HgTe, the effective pair interactions are attractive, implying the usually expected smooth layer by layer growth below some order/disorder temperature. Double-layer surface free-energy diagrams will be presented that clearly distinguish between Hg and Te stablized MBE growth. For several surfaces of CdTe, the effective pair interactions are repulsive, implying ordered arrangements of the surface atoms and vacancies will occur below some order/disorder temperature. The above calculations will be extended to ZnTe as well, and presented at the conference. We will discuss the implications of these calculated surface properties on the nature of the growing surfaces and resulting film quality. We will also discuss the extention of the current calculations to the alloys HgZnTe and HgCdTe.

*This work was supported by ONR and NASA.

[1]. S. Krishnamurthy, M.A. Berding, A. Sher, and A.-B. Chen, Phys. Rev. Lett. (in print).

STRUCTURAL CHARACTERIZATION OF THE (111) SURFACE S OF CdZnTe SUBSTRATES AND HgCdTe EPILAYERS BY X - RAY PHOTOELECTRON DIFFRACTION

M. Seelmann–Eggebert and H. J. Richter

Fraunhofer–Institut für Angewandte Festkörperphysik
D–7800 Freiburg, Federal Republic of Germany

In a previous study we have published preliminary data on x–ray photoelectron diffraction (XPD) obtained for the (111)B surfaces of CdZnTe and HgCdTe[1] . As exemplified by selected angular (polar and azimuthal) scans those first measurements already revealed characteristic anisotropies in the angle–resolved photoemission originating from the Te $3d_{5/2}$, Cd $3d_{5/2}$, and Hg $4f_{7/2}$ core levels.

In this continued and more detailed study we now present complete sets of XPD data taken for all directions of photoelectron escape with improved angular resolution, and we examine the (111)B as well the (111)A surface of CdZnTe. Moreover, we study HgCdTe epilayers grown by liquid phase epitaxy on these CdZnTe substrates in order to characterize and correlate the surface structure of epilayer and substrate.

Comparing experimental and modelling results, we find that the recorded angular distributions of the photoemission intensity give rise to photoelectron diffraction patterns which exhibit intensity peaks exclusively in the directions of internuclear axes between the photoemitting atomic species and all its neighbors if internuclear distances up to 5 times the bond distance are taken into account. Each observed peak can be assigned to a low–index crystal direction. This implies that zero–order interference (or "forward–direction fucusing") is the dominant interference phenomenon. Each diffraction pattern can then be understood as a hemispherical image of atoms in the real lattice space as mapped by a central projection, where the center of projection is the site of the relevant photoemitting atomic species.

Figs. 1 and 2 show the hemispherical display format as viewed from above for various experimental diffraction patterns in which the recorded photoemission intensity is referred to the values of a gray scale (in arbitrary units). Closer inspection of these diffraction patterns confirms [2,3,4] that there is no evidence for any reconstruction or relaxation of the (111) surfaces of CdZnTe or HgCdTe, respectively.

Fig. 1 exemplifies for CdZnTe that the examined (111)A and (111)B surfaces can be readily distinguished by their different diffraction patterns owing to a surprisingly perfect termination. Unexpected intensity discrepancies found by a comparison of these diffraction patterns can be traced to the fact that the magnitude of the generated scattering amplitude is larger for the Te than for the Cd scatterer.

The diffraction patterns on the left part of Fig.2 illustrate that ordered HgCdTe surfaces of stoichiometric composition can be realized by electrochemical etching and that a nonordered foreign contamination of about one monolayer is not an obstacle for the structural analysis of the underlying HgCdTe surface by XPD.

The diffraction patterns on the right part of Fig. 2 demonstrate that sputter–cleaning (1 keV Ar ions) of HgCdTe surfaces leads to a significant change in the peak intensity distribution of the photoemission indicating an increase in the mole fraction of CdTe in the outermost surface region. The crystallinity of the surface is maintained, however, in spite of the sputter treatment

References

1. M. Seelmann–Eggebert and H. J. Richter, Proc. SPIE **106**, 181 (1989)
2. U. Solzbach and H. J. Richter, Surf. Sci. **97**, 191 (1980)
3. G. Granozzi, G.A. Rizzi, G. S. Herman, D. J. Friedmann, C. S. Fadley, J. Osterwalder, and S. Bernardi, to appear in Physica Scripta
4. Y.–C Lu, R. S. Feigelson, and R. K. Rout, J. Appl. Phys. **67**, 2583 (1990)

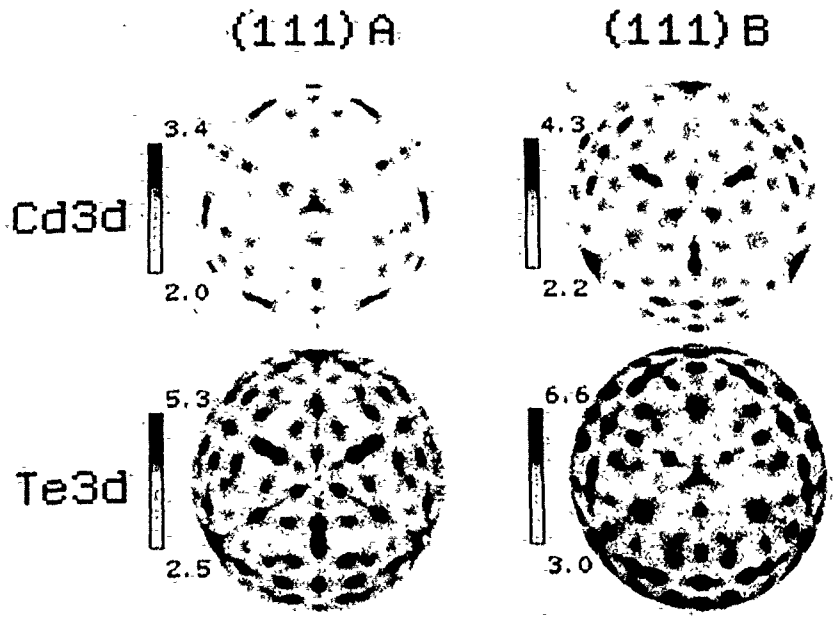

Figure 1. Diffraction patterns of the Cd $3d_{5/2}$ and the Te $3d_{5/2}$ core–level photoelectrons as obtained for the (111)A and the (111)B surface of CdZnTe.

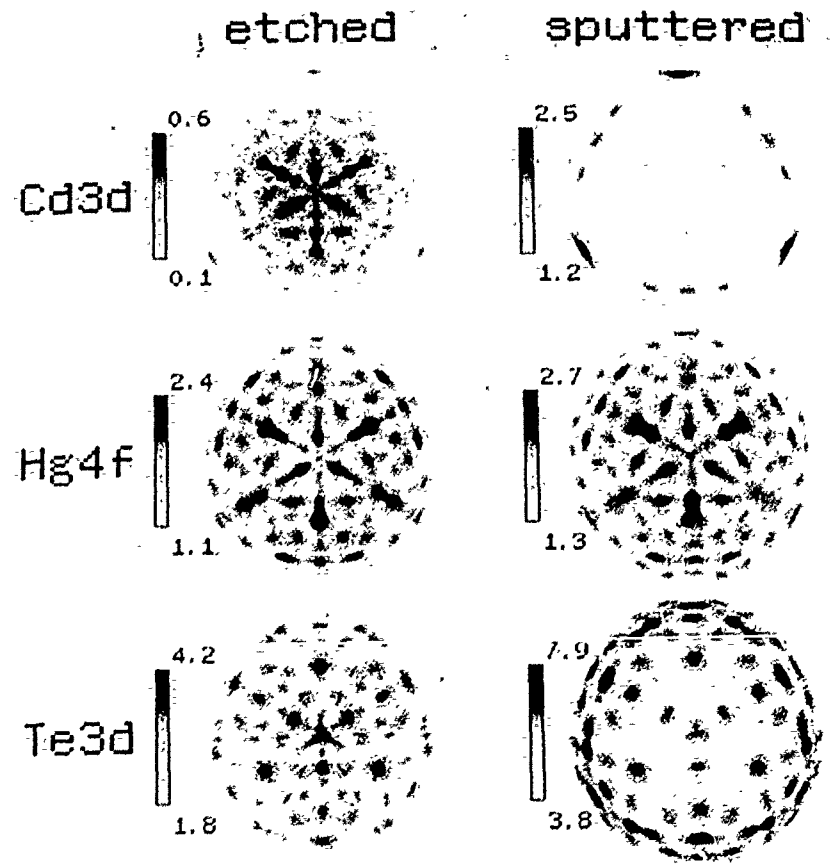

Figure 2. Diffraction patterns of the Cd $3d_{5/2}$, Hg $4f_{7/2}$, and Te $3d_{5/2}$ core–level photoelectrons as obtained for the (111)B surface of a HgCdTe epilayer after electrochemical etching (left) and sputtering with 1 keV Ar ions (right).

X-RAY PHOTOELECTRON DIFFRACTION FROM THE HgCdTe(111) SURFACE*

G.S. Herman[a], D.J. Friedman[a], C.S. Fadley[a], G. Granozzi[b], A. Rizzi[b], J. Osterwalder[c], and S. Bernardi[d]

[a]Department of Chemistry, University of Hawaii, Honolulu, HI 96822, U.S.A.

[b]Dipartimento di Chimica, Universita' di Padova, Padova, Italy

[c]Institut de Physique, Universite' de Fribourg, CH-1700 Fribourg, Switzerland

[d]Centro Studi e Laboratori Telecomunicazioni Spa, Torino, Italy

Surface polarity determinations for (111) zinc-blende structures have been of much interest as a result of their differing chemical and physical properties[1,2]. Due to the lack of a center of symmetry in the zinc-blende structure, these (111) surfaces can have either cationic (Type A) or anionic (Type B) surfaces. This paper presents a study of the HgCdTe surface using x-ray photoelectron diffraction (XPD), a uniquely powerful tool for the determination of surface structure[3,4,5]. We have obtained an extensive set of XPD data for $Hg_{1-x}Cd_xTe(111)$ with $x \approx 0.4$ as grown by liquid phase epitaxy (LPE) on Type A CdTe(111).

These data include both polar and azimuthal scans for the Hg $4f_{7/2}$, Cd $3d_{5/2}$, and Te $3d_{5/2}$ photoelectrons. Reproducible diffraction features are observed both before and after low-level ion bombardment to remove the native oxide layer. Shown in Figure 1(a) is an azimuthal scan of Cd $3d_{5/2}$ emission at a polar angle of 35° with respect to the surface (chosen to pass through near-neighbor scattering directions). A similar azimuthal scan for Te $3d_{5/2}$ emission is illustrated in Figure 1(b) at the same polar

angle. Strong modulations in XPD intensity were observed for both azimuthal diffraction patterns, with $\Delta I/I_{max}$ = 20% for Cd, and 29% for Te.

Single-scattering-cluster (SSC) calculations were used to model our experimental data for both Type A and Type B surfaces. Comparison of these experimental data with calculations, both visually and with R-factors, clearly indicates that this HgCdTe surface is Type A-terminated.

As one further aspect of this study, we consider the forward scattering origin of the various major peaks observed in Fig. 1(a) with the aid of Fig. 2, which indicates the several near-neighbor forward scattering events that are possible in a Type A-terminated surface. For the data at θ=35°, the principle peaks are due to events of the type labelled θ=35°, ϕ=60° and θ=30, ϕ=30°, 90°. The analogous Te curves in Fig. 1(b) are very different from those of Cd, with peak shifts and relative intensity changes. In particular, the peaks at θ=35°, ϕ=30° and 90° for Cd disappear in Te and are replaced by two weaker features at θ=35°, ϕ=40° and 80°. This is easily explained, since Fig. 2 shows that, in a Type A termination, the peaks which disappear are due to strong forward scattering events in the first double layer for only Cd emission; thus they are not expected to be seen for Te.

*This work has been supported by the Office of Naval Research (USA) under contract N00014-90-K-0512.

References

1. A.W. Stevenson, S.W. Wilkins, M.S. Kwietniak, and G.N. Pain, J. Appl. Phys. 66, 4198 (1989).
2. A.C. Chami, E. Ligeon, R. Danielou, and J. Fontenille, Appl. Phys. Lett. 52, 1502 (1988).
3. C.S. Fadley, Physica Scripta T17, 39 (1987).
4. D.A. Steigerwald and W.F. Egelhoff, Phys. Rev. Lett. 60, 2558 (1988).
5. P. Alnot, J. Olivier, and C.S. Fadley, J. Electron Spectrosc. Relat. Phenom. 49, 159 (1989).

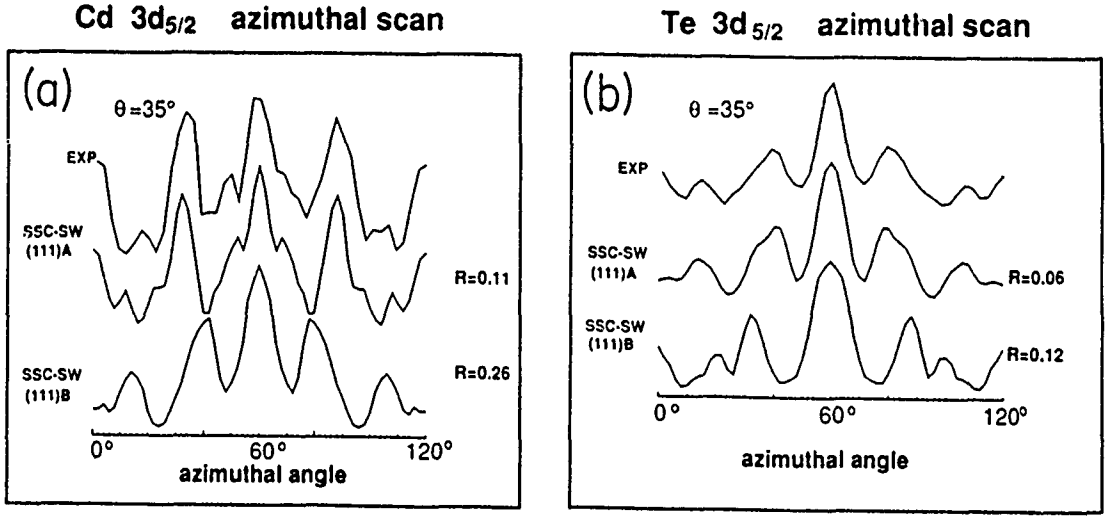

Figure 1. (a) Al Kα-excited azimuthal scans of Cd $3d_{5/2}$ intensities from $Hg_{1-x}Cd_xTe(111)$ at a polar angle 35° passing through or very close to the low-index directions in Fig. 2 shown as "θ=35°, ϕ=60°". Also shown are SSC curves for the two possible structure terminations (Type A Cd or Hg on top, Type B Te on top), together with R factors comparing experiment and theory. (b) As (a), but for Te $3d_{5/2}$ emission.

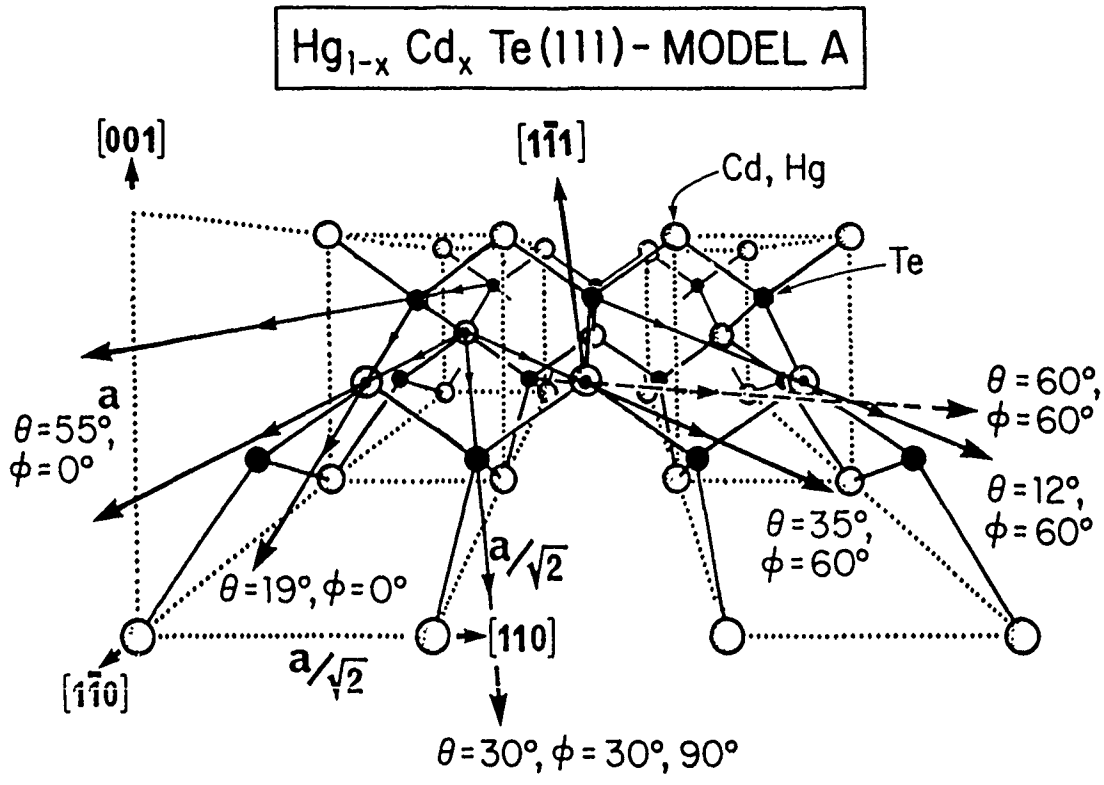

Figure 2. Perspective view of the unreconstructed (111) surface of $Hg_{1-x}Cd_xTe(111)$, with the θ, ϕ coordinates of various near-neighbor/low-index directions along which forward scattering might be expected to be strong.

ELECTROCHEMICAL APPROACHES TO CLEANING, RECONSTRUCTION AND CHARACTERIZATION OF THE (HgCd)Te SURFACE

S. Menezes, W. V. McLevige, E. R. Blazejewski and W. E. Tennant

Rockwell International Science Center, Thousand Oaks, CA 91360

J.P. Ziegler

Rockwell International Electro-Optical Center, Anaheim CA 92803-3105

Surface processes occuring at the (HgCd)Te/electrolyte (pH2) interface have been investigated with a rotating ring-(HgCdTe)disk electrode, modulated photocurrent, impedance and surface analysis. The potentials and the reaction sequence for the formation, dissolution and reduction of Hg, Cd, and Te based compounds and oxides were deduced from the results of these studies in conjunction with thermodynamic data. The relevant processes are shown in the current-voltage plot of Fig. 1. The initial anodic scan (dashed curve) in a pH 2, K_2SO_4 electrolyte shows no oxidation of (HgCd)Te components at potentials < 0.5 V. Anodic oxidation converts the defective surface layers to $CdTeO_3$ and then to $HgTeO_3$. These oxides are partially soluble in this electrolyte. The insoluble portion of the oxide components is reduced during the cathodic scan in the sequence: $HgTeO_3 > TeO_2 > CdTeO_3$. The preferentially reduced Hg film can be dissolved anodically by reoxidization as Hg_2^{2+}. The TeO_2 and $CdTeO_3$ are subsequently reduced to Te and CdTe, respectively. Excess Te dissolves as HTe^- leaving a CdTe-covered (HgCd)Te surface. The presence of dissolved Cd^{2+}, $HTeO_2^+$ or Hg^{2+} in the electrolyte can alter the course of surface reactions at (HgCd)Te.

Based on these results, we have devised a new electrochemical treatment for in-situ etching and passivation of (HgCd)Te surfaces. The method employs a sequence of potentiostatic cycles and steps applied to a (HgCd)Te specimen, immersed in a pH 2 electrolyte to oxidize the surface, remove Hg and leave a thin protective CdTe layer, reconstructed from the lattice atoms.

The electrochemically processed interface is characterized by a low density of fast interface states, a negligible concentration of slow traps and stability to prolonged air exposure and to 100 °C air anneal, as shown in Fig. 2. More than 30 samples, representing 6 layers of (HgCd)Te, were tested. MIS capacitance-voltage data from these samples showed that the best layers had consistent $N_{ss} < 5 \times 10^{10}$ cm^{-2} V^{-1} and E_{fb} -- 1.5 V. Control samples with conventional wet chemical treatment on the same layers were typically less consistent, with higher N_{ss}, more positive fixed charge and higher hysteresis for potential excursions between -10 V and +10 V.

The electrochemical approach additionally serves as an in-situ analytical tool to monitor the surface quality of (HgCd)Te. Voltammetric characterization of (HgCd)Te surfaces following various surface treatments is shown in Figs. 3 and 4. A cathodic peak, representing the dissolution of Te, produced by a Br_2/MeOH etch, appears in Fig. 3a. Depending on the solvent and the etch time, 2-10 monolayers of Te were detected on the Br_2-etched surfaces. The electrochemically reduced surface, Fig. 3b, appears clean and free of corrosion products or oxides. The Te present on the Br_2-etched surface converts to a TeO_2 on air exposure, Fig. 4a. Prolonged air exposure results in diffusion of Hg into the oxide, Fig. 4b.

These results confirm the extreme sensitivity of Br_2-etched (HgCd)Te surface to the etching parameters as well as to the post-etch conditions. A more stable surface may be attained using the electrochemical cleaning procedure in Fig. 1 or by mere electrochemical reduction of excess Te, Fig. 3b. Alternately, the excess Te may be reduced in Cd^{2+}/K_2SO_4 electrolyte to produce a thin CdTe layer. The Cd chalcogenides, including $CdTeO_3$, are thermochemically stable with respect to (HgCd)Te and produce passive surfaces [1]. Electrochemical processing offers selectivity and flexibility to manipulate the surface structure.

REFERENCES

1. C. R. Helms, J. Vac. Sci. Technol. A 8, 1178 (1990).

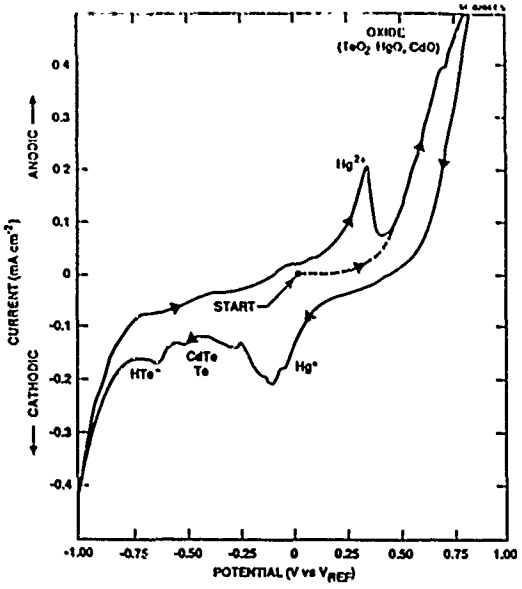

Fig. 1

Current-voltage characteristics of (HgCd)Te in 0.2M K_2SO_4.

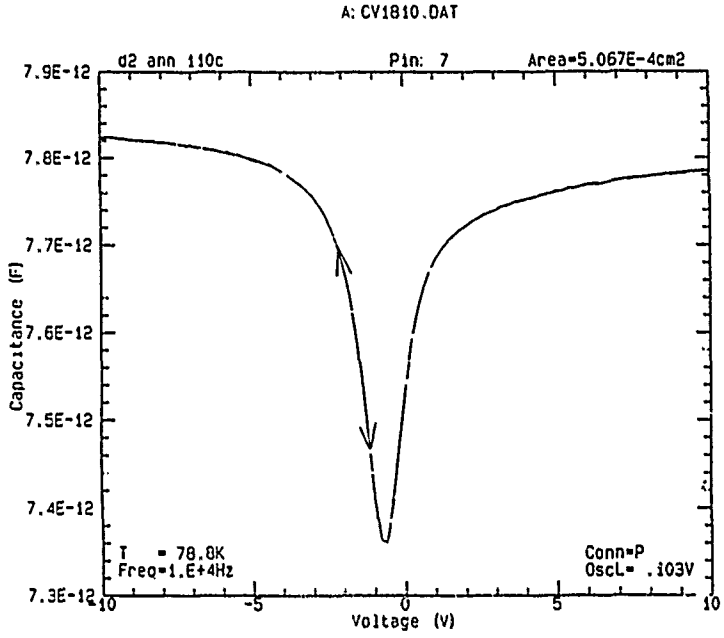

Fig. 2

Capacitance-voltage characteristics at 10 KHz for an electrochemically treated p-type MWIR (HgCd)Te/ZnS/Au structure.

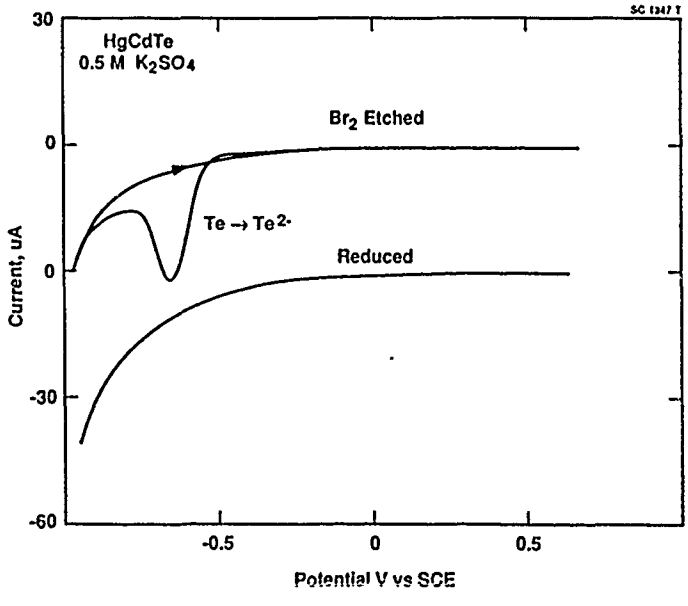

Fig. 3

Voltammetric characterization of (HgCd)Te surfaces in 0.2M K_2SO_4, following (a) Br_2/MeOH etch, (b) electrochemical reduction,

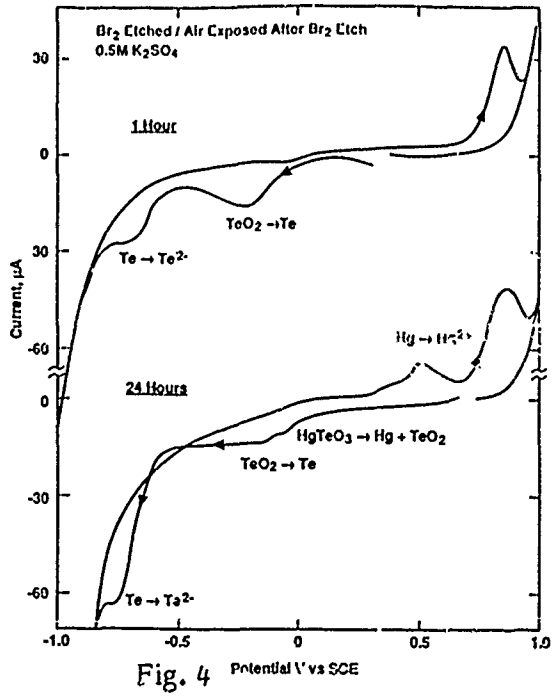

Fig. 4

Experiment of Fig. 3a after (c) 1 hour air-exposure of etched surface and (d) 24 hour air-exposure of etched surface.

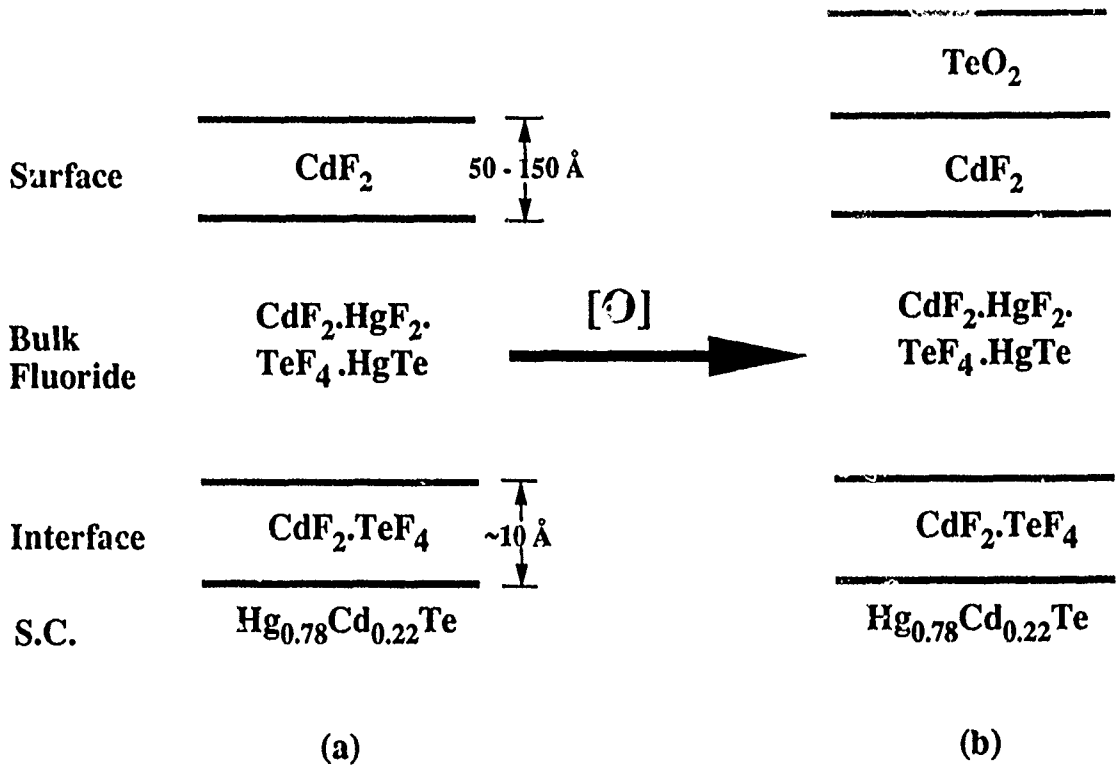

Fig. 1 Model of structure of the "as grown" anodic fluoride film and its interface with the semiconductor (a), and after exposure to room ambient (b).

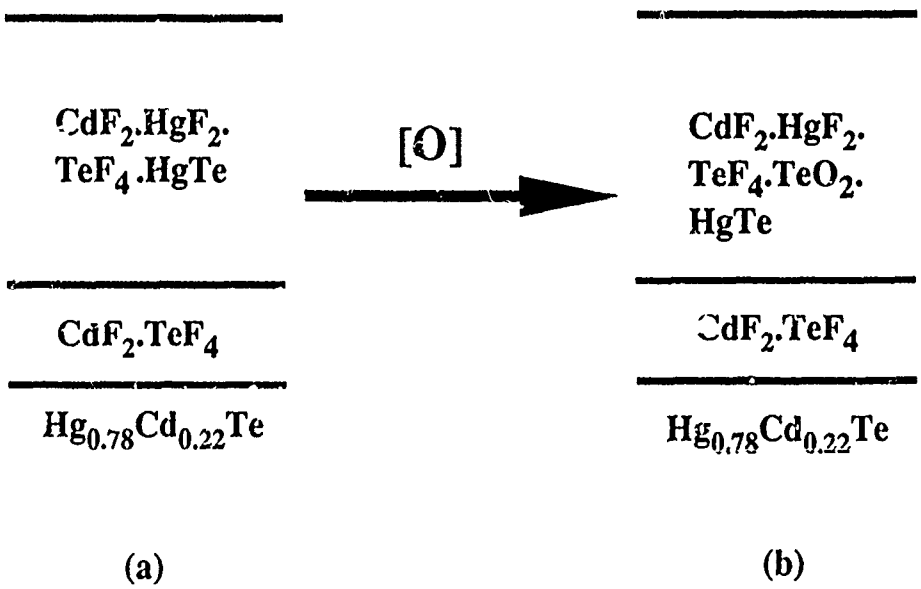

Fig. 2 Model as in Fig. 1 but for special films were the top CdF_2 rich layer is absent.

COMPOSITION, GROWTH MECHANISM AND STABILITY OF ANODIC FLUORIDE FILMS ON $Hg_{1-x}Cd_xTe$ (x~0.2)

Eliezer Weiss and C. R. Helms, Department of Electrical Engineering, Stanford University, Stanford, CA 94305.*

Recently Weiss and Mainzer reported the passivation of $Hg_{1-x}Cd_xTe$ surfaces by growing anodic layers from fluoridic solutions.[1,2] The use of anodic fluoridization or fluoro-oxidation is advantageous because the resulting interfaces are relatively thermally stable. Moreover, this method also reduces the surface recombination velocity and enables the adjustment of the amount of band bending at the surface of $Hg_{1-x}Cd_xTe$ infra-red detectors. The objective of the present work is the characterization of anodic fluorides on $Hg_{1-x}Cd_xTe$ in terms of their composition, growth mechanism, and stability. We have concentrated in this work only on the anodic growth in nonaqueous solutions of KF; that is, on the anodic fluoridization as opposed to the fluoro-oxidation process.

Using Auger electron spectroscopy and X-ray photoelectron spectroscopy combined with depth profiling, as well as microprobe analysis we discovered that the anodic film consists of three distinct regions as shown in Fig. 1a. A thick uniform region, containing the fluorides of cadmium, mercury, and tellurium, as well as HgTe, is covered by a thin CdF_2 layer. The third region — the

---

*Permanent address: SCD - semi-Conductor Devices, D.N. Misgav 20179, Israel.

film-substrate interface — poor in mercury, consists mainly of CdF_2 and TeF_4. The whole structure is covered with a thin layer of TeO_2 (Fig. 1b), due to oxidation by water vapor.

We have used ultra-thin Pd marker layers and growth from baths saturated in CdF_2 to study the growth mechanism. The film is grown by two mechanisms: the dominant one occurs by motion of the film-substrate interface into the semiconductor, consuming the original surface. There is, however, some growth at the film-electrolyte interface which forms the thin CdF_2 layer on top of the structure. It turns out that this second mechanism has a crucial effect on the stability of the film against oxidation. Films which were grown under conditions such that the top CdF_2 rich region is absent and films in which this top layer was carefully etched off (Fig. 2a) are oxidized rapidly upon exposure to room ambient (Fig. 2b). This indicates that the CdF_2 rich region acts as a diffusion barrier for the in-diffusion of oxidizing species. Tellurium ions, on the other hand, diffuse to the outer surface to be oxidized there.

The effects of thermal treatments on the film structure will also be described and discussed in terms of the thermodynamic properties of the Hg-Cd-Te-F system.

References:

[1]E. Weiss and N. Mainzer, J. Vac. Sci. Technol. A **6**, 2765 (1988).

[2]N. Mainzer, E. Weiss, D. Laser, and M. Shaanan, J. Vac. Sci. Technol. A **7**, 460 (1989).

Study of Temperature Dependent Structural Changes in MBE Grown $Hg_{1-x}Cd_xTe$ by X-ray Lattice Parameter Measurements and EXAFS

D. Di Marzio, M.B. Lee, J. DeCarlo
Grumman Corporate Research Center
Bethpage N.Y. 11714

A. Gibaud*, S.M. Heald
Brookhaven National Laboratory
Upton, N.Y. 11973

IR detectors fabricated from $Hg_{1-x}Cd_xTe$ typically operate in the 60 to 160 K range. Low temperature structural information is important for understanding the strains that may be present in device structures due to lattice mismatch at interfaces or native defects. Uniaxial stress experiments have shown significant changes in the resistivity, carrier concentration, and mobility of $Hg_{1-x}Cd_xTe$ when various stresses are applied[1,2]. We present the first detailed study of the x-ray diffraction lattice parameters of MBE grown $Hg_{1-x}Cd_xTe$ epilayers between 15 and 300K. These results are then compared to extended x-ray absorption fine structure (EXAFS) measurements. EXAFS studies at room temperature have already demonstrated a bimodal bond length distribution (Hg-Te and Cd-Te) in the HgCdTe ternary alloy[3]. This suggests that there is a significant local distortion of the atomic structure that is not readily apparent from x-ray diffraction.

The (100) oriented epilayers were grown in a Riber 2300 MBE system on (100) CdTe substrates, and they varied in thickness (6 to 11 um) and composition (x=0 to 0.172)[4]. A Huber four circle diffractometer with a rotating anode Cu $K\alpha_1$ beam was used, and the (400) reflection was measured to determine the lattice parameter, $a\perp$, normal to the film. The lattice parameters as a function of the composition, as determined by the IR cutoff, is shown in figure 1 (sample x=.244 is also included). Figure 2 shows the lattice parameters of the epilayers as a function of temperature for both cooling and heating cycles. HgTe (x=0, 6 um thick) exhibited normal linear lattice contraction ($\alpha=4.7\times10^{-6}$ K^{-1} at 300 K), with a minimum in $a\perp$ at 60K, and an expansion of $a\perp$ below 60K (fig. 2 and fig. 3). In addition to showing a minimum in $a\perp$ at 60K, some of the HgCdTe ($x\neq0$) epilayers (10 to 11 um thick) exhibited anomalous non linear

behavior with varying degrees of thermal hysteresis in $a_\perp$ (fig. 2 and fig. 3; x=.153, x=.160). This unusual non linear hysteretic behavior may be the result stress fields in the epilayer elastically coupled to the substrate[5]. Interacting with various inherent defects in the film (vacancies, dislocations, hillocks, etc.), these stress fields could lead to deviations from linear and reversible thermal behavior. The average contraction of $a_\perp$ for these epilayers from 300 to 60K is 0.006Å. The lattice parameter, $a_\perp$, of a 1000 Å cap layer of CdTe on sample x=.160 was also measured as a function of temperature. The room temperature $a_\perp$ was 6.4967, which is close the expected value of 6.5127 Å predicted by elastic theory.

These results are compared with measurements we have obtained from a temperature dependent EXAFS study[6]. The HgTe (x=0) epilayer exhibited a normal thermal contraction (linear) of the Hg-Te bond length consistent, within the error bars, with the lattice parameter results. However, in the HgCdTe epilayers this bond contracts 0.02 to 0.03Å on cooling from 300 to 10K. In figure 4, sample x=.160 exhibits a rapid contraction of the Hg-Te bond length with decreasing temperature around 100 K. This unusually large bond length contraction, as compared to the non linear, hysteretic, and relatively smaller lattice parameter contraction, suggests that a degree of local atomic relaxation is taking place that is averaged out in x-ray diffraction measurements.

* Presently at the University of Le Mans, France.

We acknowledge the support of the U.S. Department of Energy, Division of Materials Sciences, under contract No. DE-AC02-76CH00016, and No. DE-AS05-80-ER10742.

---

[1]P.S. Kireev, V.V. Ptashinskii, A.M. Sokolov, and V.G. Kovalev, Sov. Phys. Semicond., **7**, 266 (1973).

[2]P.I. Baranskii, A.I. Elizarov, V.A. Kulik, and K.R. Kubanov, Sov. Phys. Semicond., **13**, 490 (1979).

[3]R.A. Mayanovic, W.F. Pong, and B.A. Bunker, to be published.

[4]M.B. Lee, J. DeCarlo, D. Di Marzio, and M. Kesselman, *in Proceedings of the MRS Symposium on the Properties of II-VI Semiconductors: Bulk Crystals, Epitaxial Films, Quantum Well Structures, and Dilute Magnetic Systems*, Boston, 1989, edited by F.J. Bartoli, Jr., H.F. Schaake, and J.F. Schetzina (MRS, Pittsburgh, 1990), Vol. 161, p.377.

[5]R.W. Hoffman, *in Proceedings of the MRS Symposium on Materials Characterization*, Palo Alto, 1986, edited by N. Cheung, and M. Nicolet (MRS, Pittsburgh, 1986), Vol. 69, p. 95.

[6]D. Di Marzio, M.B. Lee, J. DeCarlo, and S.M. Heald, in preparation.

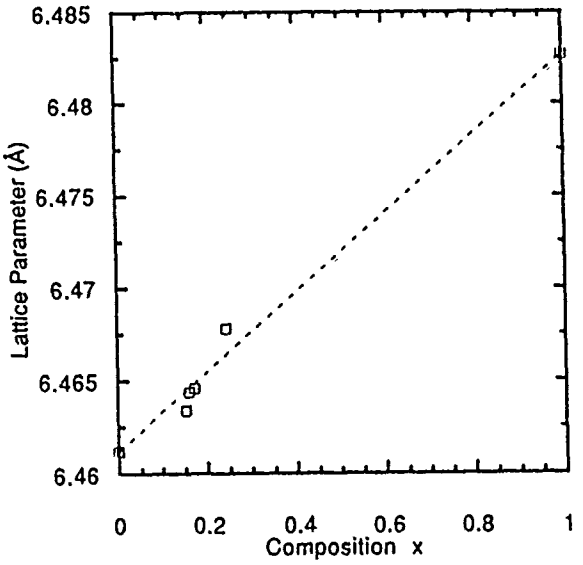

1) Room temperature lattice parameters of $Hg_{1-x}Cd_xTe$ epilayers as a function of composition. The dashed line joins the two end point compounds (HgTe and CdTe).

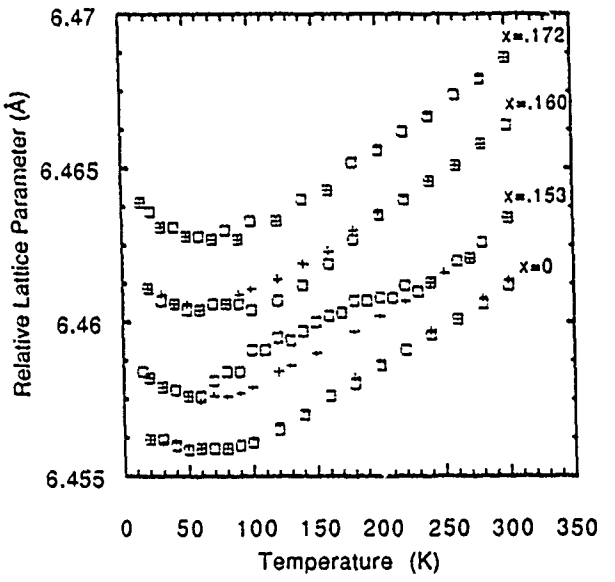

2) Relative lattice parameters of the epilayers as a function of temperature; "□" : cooling cycle, "+" : heating cycle. For clarity, the lattice parameters of sample x=.160 and x=.172 are displaced from their absolute values by +.002 Å and +.004 Å, respectively.

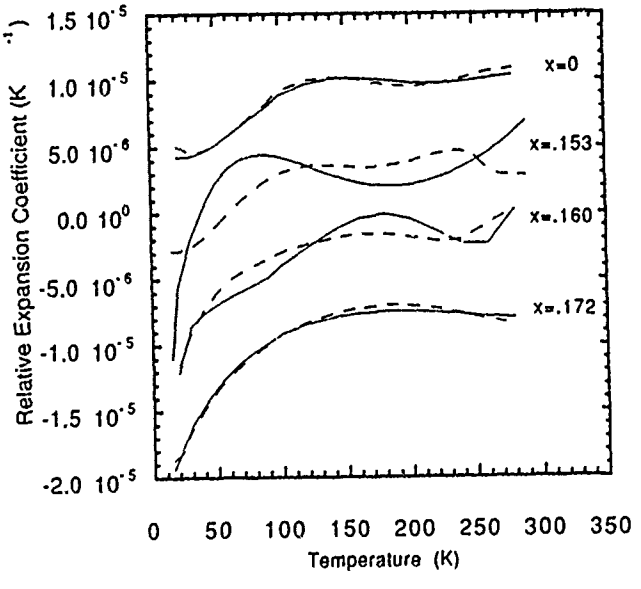

3) Relative thermal expansion coefficient, α, of the epilayers as a function of temperature. "———" cooling cycle; "– – – –" heating cycle. For clarity, the α of sample x=0, x=.160, and x=.172 are displaced from their absolute values by $+6.0\times10^{-6}$ K^{-1}, -6.0×10^{-6} K^{-1}, and -12.0×10^{-6} K^{-1}, respectively.

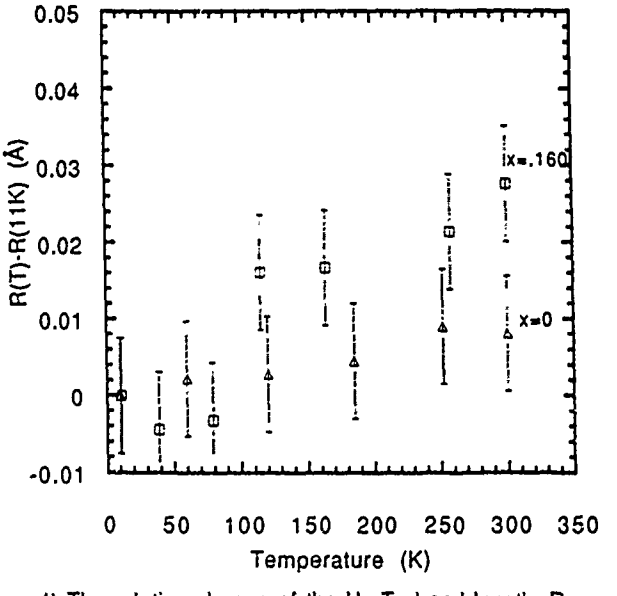

4) The relative change of the Hg-Te bond length, R, as measured by EXAFS, in sample x=0 and x=.160 between temperature T and 11 K.

CHARACTERIZATION OF CdTe, (Cd,Zn)Te AND Cd(Te,Se) SINGLE CRYSTALS BY TRANSMISSION ELECTRON MICROSCOPY

R.S. Rai, S. Mahajan, S. McDevitt* and C.J. Johnson*
Department of Metallurgical Engineering and Materials Science
Carnegie Mellon University, Pittsburgh, PA 15213
*II-VI Incorporated, Saxonburg, PA 16056

CdTe and its alloys possess many attractive properties and have application in the area of opto-electronics. However, their full potential cannot be realized because of the presence of precipitates, dislocations and microtwins. Among CdTe family, (Cd,Zn)Te is a leading candidate material for substrates for LPE growth of (Hg,Cd)Te epitaxial layers.

The performance of the heterostructure devices is strongly influenced by the quality of underlying substrate [1]. Therefore, in addition to growing large area single crystals, controlled growth of these materials is highly desirable for developing structural quality substrates. In this paper, CdTe, (Cd,Zn)Te and Cd(Te,Se) crystals, grown by the Bridgman technique have been characterized on the submicron scale by TEM.

Te precipitates consistent with earlier published results [2,3], isolated dislocations, stacking faults and arrays of dislocations are observed in as grown CdTe crystals. Fig. 1 shows a typical example in which dislocations are arranged into arrays on {111} parallel planes. It has been ascertained by diffraction contrast experiments that the Burgers vectors of the dislocations are 1/6<112>. The as-grown (Cd,Zn)Te crystals show a high density of Te precipitates. This is evident in Fig. 2 which shows a dark-field image obtained using 1010-Te reflection. The density of the precipitates in these crystals is considerably higher than that in CdTe crystals. In addition, microtwins lying on the {111} planes are observed in certain regions. One of the examples is reproduced as Fig. 3. Microtwins are similarly seen in as-grown Cd(Te,Se) crystals. Also, the density of Te precipitates in Cd(Te,Se) crystals is smaller than either (Cd,Zn)Te or in CdTe as-grown crystals.

Dislocations and microtwins shown in Fig. 1 and Fig. 3, respectively, are very likely caused by thermal-gradient-induced stresses which develop during cool down from the growth temperature. It appears from the preceding study that if one could minimize thermal induced stresses, it should be possible to grow Cd(Te,Se) crystals whose quality is superior to that of the CdTe and (Cd,Zn)Te crystals because of the reduced precipitate density [4].

References:

1. B.V. Dutt, S. Mahajan, R.J. Roedel, G.P. Schwartz, D.C. Miller and L. Derick, J. Electrochem. Soc. 128 (1981) 1573.

2. S.H. Shin, J. Bajaj, L.A. Moudy and D.T. Cheung, Appl. Phys. Lett. 43 (1983) 68.

3. M.A. Shahid, S.C. McDevitt, S. Mahajan and C.J. Johnson, Inst. Phys. Conf. No. 87 (1987) 321.

4. This work is supported by US ARMY/CNVEO, Contract No. DAAB 07-87-C-F088.

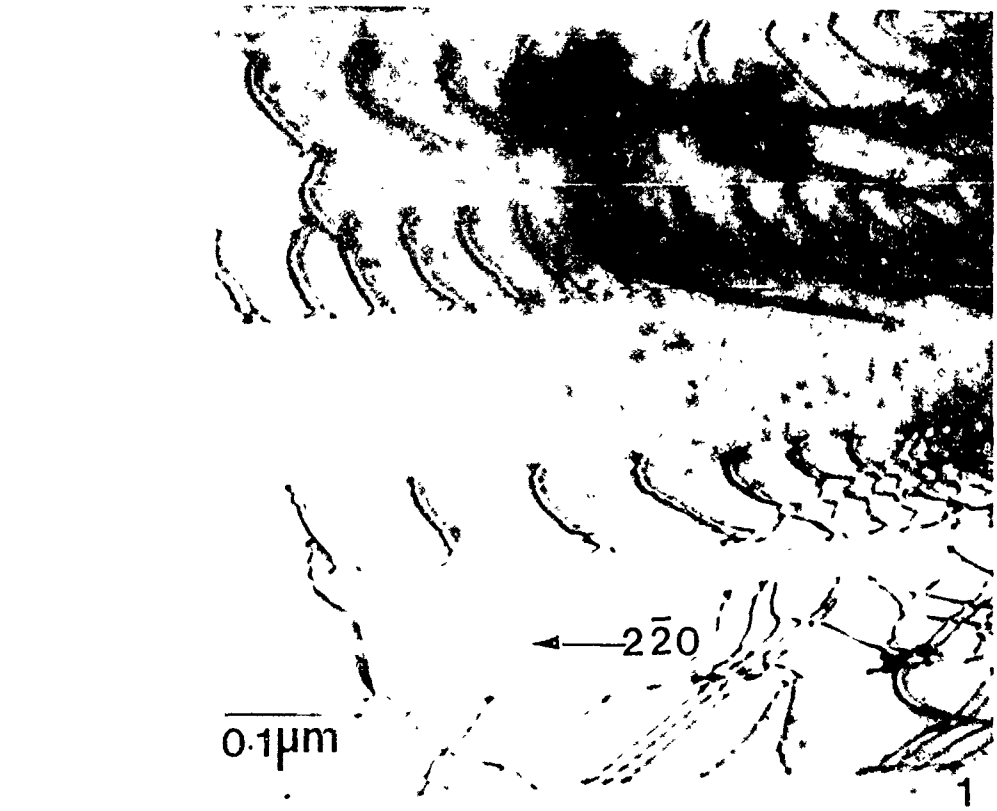

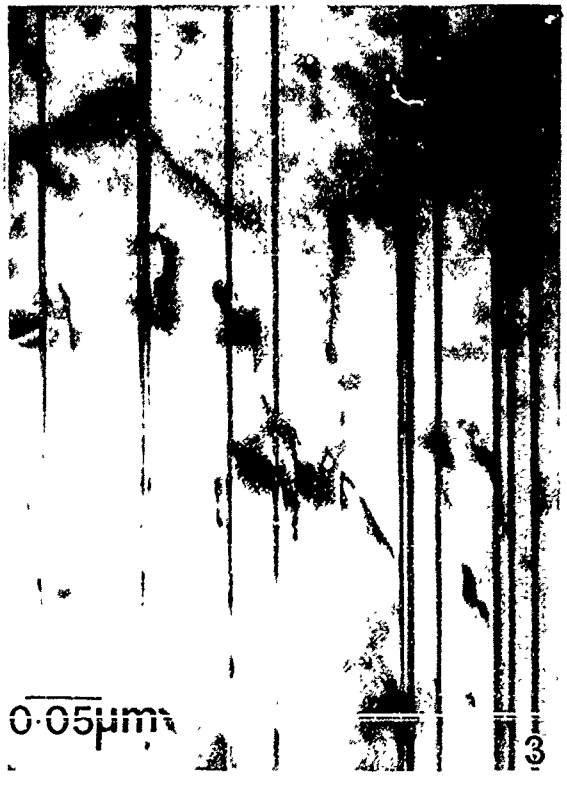

Fig. 1: Bright field electron micrograph obtained from CdTe specimen, showing arrays of dislocations due to parallel slip bands. Diffraction vector is [2$\bar{2}$0] and foil orientation [111].

Fig. 2: Centered dark field image obtained from precipitate reflection showing Te precipitates (white spots) in (Cd,Zn)Te.

Fig. 3: Bright field electron micrograph showing microtwins and precipitates in (Cd,Zn)Te. Diffraction vector is [220] and foil orientation [110].

Optical Techniques for Composition Measurement of Bulk and Thin-film $Cd_{1-y}Zn_yTe$

S.M. Johnson, S. Sen, W.H. Konkel, and M.H. Kalisher
Santa Barbara Research Center
75 Coromar Drive, Goleta, CA 93117

Lattice-matched single-crystal bulk CdZnTe is the preferred substrate for growth of high-quality epitaxial HgCdTe used for the fabrication of second-generation infrared focal-plane arrays. Thin-film alternative substrates of CdZnTe/GaAs/Si are rapidly gaining importance for improvements in size, strength, cost, and reliability of hybrid focal-plane arrays. An accurate nondestructive measurement of the magnitude and spatial uniformity of the composition of both bulk and thin-film $Cd_{1-y}Zn_yTe$ is needed to ensure uniform lattice matching to the HgCdTe epitaxial layer.

Previously, measurements of the composition of several MBE-grown $Cd_{1-y}Zn_yTe$ ($0 \le y \le 1$) layers by energy-dispersive x-ray analysis (EDX) were correlated with photoluminescence measurements done at 12K and 300K [1]. Recently, determination of the composition of bulk $Cd_{1-y}Zn_yTe$ ($0.02 \le y \le 0.07$) was done using 4.2K photoluminescence measurements correlated with lattice constants determined from x-ray powder diffraction measurements [2].

We have extended this photoluminescence calibration to compositions in the higher composition range ($0 \le y \le 0.2$) and also to T=77K, which allows immersion of large substrates in liquid nitrogen for rapid measurements rather than using a liquid-He dewar. We have further developed an accurate calibration curve for bulk substrates using a simple measurement of the 300K optical transmission cut-on wavelength. Both techniques will give an accuracy of $y \pm 0.001$. The lattice constants of the single-crystal high-quality bulk CdTe, ZnTe, and CdZnTe calibration samples were determined using the Bond technique and are accurate to ±0.0001 Å; composition was calculated using Vegard's law. With these calibration curves these optical techniques are useful for mapping the composition of both bulk and thin-film substrates over composition ranges suitable for lattice matching to HgCdTe and HgZnTe.

1. D.J. Olego, J.P. Faurie, S. Sivananthan, and P.M. Raccah, Appl. Phys. Lett. **47**, 1172 (1985).
2. W.M. Duncan, R.J. Koestner, J.H. Tregilgas, H.-Y. Liu, and M.-C. Chen, in *Properties of II-VI Semiconductors: Bulk Crystals, Epitaxial Films, Quantum Well Structures, and Dilute Magnetic Systems*, Materials Research Society Symposium Proceedings, Vol. 161 (1990), in press.